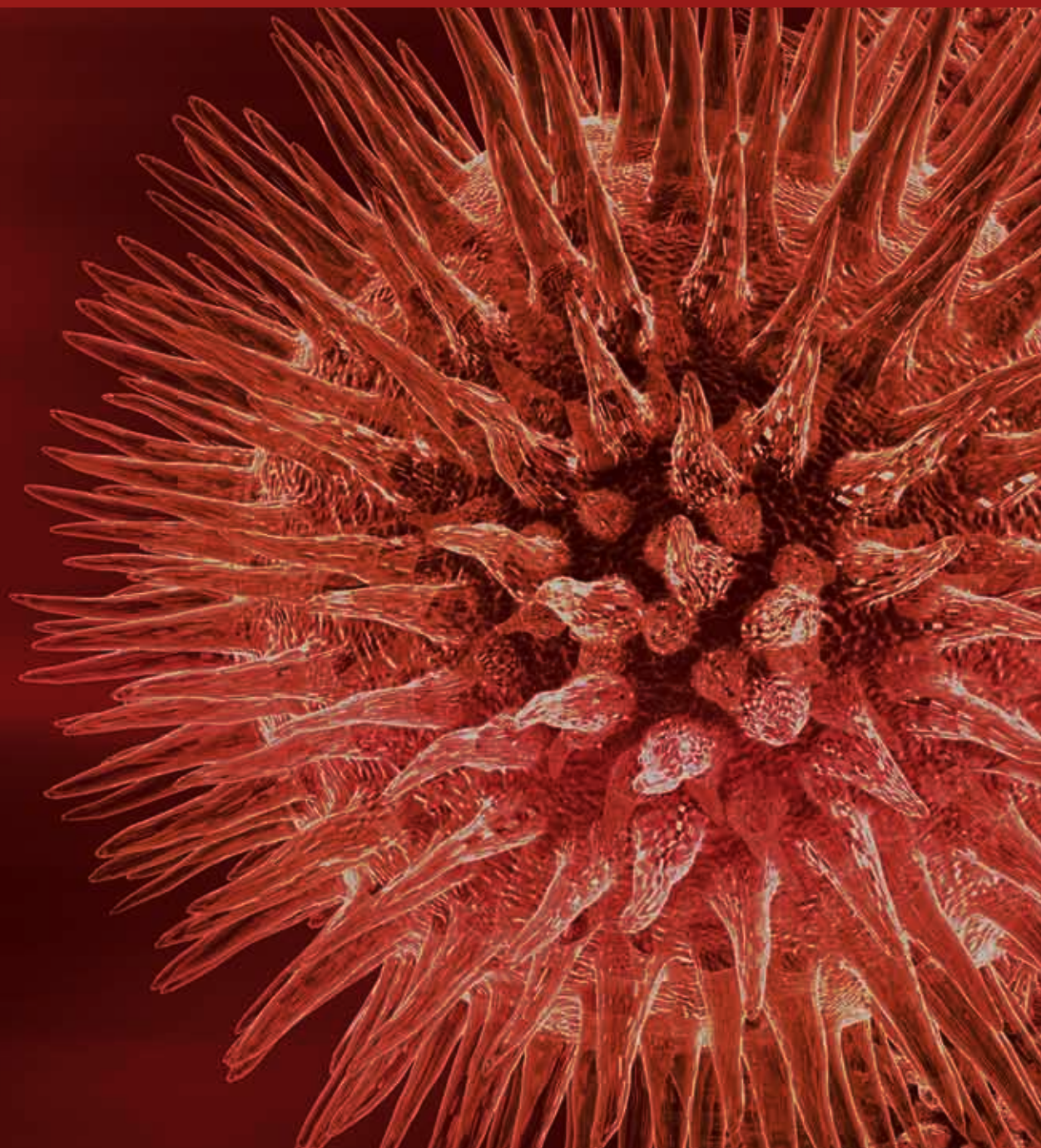


Physiology to the Pleiotropic Role of RNAs: Prospecting Novel Therapies

Guest Editors: Maria Chiara Maiuri, Daniela De Stefano,
and Ammad Ahmad Farooqi





Physiology to the Pleiotropic Role of RNAs: Prospecting Novel Therapies

Physiology to the Pleiotropic Role of RNAs: Prospecting Novel Therapies

Guest Editors: Maria Chiara Maiuri, Daniela De Stefano,
and Ammad Ahmad Farooqi



Copyright © 2014 Hindawi Publishing Corporation. All rights reserved.

This is a special issue published in “BioMed Research International.” All articles are open access articles distributed under the Creative Commons Attribution License, which permits unrestricted use, distribution, and reproduction in any medium, provided the original work is properly cited.

Contents

Physiology to the Pleiotropic Role of RNAs: Prospecting Novel Therapies, Maria Chiara Maiuri, Daniela De Stefano, and Ammad Ahmad Farooqi
Volume 2014, Article ID 735374, 1 page

Inhibition of Hepatitis B Virus Replication by Helper Dependent Adenoviral Vectors Expressing Artificial Anti-HBV Pri-miRs from a Liver-Specific Promoter, Mohube Betty Mowa, Carol Crowther, Abdullah Ely, and Patrick Arbuthnot
Volume 2014, Article ID 718743, 12 pages

Systemic Approach to Identify Serum microRNAs as Potential Biomarkers for Acute Myocardial Infarction, An Hsu, Shu-Jen Chen, Yu-Sun Chang, Hua-Chien Chen, and Pao-Hsien Chu
Volume 2014, Article ID 418628, 13 pages

Exploitation of a Very Small Peptide Nucleic Acid as a New Inhibitor of miR-509-3p Involved in the Regulation of Cystic Fibrosis Disease-Gene Expression, Felice Amato, Rossella Tomaiuolo, Fabrizia Nici, Nicola Borbone, Ausilia Elce, Bruno Catalanotti, Stefano D'Errico, Carmine Marco Morgillo, Giuseppe De Rosa, Laura Mayol, Gennaro Piccialli, Giorgia Oliviero, and Giuseppe Castaldo
Volume 2014, Article ID 610718, 10 pages

Rapid Degradation of Hfq-Free RyhB in *Yersinia pestis* by PNPase Independent of Putative Ribonucleolytic Complexes, Zhongliang Deng, Zizhong Liu, Yujing Bi, Xiaoyi Wang, Dongsheng Zhou, Ruifu Yang, and Yanping Han
Volume 2014, Article ID 798918, 7 pages

Synthesis and Gene Silencing Properties of siRNAs Containing Terminal Amide Linkages, Maria Gaglione, M. Emilia Mercurio, Nicoletta Potenza, Nicola Mosca, Aniello Russo, Ettore Novellino, Sandro Cosconati, and Anna Messere
Volume 2014, Article ID 901617, 15 pages

Transferrin-Conjugated SNALPs Encapsulating 2-O-Methylated miR-34a for the Treatment of Multiple Myeloma, Immacolata Scognamiglio, Maria Teresa Di Martino, Virginia Campani, Antonella Virgilio, Aldo Galeone, Annamaria Gullà, Maria Eugenia Gallo Cantafio, Gabriella Misso, Pierosandro Tagliaferri, Pierfrancesco Tassone, Michele Caraglia, and Giuseppe De Rosa
Volume 2014, Article ID 217365, 7 pages

Editorial

Physiology to the Pleiotropic Role of RNAs: Prospecting Novel Therapies

Maria Chiara Maiuri,¹ Daniela De Stefano,² and Ammad Ahmad Farooqi³

¹ INSERM, U848, Institut Gustave Roussy, PR1, 39 rue Camille Desmoulins, Villejuif, 94805 Paris, France

² Dipartimento di Farmacia, Università Degli Studi di Napoli Federico II, Via D. Montesano 49, 80135 Napoli, Italy

³ Laboratory for Translational Oncology and Personalized Medicine, Rashid Latif Medical College, 35 Km Ferozepur Road, 54600 Lahore, Pakistan

Correspondence should be addressed to Maria Chiara Maiuri; maiuri@igr.fr

Received 11 June 2014; Accepted 11 June 2014; Published 1 July 2014

Copyright © 2014 Maria Chiara Maiuri et al. This is an open access article distributed under the Creative Commons Attribution License, which permits unrestricted use, distribution, and reproduction in any medium, provided the original work is properly cited.

The purpose of this special issue is to point the attention to the RNA functions, which in the last decades emerged as extremely important. Particularly, physiopathological roles of microRNA, short hairpin RNA, and small interfering RNA have been reported, in turn leading to the opportunity to consider RNAs as both novel therapeutic targets and tools. The contributions of this special issue cover a variety of subjects and reflect the complexity of the field.

In particular, RNA is a difficult molecule, due to its rapid degradation. Several strategies have been described to overcome these issues, in order to render the use of RNA possible. M. Gaglione et al. reported chemical modifications of siRNAs containing terminal amide linkages by introducing hydroxyethylglycine PNA (hegPNA) moieties at 5', at 3' positions, and on both terminals and demonstrated that some of these modifications are compatible with the RNAi machinery, as they markedly increased the resistance to serum-derived nucleases. Indeed, Z. Deng et al. reported the role of PNPase as a major enzyme of sRNAs degradation.

I. Scognamiglio et al. describe the development and effects of stable nucleic acid lipid vesicles (SNALPs) encapsulating miR-34a to treat multiple myeloma. In this study, the authors show that it is possible to overcome the targeted delivery of SNALPs as well as miRNA encapsulation efficiency drawbacks by conjugating SNALPs with the transferrin and chemically modifying the miRNA with a 2'-O-methylation. The formulation was effective in reducing tumor growth.

The miRNAs are the subject of another contribution. A. Hsu et al. demonstrated that an alteration of miRNA levels

may be used as diagnostic markers of myocardial infarction. The differentially expressed miRNAs were evaluated in a separate cohort of 62 subjects to show that serum miR-486-3p and miR-150-3p were upregulated while miR-126-3p, 14 miR-26a-5p, and miR-191-5p were significantly down-regulated suggesting that serum miRNAs may be used as potential diagnostic biomarkers. F. Amato et al. reported the effectiveness of an inhibitor of miR-5093p for the regulation of cystic fibrosis-related gene expression.

Primary miRNA (pri-miRNA) is the subject of M. B. Mowa and colleagues study. The authors investigated the utility of the murine transthyretin receptor (MTTR) promoter for expression of artificial anti-HBV primary miRNA (pri-miRNA) sequences to develop their use in liver-specific transcription regulatory elements. They demonstrated that the expression of anti-HBV pri-miR mimics from MTTR promoter is well suited to countering HBV replication and development of HD Ads through attenuation of their immunostimulatory effects.

The present issue constitutes an important update in a constantly developing field. The efforts to carry on these studies will, possibly, generate new therapeutic opportunities in the near future.

Maria Chiara Maiuri
Daniela De Stefano
Ammad Ahmad Farooqi

Research Article

Inhibition of Hepatitis B Virus Replication by Helper Dependent Adenoviral Vectors Expressing Artificial Anti-HBV Pri-miRs from a Liver-Specific Promoter

Mohube Betty Mowa, Carol Crowther, Abdullah Ely, and Patrick Arbuthnot

Antiviral Gene Therapy Research Unit, School of Pathology, Health Sciences Faculty, University of the Witwatersrand, Private Bag 3, Johannesburg 2050, South Africa

Correspondence should be addressed to Patrick Arbuthnot; patrick.arbuthnot@wits.ac.za

Received 4 January 2014; Revised 25 April 2014; Accepted 8 May 2014; Published 5 June 2014

Academic Editor: Ammad Ahmad Farooqi

Copyright © 2014 Mohube Betty Mowa et al. This is an open access article distributed under the Creative Commons Attribution License, which permits unrestricted use, distribution, and reproduction in any medium, provided the original work is properly cited.

Research on applying RNA interference (RNAi) to counter HBV replication has led to identification of potential therapeutic sequences. However, before clinical application liver-specific expression and efficient delivery of these sequences remain an important objective. We recently reported short-term inhibition of HBV replication *in vivo* by using helper dependent adenoviral vectors (HD Ads) expressing anti-HBV sequences from a constitutively active cytomegalovirus (CMV) promoter. To develop the use of liver-specific transcription regulatory elements we investigated the utility of the murine transthyretin (MTTR) promoter for expression of anti-HBV primary microRNAs (pri-miRs). HD Ads containing MTTR promoter effected superior expression of anti-HBV pri-miRs in mice compared to HD Ads containing the CMV promoter. MTTR-containing HD Ads resulted in HBV replication knockdown of up to 94% in mice. HD Ads expressing trimeric anti-HBV pri-miRs silenced HBV replication for 5 weeks. We previously showed that the product of the codelivered *lacZ* gene induces an immune response, and the duration of HBV silencing *in vivo* is likely to be attenuated by this effect. Nevertheless, expression of anti-HBV pri-miRs from MTTR promoter is well suited to countering HBV replication and development of HD Ads through attenuation of their immunostimulatory effects should advance their clinical utility.

1. Introduction

Reactivation of hepatitis B virus (HBV) replication after treatment withdrawal commonly occurs with currently available anti-HBV therapies [1, 2]. This has necessitated development of more effective durable approaches to countering HBV infection. RNA interference- (RNAi-) based therapy has shown promising outcomes as an alternative to current hepatitis B treatment (reviewed in [3, 4]). Naturally, the RNAi pathway uses small RNAs (e.g., microRNAs (miRs)) to regulate gene expression in a wide range of organisms. Binding of small RNAs to the target sequence may result in degradation or translation inhibition of the target. Generally, endogenous activation of the RNAi pathway with miRs initially involves transcription of primary miRs (pri-miRs) by RNA polymerase (Pol) II. These hairpin-like structures are then processed in the nucleus by Drosha (RNase III) and

its double stranded RNA binding partner DGCR8, to form precursor miRs (pre-miRs). Pre-miRs are then exported to the cytoplasm and processed by Dicer (RNase III) to form mature miR duplexes. Mature miRs are passed on to the RNA induced silencing complex (RISC) containing the argonaute protein with RNase activity. One strand is selected as a guide, which pairs with the target to facilitate target translation inhibition or degradation (reviewed in [5]).

Manipulation of RNAi for therapeutic purposes involves the use of synthetic short interfering RNA (siRNA), expressed pri-miR or pre-miR mimics. These artificial intermediates of the RNAi pathway reprogramme the endogenous RNAi pathway to induce silencing of specific targets (reviewed in [6]). Expressed RNAi activators have advantages of sustained efficacy from continuous intracellular supply of siRNAs, ease of propagation in plasmid DNA, better stability, and compatibility with highly efficient viral vectors. These properties

make them well suited to treatment of chronic viral infections, such as caused by HBV. Pol III promoters, for example, U6 small nuclear RNA (snRNA) and human ribonuclease P RNA component H1 promoters, are commonly used to regulate transcription of short hairpin RNAs (shRNAs) that mimic pre-miRs [7, 8]. However, overexpression from Pol III promoters may be complicated by toxicity that is attributed to saturation of the endogenous RNAi machinery [9, 10]. The versatility of Pol II promoters overcomes some of these problems. These transcriptional regulatory elements are capable of achieving tissue specific transgene expression, improved transcriptional regulation, and generation of multimeric pri-miR activators of RNAi [11, 12]. Since functional coupling between intermediates of the RNAi pathway may occur, expression of earlier intermediates of the RNAi pathway, such as pri-miRs, may improve efficiency of target silencing. Moreover, use of artificial pri-miR cassettes that are expressed from Pol II promoters has been shown to be safer than employing U6 Pol III shRNA expression cassettes [11, 13–15]. Use of a liver-specific promoter to express anti-HBV sequences is also potentially useful to limit nonspecific effects that may be caused by constitutively active transcriptional regulatory elements.

Achieving safe and efficient nucleic acid delivery is important for developing RNAi-based therapy of viral infections. The natural targeting of hepatocytes by adenoviral vectors [16] and sustained transgene expression that may be attained with helper dependent adenoviral vectors (HD Ads) makes them suitable for delivering expressed RNAi activators that are designed to treat chronic HBV infection (reviewed in [17, 18]). The feasibility of using HD Ads for treating HBV infection has been demonstrated in murine and woodchuck models of the disease [19–22]. In these studies, immunotherapy-based treatment using HD Ads to deliver interferon-alpha and interleukin-12 was employed. Prolonged (~3 months) transgene expression with sustained antiviral effects was observed with HD Ads, which was not possible with first generation Ad vector expressing interferon-alpha.

Rauschhuber et al. reported the efficacy of HD Ad expressing shRNAs against HBV infection in mice [23]. However, modest silencing of HBV replication was observed and is likely to be a result of modest silencing efficacy of the antiviral shRNA expression cassettes. Using a HBV transgenic mouse model of chronic HBV infection, we recently reported high efficacy of transduction and superior silencing of HBV replication by HD Ads expressing previously designed artificial antiviral pri-miR and pre-miR mimics [11, 13]. Constitutively active U6 Pol III and cytomegalovirus (CMV) Pol II promoters were used effectively to inhibit HBV replication with pre-miR and pri-miR mimics, respectively [24, 25]. In the case of the artificial HBV-targeting pri-miRs, natural miR-122 and miR-31 sequences were used as templates to design the exogenous RNAi activators. Highly efficient inhibition of HBV replication was observed. To improve this approach we have incorporated a liver-specific modified mouse transthyretin (MTTR) promoter [26] into the pri-miR expression cassettes. Use of HD Ads to deliver these antiviral sequences to hepatocytes *in vivo* resulted in effective gene silencing without evidence of off target effects.

Moreover, *in vivo* generation of processed mature miR sequences from MTTR-containing cassettes was more efficient when compared to that achieved with the CMV promoter. Although liver-specific promoters have previously been employed to express anti-HBV RNAi activators with varying success [12, 27], use of the well characterised and highly efficient liver-specific MTTR promoter sequence has not been investigated. Demonstration here that this transcriptional regulatory element may be used to work efficiently against HBV *in vivo* indicates that the MTTR promoter has utility for therapeutic hepatic transgene expression.

2. Materials and Methods

2.1. Construction of Adenoviral Genome Bearing Plasmids. Generation of adenoviral plasmids expressing anti-HBV pri-miRs from CMV promoter has previously been described [25]. To generate adenoviral plasmids expressing anti-HBV pri-miRs from the MTTR promoter, a CMV promoter sequence in a previously described pCI-neo plasmid containing anti-HBV single or trimeric pri-miR sequences (pri-miR-122/5, pri-miR-31/5 and pri-miR-31/5-8-9) [11] was substituted with MTTR promoter sequence [26] using *Bgl* II and *Sac* I restriction sites. This generated pMTTR pri-miR-122/5, pMTTR pri-miR-31/5, and pMTTR pri-miR-31/5-8-9 plasmids. The MTTR promoter-pri-miR cassettes were then amplified using PCR with a previously described primer set (5' GAT CGG CGC GCC CTA TGG AAA AAC GCC AGC AA 3' and 5' GAT CGG CGC GCC GAA AGG AAG GGA AGA AAG CGA 3') that incorporated flanking *Asc* I restriction sites (underlined) in the amplicons [25]. Amplified fragments were then inserted into pTZ57R/T (InsTAclone PCR cloning Kit, Fermentas, MD, USA) to generate pTZMTTR-pri-miR-122/5, pTZMTTR-pri-miR-31/5, and pTZMTTR-pri-miR-31/5-8-9. Following sequencing, the inserts were removed using *Asc* I and subcloned at the *Asc* I restriction site of pΔ28E4LacZ adenoviral backbone [28] to generate pΔ28E4LacZ MTTR pri-miR-122/5, pΔ28E4LacZ MTTR pri-miR-31/5, and pΔ28E4LacZ MTTR pri-miR-31/5-8-9.

2.2. Luciferase Assay to Determine Liver-Specific Expression of MTTR Promoter. *In vitro* hepatotropic expression of luciferase from MTTR promoter was determined using the Dual-Luciferase Reporter Assay System according to manufacturer's instructions (Promega, WI, USA). Huh7 or HEK293 cells were cotransfected with 100 ng of pMTTR-FLuc or pCMV-FLuc [29] and 100 ng of pRL-CMV (Promega, WI, USA) plasmids. Forty-eight hours after transfection, cells were harvested and lysed. The cell lysates were used for luciferase activity measurement. Firefly luciferase expression was normalised to *Renilla* luciferase expression.

2.3. Production of Anti-HBV HD Ads. Production, amplification, and purification of anti-HBV HD Ads were carried out according to published methods [28]. Briefly, HEK293-derived 116 HD Ad packaging cell line was propagated in Eagle's or Joklik's minimum essential medium (MEM).

Following transfection of 116 cells with HD Ad genome-containing plasmid DNA that had been linearized by *Pme* I restriction digestion, cells were infected with helper virus (AdNG163). After 48 hours of incubation, the cells were harvested and frozen at -80°C . Transfected cell suspensions were subjected to three cycles of freeze-thawing and the lysates then used to coinfect 116 cells with helper virus, and incubated for 48 hours. This was repeated several times until viral titers were maximal. For large scale preparation of anti-HBV HD Ads, 2 liter cultures of 116 cells were coinfecting with helper virus and anti-HBV HD Ad lysates. Two days following coinfection, cells were harvested by centrifugation, the cells were then lysed and anti-HBV HD Ads were purified using CsCl gradient centrifugation. Total viral particles and helper virus contamination were determined using quantitative PCR (Q-PCR).

To determine viral infectious units, HEK293 cells infected with serial dilutions of HD Ads were stained for β -galactosidase activity as previously described [30]. Preparations of viral particles were aliquoted and stored in 10% glycerol at -80°C . The complete panel of HD Ads used in this study therefore comprised the previously described HD Ad Δ 28, HD Ad HBV CMV pri-miR-31/5, HD Ad HBV CMV pri-miR-122/5, HD Ad HBV CMV pri-miR-31/5-8-9, and newly propagated HD Ad HBV MTTR pri-miR-31/5, HD Ad HBV MTTR pri-miR-122/5, and HD Ad HBV MTTR pri-miR-31/5-8-9, which express antiviral sequences from the MTTR promoter.

2.4. Assessment of Efficacy in Cultured Cell of Anti-HBV HD Ads. To assess anti-HBV effects *in vitro*, the liver-derived Huh7 cell line was used and maintained as previously described [30]. Huh7 cells were cotransfected with a target plasmid vector containing a greater than genome length HBV sequence (pCH-9/3091) [31] and a plasmid expressing enhanced green fluorescent protein (eGFP) [32] as a transfection control. Lipofectamine 2000 was used for all transfections according to manufacturer's instructions (Life Technologies, CA, USA). Five hours after transfection, cells were washed with fresh medium and infected with HD Ads at multiplicities of infection (MOIs) ranging from 100 to 1000 infectious viral particles per cell. At 48 hours after HD Ad infection, secretion of HBV surface antigen (HBsAg) into the culture supernatants was measured as a marker of HBV replication using MONOLISA HBs Ag Assay kit (Bio-Rad, CA, USA).

2.5. Northern Blot Hybridization. To determine pri-miR expression and processing in cell culture, Huh7 cells were infected with HD Ads at a MOI of 100 infectious viral particles per cell. Two days after infection, cells were harvested and total RNA was extracted using Tri Reagent (Sigma, MI, USA). To determine pri-miR expression and processing *in vivo*, HBV transgenic mice [33] were used according to the protocols approved by the University of the Witwatersrand Animal Ethics Screening Committee. Mice were injected with a dose of 5×10^9 HD Ad infectious viral particles via the tail vein. Animals were then killed at 1 week after injection

and livers were harvested. Livers were homogenized and total RNA was isolated using Tri Reagent (Sigma, MI, USA). Thirty or sixty micrograms of RNA from cultured cells or liver tissue were analyzed using Northern blot hybridization according to previously described methods [11, 13]. Labelled probes with sequences of 5' CCG TGT GCA CTT CGC TTC 3', 5' CAA TGT CAA CGA CCG ACC 3', and 5' TAG GAG GCT GTA GGC ATA 3' were used to detect mature guides 5, 8, and 9, respectively. Blots were then stripped and probed for U6 snRNA using a labelled oligonucleotide with sequence 5' TAG TAT ATG TGC TGC CGA AGC GAG CA 3'. Band intensities were quantified by measuring photostimulated luminescence (PSL) using a FUJI FILM phosphorimager with Multi Gauge software.

2.6. Administration of Anti-HBV HD Ads to HBV Transgenic Mice. HBV transgenic mice [33] were used as a model of HBV replication, and protocols employed had been approved by the University of the Witwatersrand Animal Ethics Screening Committee. Six mice per group were infected by injecting a single dose of 5×10^9 infectious viral particles via the tail vein. Transduction of HD Ads and *lacZ* gene expression was assessed by X-gal staining of frozen liver sections. Frozen sections were prepared according to standard protocol. Blood samples were collected over a period of 13 weeks by retroorbital puncture. Serum HBsAg was measured by ELISA using the MONOLISA HBs Ag ULTRA kit (Bio-Rad, CA, USA). Circulating viral particle equivalents (VPEs) were determined by real-time Q-PCR according to previously described methods [13, 34].

To determine hepatotoxicity of the anti-HBV HD Ads, six mice per group were injected with 5×10^9 infectious viral particles via the tail vein. Blood samples were taken after infection and alanine transaminase (ALT) activity was determined in the serum.

2.7. Statistical Analysis. Data are expressed as the mean \pm standard error of the mean (SEM). Statistical difference was determined using Student's 2-tailed *t*-test and was considered significant when $P \leq 0.05$. Calculations were done with the GraphPad Prism software (GraphPad Software Inc., CA, USA).

3. Results

3.1. Structure of HD Ads Containing CMV and MTTR Pol II Artificial Anti-HBV Pri-miR Expression Cassettes. Previously described mono- and trimeric anti-HBV pri-miR sequences were inserted downstream of the constitutively active CMV or liver-specific MTTR Pol II promoter sequences (Figure 1(a)) [11]. Artificial monomeric pri-miR sequences, pri-miR-122/5, pri-miR-31/5, used the pri-miR-122 or pri-miR-31 sequences as a scaffold for incorporating a HBV-targeting guide sequence. The pri-miR-31/5-8-9 sequence was incorporated into trimeric cassettes and

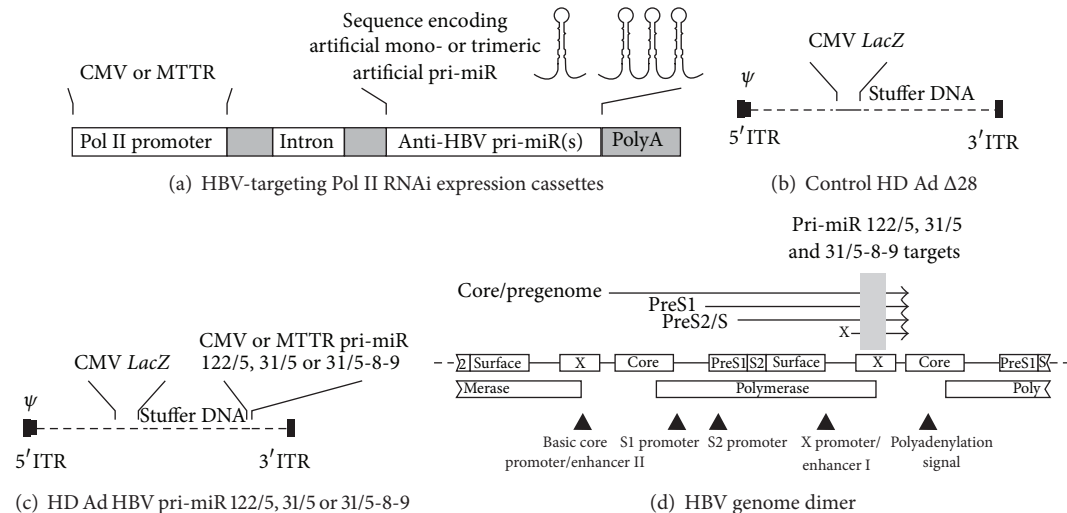


FIGURE 1: Schematic illustration of artificial pri-miR expression cassettes, recombinant HD Ads and HBV target sites. (a) Mono- or trimeric anti-HBV pri-miR sequences are transcribed under control of either a CMV or MTTR promoter. The cassettes also include an intron and polyA transcription termination signal. (b) The control HD Ad $\Delta 28$ vector contains no HBV-targeting cassettes but does include the CMV *LacZ* reporter cassette. Apart from ITRs and viral packaging signal (Ψ) the remainder of the vector DNA comprises stuffer sequence with all Ad open reading frames (ORFs) removed. (c) Anti-HBV HD Ads contain the mono- or trimeric artificial pri-miR expression cassettes under control of the CMV or MTTR Pol II promoters. (d) Tandem arrangement of a dimer of the hepatitis B virus genome, comprising 6.4 kb, showing sites targeted by antiviral artificial pri-miRs. The overlapping *surface*, *core*, *polymerase*, and *HBx* viral ORFs are indicated by labelled rectangles. The four arrows above the genome represent the HBV transcripts that are initiated from different viral promoter elements and a common 3' end. Essential cis elements controlling transcription are indicated by arrowheads. The sites targeted by the artificial pri-miRs, indicated by the shaded rectangle, are located within the *HBx* ORF and are found in all of the viral transcript.

comprised a tandem arrangement of three different HBV-targeting pri-miR-31 derivatives. These cassettes had previously been shown to produce transcripts that were efficiently processed and capable of silencing HBV replication in cultured liver cells and *in vivo*. Expression cassettes were incorporated into HD Ads to generate a panel of six vectors that each expressed pri-miR-122/5, pri-miR-31/5, or pri-miR-31/5-8-9 from either the CMV or MTTR Pol II promoters (Figure 1(b)). A control vector, HD Ad $\Delta 28$, did not contain any anti HBV sequence. All HD Ads also included a reporter cassette encoding Beta-galactosidase to enable convenient tracking of cells infected by the viral vectors. The targets of the guides generated from the artificial expressed RNAi activators are located in the *HBx* open reading frame (ORF) of HBV (Figure 1(c)) [30]. This viral sequence is conserved in HBV genotypes and is also present in all of the viral transcripts. The replication-competent integrant that had been inserted into the transgenic mice used as a model of viral replication in this study comprised a dimer of HBV sequences (Figure 1(c)) [33].

3.2. Inhibition of HBV Replication by HD Ads Carrying CMV Promoter Driven Anti-HBV Sequences in Mice. We previously reported a significant decrease in serum HBsAg levels and VPEs at one and two weeks after treatment of HBV transgenic mice with HD Ads expressing anti-HBV pri-miR mimics from a CMV promoter [25]. To assess long-term anti-HBV effect in mice, six mice per group were injected with HD Ads carrying CMV promoter-anti-HBV pri-miR cassettes

and monitored over a 13-week period. In agreement with the previous report, significant decrease in HBsAg levels was observed at one week following the injection of mice with either HD Ad HBV pri-miR-122/5, HD Ad HBV pri-miR-31/5, or HD Ad HBV pri-miR-31/5-8-9 (Figure 2(a)). In mice treated with HD Ad HBV pri-miR-122/5 or HD Ad HBV pri-miR-31/5, the serum concentrations of HBsAg increased at time points after one week and were no longer significantly different from the baseline values. However, HD Ad HBV pri-miR-31/5-8-9 administration resulted in the most efficient silencing of HBsAg expression. Inhibition of up to 94% was achieved at 1 week and prolonged anti-HBV effects were observed for five weeks following administration of HD Ad HBV pri-miR-31/5-8-9. Similar, although less statistically significant, results were observed when VPEs were measured as a marker of HBV replication (Figure 2(b)).

3.3. Expression of Anti-HBV Sequences from MTTR Promoter and HBV Replication Inhibition in Cell Culture. Despite the high efficacy and prolonged knockdown of HBV replication by HD Ad HBV pri-miR-31/5-8-9, previous studies have shown that hepatic transgene expression from the CMV promoter is not durable [35, 36]. To address this limitation, HD Ad vectors expressing anti-HBV pri-miRs from a liver-specific MTTR promoter were generated. Initially, liver-specific expression of the MTTR promoter was assessed using a reporter gene assay following transfection of liver-derived (Huh7) and kidney-derived (HEK293) cells (Figure 3(a)). Measurement of Firefly luciferase activity showed reporter

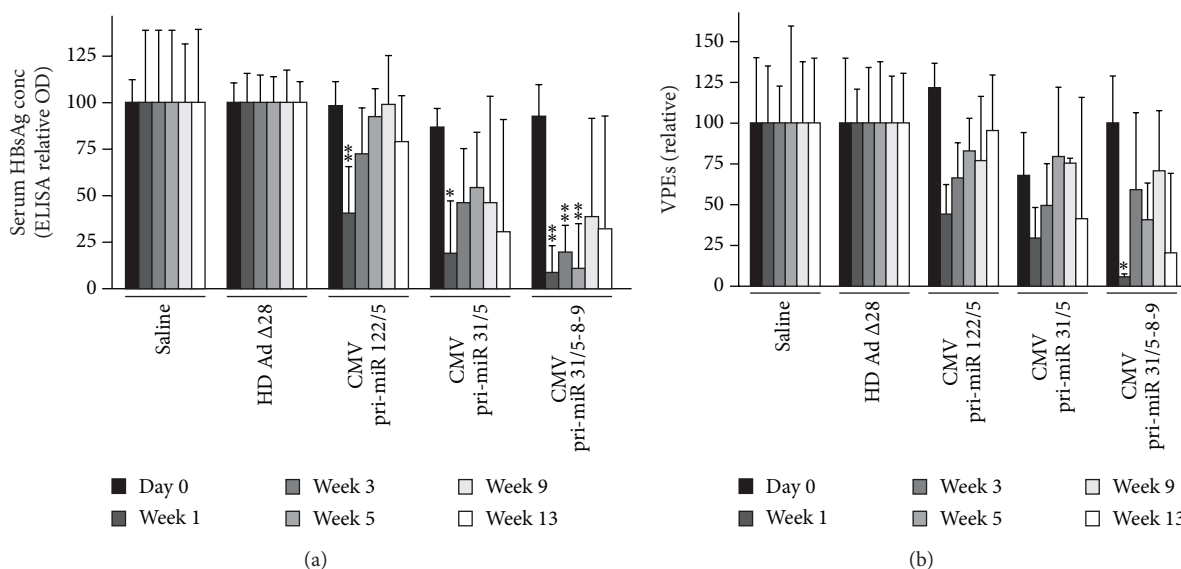


FIGURE 2: Silencing of HBV replication in mice by HD Ads expressing anti-HBV pri-miR mimics from a CMV promoter. Mice were infected with a single dose of 5×10^9 infectious HD Ad particles expressing pri-miR-122/5, pri-miR-31/5, and pri-miR-31/5-8-9. Animals injected with saline or HD Ad Δ28 served as negative controls. (a) Time course of serum HBsAg concentrations, as measured by ELISA, following HD Ad administration. (b) Circulating viral particle equivalents (VPEs) were measured using qPCR following injection of HBV transgenic mice with HD Ads. Data are expressed as means with SEMs from each group of six mice. The statistical significance was calculated using a pair-wise comparison according to the Student *t*-test. *P* values less than 0.05 (*) or less than 0.01 (**) were considered statistically significant.

gene activity in both cell lines receiving the plasmid containing the constitutively active CMV promoter. However, when cells were transfected with cassettes containing the MTTR transcriptional regulatory element, Firefly luciferase activity was barely detectable in the kidney derived cell line, and activity was significantly higher in the liver-derived cell line. To assess processing of the artificial pri-miRs, RNA isolated from Huh7 cells infected with the MTTR-containing HD Ads at a MOI of 100 infectious viral particles per cell were analyzed by low molecular weight northern blot hybridization (Figure 3(b)). Hybridization using a probe complementary to guide 5 confirmed efficient generation of anti-HBV pri-miRs from each of the MTTR promoter-containing monomeric and trimeric HD Ads. This was evident from the detection of a band of approximately 21 nucleotides in length, which was absent from control cells infected with the empty HD Ad Δ28 vector. Higher molecular weight bands representing unprocessed or partially processed intermediates were present in low amounts. As expected, hybridization to a probe complementary to the guide 8 sequence resulted in detection of a putative guide in RNA samples isolated from cells infected with HD Ad HBV pri-miR-31/5-8-9 but not in HD Ad HBV pri-miR-122/5 or HD Ad HBV pri-miR-31/5. Similarly, the probe detecting guide 9 sequences only detected a band in RNA isolated from cells treated with the trimeric HD Ad vector. The lower concentration of the guide 9 sequence is in accordance with our previous observation that this sequence is the least efficiently processed guide derived from the artificial tricistronic cassette [11]. A band of approximately 21 nucleotides was not detected in RNA samples isolated from cells infected with empty vector (HD Ad Δ28) or uninfected cells (Figure 3(b)).

To assess HBV silencing efficacy of MTTR promoter-containing HD Ads in cell culture, HBsAg concentrations in culture supernatants were measured as a marker for HBV replication. Huh7 cells were initially transfected with the pCH-9/3091 HBV replication competent target plasmid [31]. Five hours after transfection, cells were infected with HD Ads at MOIs ranging from 100 to 1000 infectious viral particles per cell. HBsAg levels were measured 48 hours after infection. All three anti-HBV HD Ads (HD Ad HBV pri-miR-31/5-8-9 M, HD Ad HBV pri-miR-31/5 M, and HD Ad HBV pri-miR-122/5 M) resulted in a significant dose dependent decrease in HBsAg levels. As expected most efficient inhibition of this HBV replication marker was observed at MOIs of 500 and 1000 infectious viral particles per cell, with knockdown of up to 91% (Figure 3(c)).

3.4. Comparison of Expression and Processing In Vivo of CMV- and MTTR-Derived Anti-HBV Sequences. To assess expression *in vivo* of anti-HBV pri-miRs derived from CMV and MTTR promoters, groups of mice were treated intravenously with 5×10^9 HD Ad particles from each of the panel of HD Ad vectors. Seven days after vector administration, RNA was isolated from the livers and 30 μg (Figure 4(a)) or 60 μg (Figure 4(b)) was analyzed by northern blot hybridization. Detection of putative guide sequences correlated with analysis of RNA isolated from cultured liver-derived cells (Figure 3). Probing for guide 5 showed efficient expression and processing of anti-HBV pri-miRs in livers of animals that had been treated with mono- and trimeric HD Ads containing CMV or MTTR promoters. The guide 8 band was only detectable in RNA extracted from mice that received

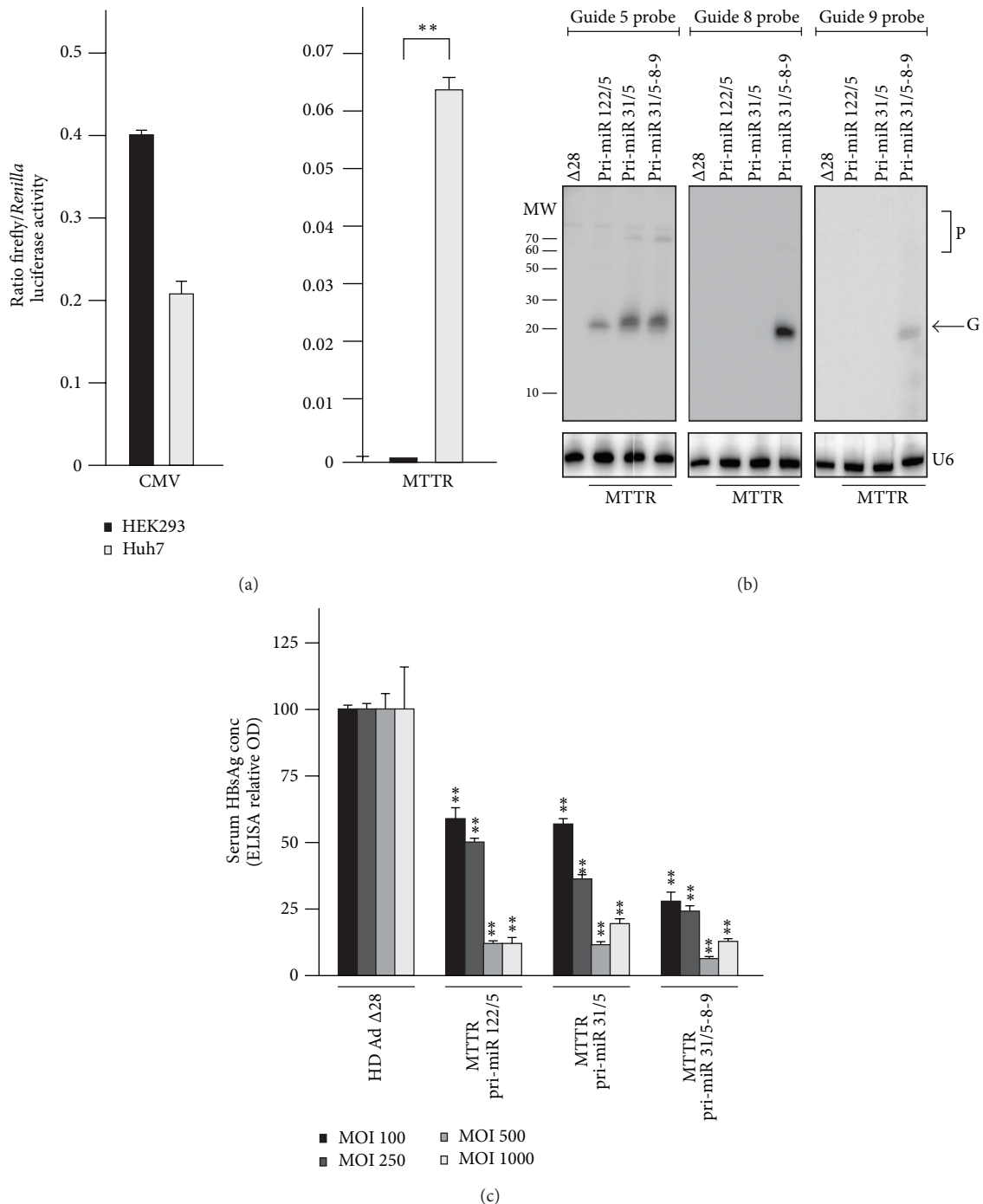


FIGURE 3: Liver specificity of MTTR promoter, RNA processed from anti-HBV pri-miR cassettes, and effect on HBsAg concentration in supernatants of cultured Huh7 cells. (a) Liver-derived Huh7 or kidney-derived HEK293 cells were transfected with 100 ng of pMTTR-FLuc or pCMV-FLuc, which contained the *Firefly luciferase* reporter gene under control of MTTR or CMV promoters, respectively. In addition the phRL-CMV (Promega) plasmid, constitutively expressing *Renilla luciferase*, was cotransfected to normalize the Firefly luciferase measurements. Forty-eight hours after transfection cells were harvested and activity of the two reporter genes was determined independently. Mean Firefly to *Renilla* luciferase activity is presented and error bars indicate the standard error of the mean ($n = 4$). (b) Northern blot analyses of 30 μ g RNA isolated from Huh 7 cells infected with HD Ads at a multiplicity of infection (MOI) of 100 infectious viral particles per cell. The probes used were complementary to the predicted 5, 8, or 9 guide sequences derived from the panel of vectors expressing antiviral pri-miRs from the MTTR promoter. Equal loading of the lanes was verified by stripping and reprobing the blot with a labelled oligonucleotide complementary to U6 small nuclear RNA. Putative guide (G) and precursor (P) bands are indicated. (c) Inhibition of HBV replication *in vitro* was determined by measuring HBsAg levels using ELISA. Cell culture supernatants were obtained from Huh7 cells that had been transfected with the pCH-9/3091 replication-competent plasmid and then infected with the indicated HD Ads at MOIs of 100, 250, 500, or 1000. Data is expressed as SEM from three replicates. The statistical significance was calculated using a pair-wise comparison according to the Student *t*-test. *P* values less than 0.05 (*) or less than 0.01 (**) were considered statistically significant.

the HD Ads that contained the pri-miR-31/5-8-9 sequence. However the guide 9 sequence was not detectable in murine liver RNA samples and confirms inefficient processing of this component of the anti-HBV trimer. Production of guide strands from CMV- and MTTR-driven pri-miR cassettes was compared by determining guide strand band intensities following probe hybridization to 30 μ g (Figure 4(a)) or 60 μ g (Figure 4(b)) of RNA. Northern blot analysis of 30 μ g of RNA isolated from cells infected with HD Ad carrying cassettes containing the CMV promoter revealed a very faint band corresponding to the expected guides. Increasing the amount of RNA loaded onto the northern blots to 60 μ g improved detection of processed transcripts. Importantly, guide strands from RNA isolated from mice that had been treated with MTTR-containing plasmids were more easily measurable. Ratios of the guide strand to U6 snRNA loading control band intensities were used as an indicator of intrahepatocyte guide RNA concentrations (Figure 4(c)). This analysis revealed pri-miR expression and processing from the MTTR promoter was more efficient than that achieved with the CMV promoter.

To correlate detection of processed miR sequences with efficiency of hepatocyte transduction, we took advantage of HD Ad-mediated codelivery of the β -galactosidase expression cassette with the pri-miR expression cassettes. Liver sections stained for reporter gene activity confirmed previous observations that approximately 90% of murine hepatocytes had been transduced at two days after intravenous administration of the vector [24, 25]. However, a significant and rapid decline in the number of cells positive for β -galactosidase activity occurred thereafter (Figure 6(b)). By 6 weeks, reporter gene activity was barely detectable. Our previous reports indicate that the decline in cells positive for reporter gene activity is likely to be a result of an immune response to the cells expressing the reporter transgene [24].

3.5. Silencing of HBV Replication In Vivo by HD Ads Expressing Pri-miR Mimics from the MTTR Promoter. To assess the silencing *in vivo* of HBV replication by HD Ads carrying the MTTR promoter-derived cassettes, both HBsAg levels and VPEs were determined in mice transduced with HD Ads. Six mice per group were injected with 5×10^9 HD Ad infectious particles and blood samples collected over a period of 13 weeks. Control groups of animals were treated with saline or the HD Ad Δ 28 empty vector. As with mice treated with the HD Ads expressing anti-HBV sequences from CMV promoter, a significant reduction in HBsAg levels was observed one week after vector administration (Figure 5(a)). HBsAg levels then increased significantly at 3 weeks after infection with HD Ads expressing the monomeric artificial pri-miRs from the MTTR promoter. However, HBsAg levels in mice treated with the cassette expressing the pri-miR trimer from the MTTR promoter remained significantly low at 3 and 5 weeks after infection (Figure 5(a)). Analysis of VPEs showed a similar trend in viral replication (Figure 5(b)).

3.6. HD Ad Vector Clearance and Toxicity in Mice. To determine whether vector clearance correlated with diminished

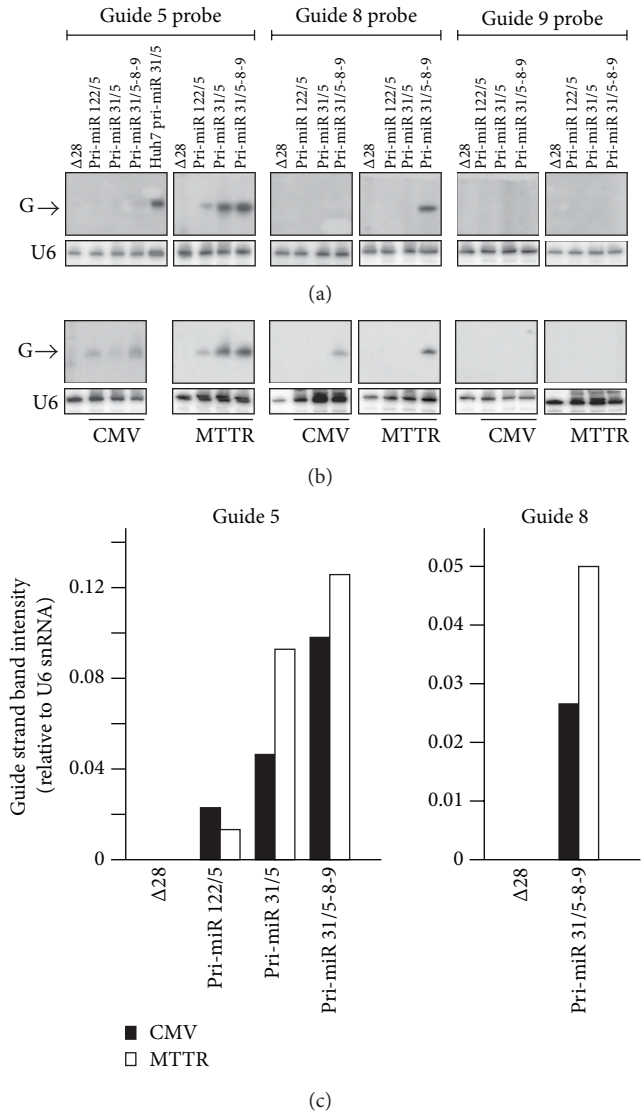


FIGURE 4: Anti-HBV pri-miR expression in livers of HBV transgenic mice following treatment with HD Ads expressing artificial mono- or trimeric pri-miRs under control of the CMV or MTTR promoters. Northern blot analyses of 30 μ g (a) and 60 μ g (b) of RNA isolated from mouse livers 1 week after infection with HD Ads. Blots hybridized with probes complementary to predicted guides 5, 8, or 9 were stripped and reprobed for U6 snRNA to confirm equal loading. (c) Quantification of indicated anti-HBV guide sequences generated from CMV and MTTR promoters was determined using a phosphorimager. Data were normalized to U6 snRNA expression and a representative example is shown.

efficacy against HBV replication, HD Ad genome copies were quantified in mouse livers. DNA isolated from liver samples collected at 48 hours, 1 week, and 3 and 6 weeks after HD Ad Δ 28 infection were used to determine HD Ad vector genome copies in the liver. HD Ad Δ 28 vector copies remained constant at approximately 2×10^5 copies per μ g of hepatocyte DNA for the first three weeks after administration of HD Ads. Thereafter, the vector copies detectable in the livers diminished significantly at week 6 (Figure 6(a)), and

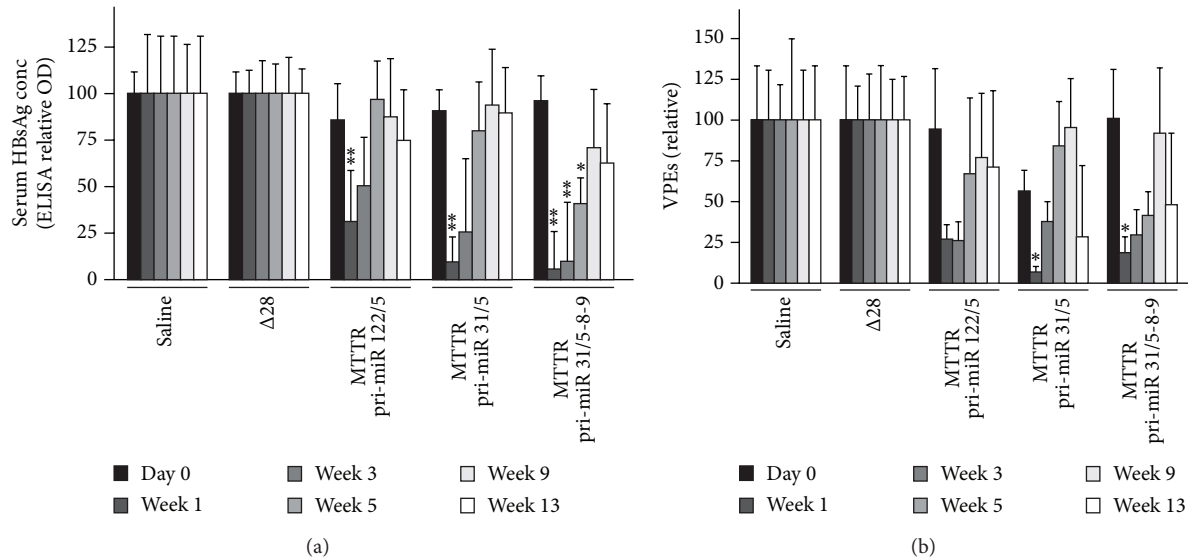


FIGURE 5: Silencing of HBV replication *in vivo* and reporter gene expression following administration of HD Ads expressing anti-HBV pri-miR mimics from the MTTR promoter. Mice were infected with a single dose of 5×10^9 infectious HD Ad particles expressing pri-miR-122/5, pri-miR-31/5 and pri-miR-31/5-8-9. Animals injected with saline or HD Ad $\Delta 28$ served as negative controls. (a) Time course of serum HBsAg concentrations, as measured by ELISA, following HD Ad administration. (b) Circulating viral particles (VPEs) were measured using Q-PCR following injection of HBV transgenic mice with HD Ads. Data are expressed as means with SEMs from each group of six mice. The statistical significance was calculated using a pair-wise comparison according to the Student *t*-test. *P* values less than 0.05 (*) or less than 0.01 (**) were considered statistically significant.

this result correlated with disappearance of histochemically detectable Beta-galactosidase activity (Figure 6(b)). Q-PCR data from anti-HBV HD Ads showed similar trends of vector clearance (not shown) and indicated that the promoter sequences had little effect on viral vector clearance. Previously it has been reported that expression of anti-HBV shRNAs from a U6 Pol III promoter within adeno-associated vectors resulted in hepatotoxicity [9]. To assess toxicity of HD Ads in mice, ALT activity was measured 48 hours after injection of HD Ads. After 48 hours, ALT levels in control mice and animals injected with anti-HBV HD Ads were 51–69 U/L (Figure 6(c)). There were no statistically significant differences between the groups, which indicated that at an early time point, the anti-HBV HD Ads used in this study were not toxic to mice.

4. Discussion

Harnessing RNAi for the silencing of viral genes has demonstrated promising therapeutic potential. Several studies have shown that replication of viral pathogens can be inhibited with engineered mimics of the RNAi pathway. Chronic HBV infection is an important global public health problem and the inadequacies of currently available therapy have prompted investigation of the utility of RNAi-based treatment of the infection. Many studies have shown that HBV replication is susceptible to silencing by both synthetic and expressed RNAi activators. An advantage of using expressed RNAi activators to silence HBV gene expression is that it is possible to achieve more sustained silencing than with synthetic RNAi activators. This is critically important to effect

lasting silencing that is required to counter chronic HBV infection. Although there is enthusiasm for developing use of expressed RNAi activators as a therapeutic option for treating HBV persistence, important hurdles remain to be overcome before the approach becomes feasible. Particularly important are the controlled expression in target tissues, coupled to safe and efficient delivery of the expression cassettes to the liver.

Pol III promoters have been commonly used to express anti-HBV RNAi activator sequences [30, 37]. However, powerful constitutive activity of the U6 Pol III promoter may result in saturation of the RNAi pathway with resultant hepatotoxicity [9]. To address this concern, studies have aimed to use more versatile Pol II promoters to control production of antiviral sequences. Efficacy of shRNA mimics expressed from Pol II promoters is however variable and it appears that the flanking sequences naturally found in pri-miR sequences are important to facilitate expression and processing from Pol II promoters. As a result sequences that simulate the natural production of artificial pri-miR RNAi mimics have been engineered for incorporation into Pol II expression cassettes. In addition to compatibility with Pol II promoters, pri-miR sequences may be multimerized to enable simultaneous silencing at multiple viral targets. In this study we have demonstrated that the efficient liver-specific MTTR promoter may be used to express mono- and trimeric anti-HBV RNAi activators. Although the HBV genome is compact and not plastic, simultaneous targeting of three viral targets by the MTTR-controlled multimeric cassettes should prevent the emergence of viral escape mutants. Our observations demonstrated that the MTTR promoter functioned

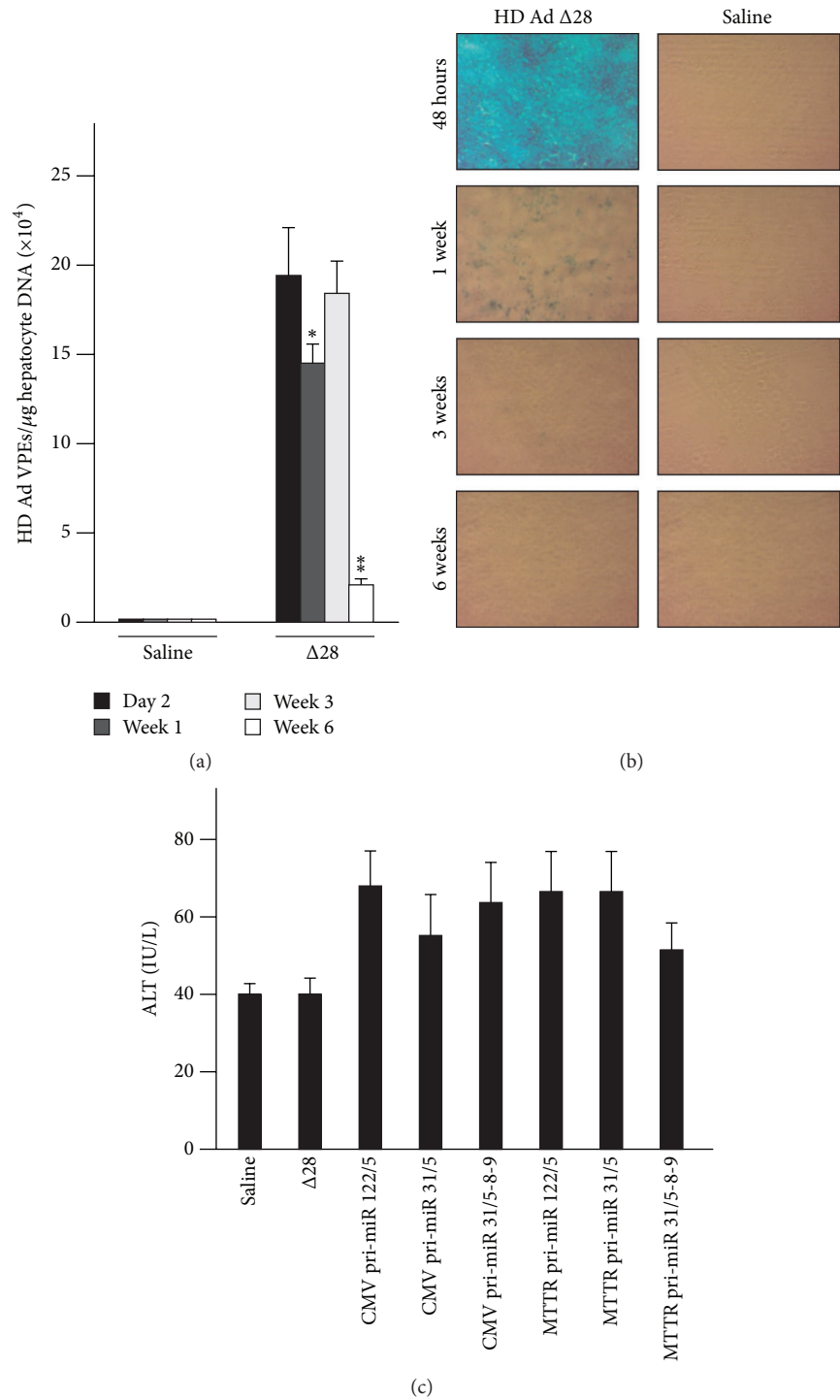


FIGURE 6: Intrahepatic HD Ad copy numbers and alanine transaminase activity following HD Ad administration to HBV transgenic mice. (a) Mice were injected intravenously with saline or a single dose of 5×10^9 infectious viral particles. DNA isolated from mice livers harvested at 48 hours, 1 week, and 3 and 6 weeks after injection was subjected to Q-PCR analysis to determine viral particle equivalents (VPEs). Data are expressed as means (\pm SEM) from three mice. Statistically significant differences were determined by comparisons to values obtained at 2 days. Analyses were carried out using a pair-wise Student's *t*-test. *P* values less than 0.05 (*) or less than 0.01 (**) were considered statistically significant. (b) Histochemical detection of Beta-galactosidase activity in livers of mice treated with saline or HD Ad $\Delta 28$. Frozen liver sections were stained for reporter gene activity at 48 hours, 1 week, 3 weeks, and 6 weeks after saline or HD Ad $\Delta 28$ administration. (c) Serum ALT activity in HD Ad infected mice. Serum activity of ALT was measured 48 hours following injection with saline or 5×10^9 infectious particles of the indicated HD As. Data is expressed as means (\pm SEM) from groups of six mice. The statistically significant differences were calculated as indicated above.

efficiently *in vivo* and was capable of significant silencing of HBV replication in a HBV transgenic mouse model.

We recently reported on efficacy *in vivo* of HD Ads that deliver anti-HBV pri-miR expression cassettes that are under control of the CMV promoter. Although effective against HBV *in vivo* [25], a concern of using the CMV promoter is that it is not specific to liver tissue and the transcription from this regulatory element is not sustained in hepatic tissue [35, 36]. The results reported here confirm that this is potentially problematic. Although concentrations of HD Ad DNA were maintained in murine liver tissue for at least 6 weeks, expression of the *lacZ* reporter gene, which was under control of the CMV transcriptional regulatory element, rapidly diminished 7 days after vector administration. A study by Löser and colleagues supports our observations [35]. In their investigation, expression of human low density lipoprotein (LDL) receptor from a CMV promoter was reduced after a week. However the protein was undetectable 4 weeks after vector administration despite the vector genome copy number remaining high at this time point. NF κ B deficiency and methylation of CpG sites within the CMV promoter sequence may be responsible for the attenuation of expression from this transcriptional regulatory element [35, 38].

Ads are highly efficient hepatotropic vectors that are well suited to delivery of RNAi expression cassettes that target HBV. However, the immunostimulatory effects of Ads [39–45] are concerning as they may cause toxicity, reduce efficiency of gene delivery, and limit transgene expression. Removal of ORFs to form HD Ads diminishes longer term humoral and cell mediated adaptive immunity to the vectors and has been useful to prolong transgene expression through [46]. Other modifications to HD Ads, such as conjugation of polymers, may also be used to diminish immunostimulatory effects. An additional important property of HD Ads is their capacity for accommodating large transgene sequences. Therefore as well as RNAi activating cassettes, other antiviral components may be incorporated into HD Ads to generate multifunctional vectors for HBV therapy. Recent advances in the use of transcription activator like effector nucleases (TALENs) and zinc finger nucleases have been impressive [47]. These engineered gene-modifying enzymes may be particularly useful in combination with HBV-targeting RNAi activators to disable the stable HBV cccDNA minichromosome. Our data show that HD Ads have utility for hepatotropic delivery of a liver-specific expression cassette. Generating HD Ads that also include other antiviral sequences, a focus of our current research, should further add to their therapeutic utility.

5. Conclusions

The observation that the MTTR Pol II promoter achieves good expression of anti-HBV sequences is a useful property for the development of gene therapy requiring liver-specific expression of antiviral RNAi mimics. Transcription of HBV-targeting artificial mono- and trimeric pri-miRs under control of the MTTR element silenced HBV replication *in vivo*

and generation of antiviral guides was more efficient than that achieved with the constitutively active CMV promoter. Moreover, expression of the antiviral sequences did not result in the hepatotoxicity that has been reported when U6 shRNA cassettes were delivered with adeno-associated viral vectors. The good delivery efficiency of recombinant HD Ads also reinforces the potential utility of these vectors. However diminishing immunostimulatory effects of the HD Ads, which may be achieved through removal of the codelivered *lacZ* and their modification with polymers, will need to be achieved before these vectors achieve clinical utility. HD Ads have the important property of being capable of carrying large transgene sequences. This will make it possible to augment their therapeutic efficacy by incorporating additional anti-HBV elements, such as those encoding engineered HBV DNA binding proteins. Advancing this approach, as well as attenuation of immunostimulatory effects of HD Ads are an active field of investigation in our laboratory.

Conflict of Interests

The authors declare that there is no conflict of interests regarding the publication of this paper.

Acknowledgments

Financial support from the South African National Research Foundation, Carnegie Research Fund, Poliomyelitis Research Foundation, and Medical Research Council is gratefully acknowledged. Technical assistance with preparing liver frozen sections and measuring ALT activity from the South African National Health Laboratory Services is gratefully acknowledged.

References

- [1] M. Esteve, C. Saro, F. González-Huix, F. Suarez, M. Forné, and J. M. Viver, "Chronic hepatitis B reactivation following infliximab therapy in Crohn's disease patients: need for primary prophylaxis," *Gut*, vol. 53, no. 9, pp. 1363–1365, 2004.
- [2] J. Fang, W. Li, Z. Tan, and D. Li, "Comparison of prednisolone and lamivudine combined therapy with prednisolone monotherapy on carriers of hepatitis B virus with IgA nephropathy: a prospective cohort study," *International Urology and Nephrology*, vol. 46, no. 1, pp. 49–56, 2014.
- [3] P. Arbuthnot, S. Carmona, and A. Ely, "Exploiting the RNA interference pathway to counter hepatitis B virus replication," *Liver International*, vol. 25, no. 1, pp. 9–15, 2005.
- [4] D. Ivacic, A. Ely, and P. Arbuthnot, "Countering hepatitis B virus infection using RNAi: how far are we from the clinic?" *Reviews in Medical Virology*, vol. 21, no. 6, pp. 383–396, 2011.
- [5] S. Azimzadeh Jamalkandi, E. Azadian, and A. Masoudi-Nejad, "Human RNAi pathway: crosstalk with organelles and cells," *Funct Integr Genomics*, vol. 14, no. 1, pp. 31–46, 2014.
- [6] B. L. Davidson and P. B. McCray Jr., "Current prospects for RNA interference-based therapies," *Nature Reviews Genetics*, vol. 12, no. 5, pp. 329–340, 2011.
- [7] D. Shin, H. Lee, S. I. Kim, Y. Yoon, and M. Kim, "Optimization of Linear double-stranded RNA for the production of multiple

- siRNAs targeting hepatitis C virus," *RNA*, vol. 15, no. 5, pp. 898–910, 2009.
- [8] C. P. Sun, T. Wu, C. Chen et al., "Studies of efficacy and liver toxicity related to adeno-associated virus-mediated RNA interference," *Human Gene Therapy*, vol. 24, no. 8, pp. 739–750, 2013.
 - [9] D. Grimm, K. L. Streetz, C. L. Jopling et al., "Fatality in mice due to oversaturation of cellular microRNA/short hairpin RNA pathways," *Nature*, vol. 441, no. 7092, pp. 537–541, 2006.
 - [10] D. Grimm, L. Wang, J. S. Lee et al., "Argonaute proteins are key determinants of RNAi efficacy, toxicity, and persistence in the adult mouse liver," *Journal of Clinical Investigation*, vol. 120, no. 9, pp. 3106–3119, 2010.
 - [11] A. Ely, T. Naidoo, and P. Arbuthnot, "Efficient silencing of gene expression with modular trimeric Pol II expression cassettes comprising microRNA shuttles," *Nucleic Acids Research*, vol. 37, no. 13, p. e91, 2009.
 - [12] J. C. Giering, D. Grimm, T. A. Storm, and M. A. Kay, "Expression of shRNA from a tissue-specific pol II promoter is an effective and safe RNAi therapeutic," *Molecular Therapy*, vol. 16, no. 9, pp. 1630–1636, 2008.
 - [13] A. Ely, T. Naidoo, S. Mufamadi, C. Crowther, and P. Arbuthnot, "Expressed anti-HBV primary microRNA shuttles inhibit viral replication efficiently in vitro and in vivo," *Molecular Therapy*, vol. 16, no. 6, pp. 1105–1112, 2008.
 - [14] J. L. McBride, R. L. Boudreau, S. Q. Harper et al., "Artificial miRNAs mitigate shRNA-mediated toxicity in the brain: implications for the therapeutic development of RNAi," *Proceedings of the National Academy of Sciences of the United States of America*, vol. 105, no. 15, pp. 5868–5873, 2008.
 - [15] C. Mueller, Q. Tang, A. Gruntman et al., "Sustained miRNA-mediated knockdown of mutant AAT with simultaneous augmentation of wild-type AAT has minimal effect on global liver miRNA profiles," *Molecular Therapy*, vol. 20, no. 3, pp. 590–600, 2012.
 - [16] S. N. Waddington, J. H. McVey, D. Bhella et al., "Adenovirus serotype 5 hexon mediates liver gene transfer," *Cell*, vol. 132, no. 3, pp. 397–409, 2008.
 - [17] N. Brunetti-Pierri and P. Ng, "Progress towards liver and lung-directed gene therapy with helper-dependent adenoviral vectors," *Current Gene Therapy*, vol. 9, no. 5, pp. 329–340, 2009.
 - [18] M. B. Mowa, C. Crowther, and P. Arbuthnot, "Therapeutic potential of adenoviral vectors for delivery of expressed RNAi activators," *Expert Opinion on Drug Delivery*, vol. 7, no. 12, pp. 1373–1385, 2010.
 - [19] L. Aurisicchio, A. De Tomassi, N. La Monica, G. Ciliberto, C. Traboni, and F. Palombo, "Regulated and liver-specific tamarin alpha interferon gene delivery by a helper-dependent adenoviral vector," *Journal of Virology*, vol. 79, no. 11, pp. 6772–6780, 2005.
 - [20] L. Aurisicchio, P. Delmastro, V. Salucci et al., "Liver-specific alpha 2 interferon gene expression results in protection from induced hepatitis," *Journal of Virology*, vol. 74, no. 10, pp. 4816–4823, 2000.
 - [21] J. Cretaz, I. Otano, L. Ochoa et al., "Treatment of chronic viral hepatitis in woodchucks by prolonged intrahepatic expression of interleukin-12," *Journal of Virology*, vol. 83, no. 6, pp. 2663–2674, 2009.
 - [22] M. Fiedler, F. Röddicker, V. Salucci et al., "Helper-dependent adenoviral vector-mediated delivery of woodchuck-specific genes for alpha interferon (IFN- α) and IFN- γ : IFN- α but not IFN- γ reduces woodchuck hepatitis virus replication in chronic infection in vivo," *Journal of Virology*, vol. 78, no. 18, pp. 10111–10121, 2004.
 - [23] C. Rauschhuber, H. Xu, F. H. Salazar, P. L. Marion, and A. Ehrhardt, "Exploring gene-deleted adenoviral vectors for delivery of short hairpin RNAs and reduction of hepatitis B virus infection in mice," *Journal of Gene Medicine*, vol. 10, no. 8, pp. 878–889, 2008.
 - [24] C. Crowther, M. B. Mowa, A. Ely, and P. B. Arbuthnot, "Inhibition of hepatitis B virus replication in vivo using helper-dependent adenovirus vectors to deliver antiviral RNAi expression cassettes," *Antiviral Therapy*, 2013.
 - [25] M. B. Mowa, C. Crowther, A. Ely, and P. Arbuthnot, "Efficient silencing of hepatitis B virus by helper-dependent adenovirus vector-mediated delivery of artificial antiviral primary Micro RNAs," in *MicroRNA*, vol. 1, pp. 19–25, 2012.
 - [26] R. H. Costa and D. R. Grayson, "Site-directed mutagenesis of hepatocyte nuclear factor (HNF) binding sites in the mouse transthyretin (TTR) promoter reveal synergistic interactions with its enhancer region," *Nucleic Acids Research*, vol. 19, no. 15, pp. 4139–4145, 1991.
 - [27] A. Ely and P. Arbuthnot, "Silencing hepatitis B virus replication with antiviral pri-miR shuttles generated from liver-specific Pol II promoter," in *Gene Silencing: Theory, Techniques and Applications*, A. J. Catalano, Ed., Nova Publishers, New York, NY, USA, 2010.
 - [28] D. Palmer and P. Ng, "Improved system for helper-dependent adenoviral vector production," *Molecular Therapy*, vol. 8, no. 5, pp. 846–852, 2003.
 - [29] S. Chattopadhyay, A. Ely, K. Bloom, M. S. Weinberg, and P. Arbuthnot, "Inhibition of hepatitis B virus replication with linear DNA sequences expressing antiviral micro-RNA shuttles," *Biochemical and Biophysical Research Communications*, vol. 389, no. 3, pp. 484–489, 2009.
 - [30] S. Carmona, A. Ely, C. Crowther et al., "Effective inhibition of HBV replication in vivo by anti-HBx short hairpin RNAs," *Molecular Therapy*, vol. 13, no. 2, pp. 411–421, 2006.
 - [31] M. Nassal, "The arginine-rich domain of the hepatitis B virus core protein is required for pregenome encapsidation and productive viral positive-strand DNA synthesis but not for virus assembly," *Journal of Virology*, vol. 66, no. 7, pp. 4107–4116, 1992.
 - [32] M. Passman, M. Weinberg, M. Kew, and P. Arbuthnot, "In situ demonstration of inhibitory effects of hammerhead ribozymes that are targeted to the hepatitis Bx sequence in cultured cells," *Biochemical and Biophysical Research Communications*, vol. 268, no. 3, pp. 728–733, 2000.
 - [33] P. L. Marion, F. H. Salazar, K. Liittschwager, and B. B. Bordier, "A transgenic mouse lineage useful for testing antivirals targeting hepatitis B virus," in *Frontiers in Viral Hepatitis*, R. F. Schinazi, J. -P. Sommadossi, and C. M. Rice, Eds., pp. 197–202, Elsevier Science, Amsterdam, The Netherlands, 2003.
 - [34] S. Carmona, A. Ely, C. Crowther et al., "Effective inhibition of HBV replication in vivo by anti-HBx short hairpin RNAs," *Molecular Therapy*, vol. 13, no. 2, pp. 411–421, 2006.
 - [35] P. Loser, G. S. Jennings, M. Strauss, and V. Sandig, "Reactivation of the previously silenced cytomegalovirus major immediate-early promoter in the mouse liver: involvement of NF κ B," *Journal of Virology*, vol. 72, no. 1, pp. 180–190, 1998.
 - [36] S. Prost, S. Sheahan, D. Rannie, and D. J. Harrison, "Adenovirus-mediated Cre deletion of floxed sequences in primary mouse cells is an efficient alternative for studies of gene deletion," *Nucleic Acids Research*, vol. 29, no. 16, p. E80, 2001.

- [37] C. Crowther, A. Ely, J. Hornby et al., "Efficient inhibition of hepatitis B virus replication in vivo, using polyethylene glycol-modified adenovirus vectors," *Human Gene Therapy*, vol. 19, no. 11, pp. 1325–1331, 2008.
- [38] S. Prösen, J. Stein, K. Staak, C. Liebenthal, H. Volk, and D. H. Krüger, "Inactivation of the very strong HCMV immediate early promoter by DMA CpG methylation in Vitro," *Biological Chemistry Hoppe-Seyler*, vol. 377, no. 3, pp. 195–201, 1996.
- [39] Q. Chen, H. Wei, R. Sun, J. Zhang, and Z. Tian, "Therapeutic RNA silencing of Cys-X3-Cys chemokine ligand 1 gene prevents mice from adenovirus vector-induced acute liver injury," *Hepatology*, vol. 47, no. 2, pp. 648–658, 2008.
- [40] L. G. Guidotti and F. V. Chisari, "Noncytolytic control of viral infections by the innate and adaptive immune response," *Annual Review of Immunology*, vol. 19, pp. 65–91, 2001.
- [41] A. P. McCaffrey, P. Fawcett, H. Nakai et al., "The host response to adenovirus, helper-dependent adenovirus, and adeno-associated virus in mouse liver," *Molecular Therapy*, vol. 16, no. 5, pp. 931–941, 2008.
- [42] D. A. Muruve, "The innate immune response to adenovirus vectors," *Human Gene Therapy*, vol. 15, no. 12, pp. 1157–1166, 2004.
- [43] D. A. Muruve, M. J. Cotter, A. K. Zaiss et al., "Helper-dependent adenovirus vectors elicit intact innate but attenuated adaptive host immune responses in vivo," *Journal of Virology*, vol. 78, no. 11, pp. 5966–5972, 2004.
- [44] M. A. Schnell, Y. Zhang, J. Tazelaar et al., "Activation of innate immunity in nonhuman primates following intraportal administration of adenoviral vectors," *Molecular Therapy*, vol. 3, no. 5, part 1, pp. 708–722, 2001.
- [45] M. Taniguchi, K. Seino, and T. Nakayama, "The NKT cell system: bridging innate and acquired immunity," *Nature Immunology*, vol. 4, no. 12, pp. 1164–1165, 2003.
- [46] M. J. Cotter and D. A. Muruve, "The induction of inflammation by adenovirus vectors used for gene therapy," *Frontiers in Bioscience*, vol. 10, pp. 1098–1105, 2005.
- [47] J. T. Schiffer, M. Aubert, N. D. Weber, E. Mintzer, D. Stone, and K. R. Jerome, "Targeted DNA mutagenesis for the cure of chronic viral infections," *Journal of Virology*, vol. 86, no. 17, pp. 8920–8936, 2012.

Research Article

Systemic Approach to Identify Serum microRNAs as Potential Biomarkers for Acute Myocardial Infarction

An Hsu,¹ Shu-Jen Chen,^{1,2} Yu-Sun Chang,³ Hua-Chien Chen,^{1,2} and Pao-Hsien Chu^{4,5,6}

¹ Graduate Institute of Biomedical Sciences, School of Medicine, Chang Gung University, 259 Wen-Hwa 1st Road, Kwei-Shan, Tao-Yuan 333, Taiwan

² Department of Biomedical Sciences, School of Medicine, Chang Gung University, 259 Wen-Hwa 1st Road, Kwei-Shan, Tao-Yuan 333, Taiwan

³ Molecular Medicine Research Center, Chang Gung University, 259 Wen-Hwa 1st Road, Kwei-Shan, Tao-Yuan 333, Taiwan

⁴ Department of Cardiology, Chang Gung Memorial Hospital, Chang Gung University College of Medicine, 199 Tun-Hwa North Road, Taipei 105, Taiwan

⁵ Healthcare Center, Chang Gung Memorial Hospital, Chang Gung University College of Medicine, 199 Tun-Hwa North Road, Taipei 105, Taiwan

⁶ Heart Failure Center, Chang Gung Memorial Hospital, Chang Gung University College of Medicine, 199 Tun-Hwa North Road, Taipei 105, Taiwan

Correspondence should be addressed to Hua-Chien Chen; hcchen@mail.cgu.edu.tw and Pao-Hsien Chu; pchu@adm.cgmh.org.tw

Received 4 December 2013; Accepted 14 April 2014; Published 12 May 2014

Academic Editor: Ammad Ahmad Farooqi

Copyright © 2014 An Hsu et al. This is an open access article distributed under the Creative Commons Attribution License, which permits unrestricted use, distribution, and reproduction in any medium, provided the original work is properly cited.

Background. Recent studies have revealed the role of microRNAs (miRNAs) in a variety of biological and pathological processes, including acute myocardial infarction (AMI). We hypothesized that ST-segment elevation myocardial infarction (STEMI) may be associated with an alteration of miRNAs and that circulating miRNAs may be used as diagnostic markers for STEMI. **Methods.** Expression levels of 270 serum miRNAs were analyzed in 8 STEMI patients and 8 matched healthy controls to identify miRNAs differentially expressed in the sera of patients with AMI. The differentially expressed miRNAs were evaluated in a separate cohort of 62 subjects, including 31 STEMI patients and 31 normal controls. **Results.** The initial profiling study identified 12 upregulated and 13 downregulated serum miRNAs in the AMI samples. A subsequent validation study confirmed that serum miR-486-3p and miR-150-3p were upregulated while miR-126-3p, miR-26a-5p, and miR-191-5p were significantly downregulated in the sera of patients with AMI. Ratios between the level of upregulated and downregulated miRNAs were also significantly different in those with AMI. Receiver operator characteristics curve analysis using the expression ratio of miR-486-3p and miR-191-5p showed an area under the curve of 0.863. **Conclusion.** Our results suggest that serum miRNAs may be used as potential diagnostic biomarkers for STEMI.

1. Introduction

Cardiovascular disease is the leading cause of death for both men and women worldwide [1, 2]. According to the newly revised guidelines from the World Health Organization in 2000, a cardiac biomarker rise accompanied by typical symptoms or ST elevation is diagnostic of acute myocardial infarction (AMI) [3]. Percutaneous coronary intervention is one of the most important treatments for patients with ST-segment elevation myocardial infarction (STEMI) [2, 4, 5]. The door-to-balloon time should be less than 90 minutes,

because any delay in time of reperfusion after arrival at the hospital is associated with a higher adjusted risk of in-hospital mortality [3, 5]. It would therefore be of great help to find biomarkers that could provide information on the pathophysiology and identify patients with STEMI to allow for early percutaneous coronary intervention.

In the first hours after AMI, myocardial fibers lose their transversal striations and nuclei. At the same time, there are robust upregulations of intramyocardial cytokines to enhance survival or accelerate myocyte necrosis and apoptosis and decrease contractility [6–8]. This is followed by cytokine

TABLE 1: Characteristics of the patients.

	Exploration cohort			Validation cohort		
	Ctrl (<i>n</i> = 8)	AMI (<i>n</i> = 8)	<i>P</i> value	Ctrl (<i>n</i> = 31)	AMI (<i>n</i> = 31)	<i>P</i> value
Age (years)	44.6 ± 10.3	53.3 ± 9.2	0.0980	53.7 ± 14.8	59.0 ± 11.5	0.1235
Male/female (<i>n/n</i>)	6/2	8/0		29/2	29/2	
Hypertension (%)	16	20	0.2873	17	19	0.323
Diabetes mellitus	12	14	0.765	11	14	0.635
Hypercholesterolemia	12	14	0.864	14	16	0.123
Smoking	14	14	0.125	14	15	0.110
Troponin I (<0.2 ng/mL)	NA	25.9 ± 65.3		NA	11.7 ± 28.2	
Triglyceride (mg/dL)	138.9 ± 73.7	144.0 ± 52.9	0.8750	161.1 ± 94.1	154.0 ± 86.7	0.7685
Cholesterol (mg/dL)	187.0 ± 26.1	164.6 ± 30.9	0.1400	197.9 ± 41.2	160.9 ± 37.8	0.0008
White blood cells (×10 ³ /uL)	6.35 ± 1.76	11.19 ± 2.19	<0.0001	6.48 ± 1.84	11.15 ± 3.99	<0.0001
Creatinine (md/dL)	0.91 ± 0.22	0.95 ± 0.13	0.6560	0.96 ± 0.22	1.28 ± 1.20	0.1505

Ctrl: control; AMI: acute myocardial infarction; NA: not available; Troponin I was the highest value.

amplification through transmigration of macrophages and neutrophils. The later cardiac remodeling includes phagocytosis and resorption of the necrotic tissue, hypertrophy of the surviving myocytes, degradation and synthesis of matrices, proliferation of myofibroblasts and angiogenesis, and, to a limited extent, progenitor cell proliferation [9, 10].

Recent studies have revealed the role of microRNAs (miRNAs) in a variety of basic biological and pathological processes [11–16] and in the association of miRNA signatures with cardiovascular diseases, including AMI [17–22]. Circulating miRNAs have been proposed to be sensitive and informative biomarkers for multiple cancers and in the diagnosis of cardiovascular diseases [23–28]. In particular, several muscle-specific miRNAs, including miR-1, miR-133a, and miR-133b, have been found to be significantly elevated in the sera of animals and patients with AMI. The identification of specific miRNAs acting as key regulators of AMI has opened new clinical avenues for research.

In this study, we first established a platform to quantify serum miRNAs, and we detected that the expression patterns of 25 miRNAs were altered in the sera of patients with AMI. Using an independent group, we confirmed that the serum levels of five miRNAs, including miR-486-3p, miR-191-5p, miR-126-3p, miR-26a-5p, and miR-150-3p, were significantly different in the AMI patients and that their expression levels can be used to differentiate AMI patients from normal patients. We further calculated the ratio between the upregulated and downregulated miRNAs and discovered that the ratio of these miRNAs had a much better predictive power to distinguish AMI patients from normal subjects. Taken together, our findings implicate circling miRNAs as potential diagnostic biomarkers for STEMI.

2. Methods

2.1. Patients' Data. This prospective study was conducted from November 2009 to January 2010 with approval from of the Institutional Regulation Board of Chang Gung Memorial Hospital, Taiwan, and it conformed to the tenets of

the Declaration of Helsinki. In total, 39 consecutive patients with STEMI were enrolled. A presumptive diagnosis of STEMI was made based on the American College of Cardiology/American Heart Association Task Force on Practice Guidelines [1]. Thirty-nine age- and gender-matched normal controls who were undergoing routine medical examinations at the same hospital were also enrolled. All of the controls had normal physical and ocular examination results and no history of cardiovascular diseases [29]. The patient records were reviewed for demographic data and medical history [30, 31]. Table 1 lists the clinical characteristics of the healthy controls and AMI patients.

2.2. Sample Collection and RNA Preparation. Blood samples from the patients diagnosed with STEMI in the emergency department or the intensive care units were processed by two-step centrifugation. The supernatant was stored at −80°C. Total RNA was prepared from serum samples using TRIzol LS reagent (Invitrogen, Carlsbad, CA) according to the manufacture's protocol. In brief, 900 µL of TRIzol LS reagent was added to 300 µL of serum. The samples were mixed well and allowed to stand for 5 minutes at room temperature. A synthetic RNA (5'-CGAUGGGCAGCUAUUUCACCUUG-3') was added to the mixture as the spike-in control. After phase separation, the upper layer aqueous solution was transferred to a separate vial and RNA was precipitated with an equal volume of 2-propanol. The precipitation was carried out at −20°C for 1 hour to increase the yield of RNA. In general, we harvested approximately 300 ng of total RNA from each sample. The total RNA was then dissolved in 15 µL of diethylpyrocarbonate-treated water, quantified by NanoDrop (Thermo Fisher Scientific Inc., Wilmington, USA), and stored at −80°C.

2.3. Reverse Transcription (RT). A pulsed reverse transcription reaction was performed to convert all miRNAs into corresponding cDNAs in one RT reaction [32]. Briefly, 10 µL of reaction mixture containing miRNA-specific stem-loop RT

primers (final 2 nM each), 500 μ M dNTP, 0.5 μ L Superscript III (Invitrogen, Carlsbad, CA), and 3 μ L total RNA was used for the pulsed RT reaction, which was performed as follows: 16°C for 30 minutes, followed by 50 cycles at 20°C for 30 seconds, 42°C for 30 seconds, 50°C for 1 second, and 70°C for 10 minutes. The RT products were diluted 10-fold before being used for the miRNA quantitative real-time PCR reaction.

2.4. Quantitative Real-Time PCR (qPCR). For miRNA quantification, 1 μ L of diluted RT product was used as the template for a 10 μ L qPCR. Briefly, 1X SYBR Master Mix (Applied Biosystems, Foster City, CA), 200 nM miRNA-specific forward primer, and 200 nM universal reverse primer were used for each qPCR reaction. The following conditions were used for qPCR: 95°C for 10 minutes, followed by 40 cycles of 95°C for 15 seconds and 63°C for 32 seconds, and a dissociation stage. End-point reaction products were analyzed on a 10% polyacrylamide gel stained with ethidium bromide to discriminate between the correct amplification product (57–60 bp) and the potential primer dimers (<44 bp). All qPCR reactions were performed on an ABI Prism 7900 real-time PCR system (Applied Biosystems, Foster City, CA).

2.5. Data Analysis. The threshold cycle (Ct) for qPCR was defined as the cycle number at which the change of fluorescence intensity crossed the threshold of 0.2. Expression levels of miRNA were converted to 39-Ct [32]. For the profiling study, the expression data were normalized by global median normalization before further analysis. For the validation studies, the synthetic spiked-in miRNA was used for normalization.

2.6. Statistical Analysis. Quantitative data were expressed as mean \pm standard deviation and analyzed using the Student's *t*-test. Receiver operator characteristics (ROC) curves and areas under the curves (AUC) were calculated using Prism 5 software (GraphPad). Prism calculates $z = (\text{AUC} - 0.5)/\text{SE}$ area and then determines *P* values from the *z* ratio (normal distribution). Cutoff values corresponded to the highest sum of sensitivity and specificity. A *P* value less than 0.05 was considered to be statistically significant. The statistical analyses used for miRNA expression data, including the *t*-test (two-tailed), principle component analysis, and hierarchical clustering, were performed with the Partek Genomics Suite (version 6.3, St. Louis, MO).

3. Results

3.1. Identification of Differentially Expressed miRNAs in the Sera from the STEMI Patients and Healthy Controls. Recent studies have identified several cardiac-specific or -enriched miRNAs in the circulation as potential biomarkers for the diagnosis of AMI. As AMI is a complex disease, it is possible that additional circulating miRNAs may also be altered and can then be used as potential markers for AMI. To explore this possibility, we quantified the expression levels of 270 miRNAs in serum samples from 8 healthy controls and 8 patients with STEMI using a qPCR assay platform previously

established in our laboratory [32]. The clinical characteristics of the subjects in the validation study are shown in Table 1. In order to detect a large number of miRNAs from small quantities of serum, we implemented a multiplexed reverse transcription reaction and used SYBR Green-based qPCR method for miRNA quantification. The assay was modified from the stem-loop RT-PCR assay originally designed by Chen et al. [33]. The SYBR Green-based RT-qPCR assay for miRNA detection has been reported by other laboratories [34]. A pilot study using RNA prepared from 300 μ L of serum samples from three healthy subjects detected approximately 100 miRNAs with high confidence ($C_t < 32$) in each sample, similar to the results reported by Wang et al. using the TaqMan method [23]. The expression levels of the serum miRNAs detected in our assay also correlated well with the expression levels of serum miRNAs reported by Wang et al. [23] (Figure 1(a)), suggesting that the SYBR Green-based RT-qPCR assay was suitable for the profiling study.

Expression levels of the 270 miRNAs were normalized and used to identify differentially expressed miRNAs. As there is currently no consensus on the best internal control for circulating miRNA profiling analysis, global median normalization was used to correct the technical variations arising from RNA preparation and qPCR detection. Principle component analysis revealed that the overall expression pattern of the 270 miRNAs in the sera from the patients with AMI was significantly different from the healthy controls (Figure 1(b)). Using the criteria of $P < 0.05$ (*t*-test, two-tailed) and fold-change ≥ 2 , we identified 25 serum miRNAs whose expression levels were significantly altered in the AMI samples (Figure 1(c)). Unsupervised hierarchical clustering using the expression levels of these 25 serum miRNAs completely separated the AMI patients from the healthy controls (Figure 1(d)).

The list of differentially expressed serum miRNAs, including 12 upregulated and 13 downregulated miRNAs, is shown in Table 2. These results confirmed that sera from the AMI patients contained multiple differentially expressed miRNAs and suggested that some of these differentially expressed miRNAs could be used as markers for the diagnosis of AMI. Previous studies have identified several serum miRNAs, including miR-1, miR-133, and miR-208, whose levels are significantly increased in the sera from AMI patients and experimental animals [23, 24, 35]. In our profiling study, levels of both miR-1 and miR-208 were found to be increased in sera from the AMI patients. miR-1 showed a 1.46-fold increase ($P = 0.206$) and miR-208 showed a 1.87-fold increase ($P = 0.074$) in the AMI samples. In contrast, we did not detect any difference in the level of miR-133 between the AMI and control subjects (fold-change = -1.042 , $P = 0.819$). This result is consistent with the study by Ai et al. [24].

3.2. Validation of Candidate miRNAs in an Independent Cohort. To determine whether the differentially expressed serum miRNAs could be used as blood-based biomarkers to differentiate AMI patients from healthy subjects, we conducted a validation study of the 25 differentially expressed miRNAs using an independent cohort including 31 AMI

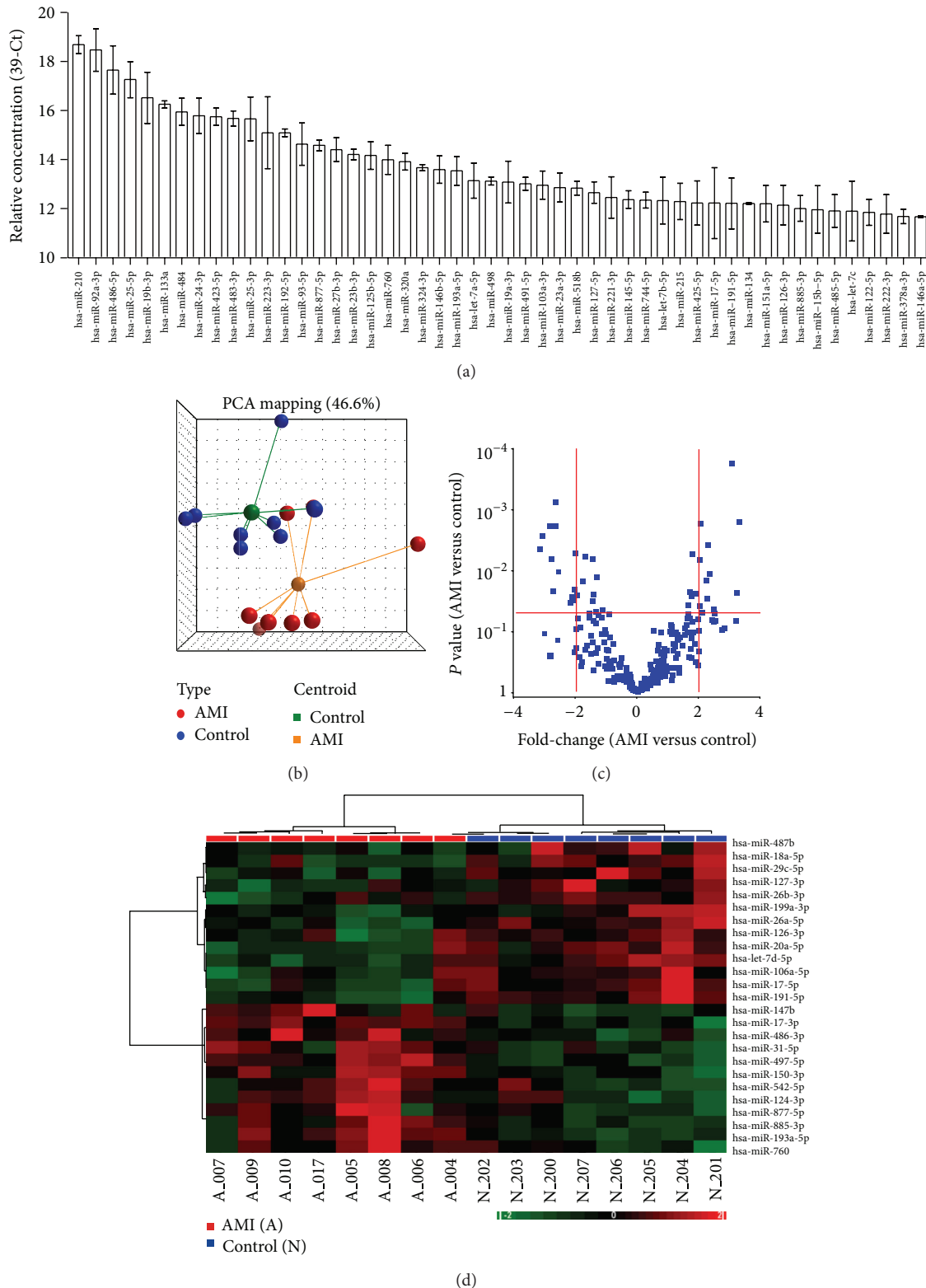


FIGURE 1: Detection of differentially expressed circulating miRNAs in serum samples. (a) Detection of miRNAs in serum from healthy subjects. Expression levels of 270 miRNAs in 300 μ L of serum were quantified using a multiplexed RT-qPCR assay. The relative expression levels of the top 50 miRNAs detected in serum from three healthy subjects (mean \pm SD) are shown. (b) Principle component analysis using expression levels of the 270 human miRNAs in serum samples from 8 healthy (blue) and 8 AMI (red) subjects. (c) Volcano plot indicated that 25 miRNAs were significantly altered in sera from the AMI patients. Red lines indicate the Student's *t*-test $P = 0.05$ and ± 2 -fold change. (d) Unsupervised hierarchical clustering of healthy and AMI samples using the 25 differentially expressed serum miRNAs. The hierarchical clustering was generated using Pearson's dissimilarity as the distance measure and Ward's method for linkage analysis. A: AMI patients; N: healthy subjects.

TABLE 2: miRNAs differentially expressed in the sera from patients with acute myocardial infarction.

miRNA name	Chromosome location	AMI (mean \pm SD)	Ctrl. (mean \pm SD)	Fold-change (AMI versus Ctrl.)	<i>t</i> -test <i>P</i> value
miRNA upregulated in AMI					
miR-193a-5p	17q12	13.15 \pm 1.02	11.49 \pm 0.48	3.17	0.0016
miR-147b	15q21.1	5.96 \pm 1.47	4.34 \pm 0.85	3.07	0.0232
miR-497-5p	17p13.1	9.12 \pm 0.57	7.58 \pm 0.57	2.91	0.0002
miR-542-5p	Xq26.3	6.34 \pm 1.07	5.09 \pm 1.05	2.36	0.0431
miR-885-3p	3p25.3	11.05 \pm 0.99	9.88 \pm 0.42	2.25	0.0113
miR-150-3p	19q13.32	9.87 \pm 0.66	8.72 \pm 0.58	2.21	0.0038
miR-877-5p	6p21.33	13.40 \pm 1.06	12.26 \pm 0.66	2.20	0.0290
miR-31-5p	9p21.3	7.74 \pm 0.84	6.63 \pm 0.66	2.17	0.0145
miR-760	1p22.1	13.01 \pm 0.91	11.96 \pm 0.94	2.07	0.0490
miR-17-3p	13q31.3	7.24 \pm 0.23	6.21 \pm 0.67	2.04	0.0017
miR-486-3p	8p11.21	9.19 \pm 0.66	8.17 \pm 0.54	2.02	0.0068
miR-124-3p	8p23.1, 8q12.3	7.23 \pm 0.79	6.21 \pm 0.90	2.02	0.0390
miRNA downregulated in AMI					
miR-20a-5p	13q31.3	7.20 \pm 1.00	8.79 \pm 0.76	-3.01	0.0045
miR-18a-5p	13q31.3	4.86 \pm 0.83	6.41 \pm 0.78	-2.94	0.0027
miR-26a-5p	12q14.1, 3p22.2	7.96 \pm 0.75	9.38 \pm 0.65	-2.69	0.0019
miR-17-5p	13q31.3	8.36 \pm 0.92	9.76 \pm 0.72	-2.64	0.0066
miR-106a-5p	Xq26.2	6.82 \pm 1.15	8.19 \pm 0.84	-2.59	0.0216
let-7d-5p	9q22.32	8.44 \pm 0.66	9.77 \pm 0.65	-2.52	0.0019
miR-191-5p	3p21.31	9.68 \pm 0.62	11.01 \pm 0.54	-2.51	0.0008
miR-26b-3p	2q35	6.62 \pm 1.09	7.91 \pm 0.42	-2.44	0.0107
miR-126-3p	9q34.3	9.15 \pm 1.17	10.25 \pm 0.44	-2.14	0.0340
miR-487b	14q32.31	5.10 \pm 0.56	6.16 \pm 1.01	-2.09	0.0278
miR-127-3p	14q32.31	6.25 \pm 0.71	7.29 \pm 0.93	-2.06	0.0313
miR-199a-3p	1q25.1, 19p13.2	7.31 \pm 0.60	8.34 \pm 0.86	-2.04	0.0205
miR-29c-5p	1q32.2	7.56 \pm 0.56	8.57 \pm 0.60	-2.02	0.0052

Ctrl.: control; and AMI: acute myocardial infarction.

patients and 31 age- and gender-matched healthy controls. The expression levels of these candidate miRNAs were quantified using multiplexed RT-qPCR, and a synthetic miRNA was used as a spike-in control to correct the variations in sample preparation and RT-qPCR. The expression data of the miRNAs were normalized to the spike-in control before further analysis. Five of the candidate miRNAs (2 upregulated and 3 downregulated) showed statistically significantly different expressions (*t*-test, *P* < 0.05, fold-change > 1.5) in the AMI samples compared to the healthy controls. Figure 2(a) shows the expression levels of these five validated miRNAs in individual samples from AMI patients and healthy controls.

To evaluate the diagnostic value of these validated miRNAs, ROC curves were constructed and the AUC values were determined (Table 3, Figure 2(b)). Among the 5 validated miRNAs, miR-150-3p, which was upregulated in the AMI samples, showed the best diagnostic power with an AUC of 0.715 ± 0.067 (*P* = 0.0036) and a 95% confidence interval of 0.584 to 0.847. The cutoff value for miR-150-3p was 7.29 with a sensitivity of 70.97% and a specificity of 70.97%. miRNA miR-126-3p, which was downregulated in the AMI

samples, showed the second best diagnostic power with an AUC of 0.694 ± 0.070 (*P* = 0.0087) and a 95% confidence interval of 0.557 to 0.832. The cutoff value for miR-126-3p was 8.835 with a sensitivity of 60.52% and a specificity of 80.65%. Interestingly, previous studies have shown that miR-150 is an inflammatory-related miRNA while miR-126 is associated with angiogenesis. These results suggest that miRNAs associated with pathological conditions other than cardiac damage may also be useful as biomarkers for the diagnosis of AMI.

3.3. Evaluation of miRNA Expression Ratio as a Biomarker for AMI. Previous studies have shown that the expression ratio of two miRNAs provides a better predictive power in the diagnosis of head and neck cancer [36]. As miR-150-3p and miR-486-3p showed significant upregulation and miR-26a-5p, miR-126-3p, and miR-191-5p showed significant downregulation in the AMI samples, we next sought to determine if expression ratios constructed between these miRNAs could improve their predictive power for the diagnosis of AMI. For each miRNA pair, the expression ratio

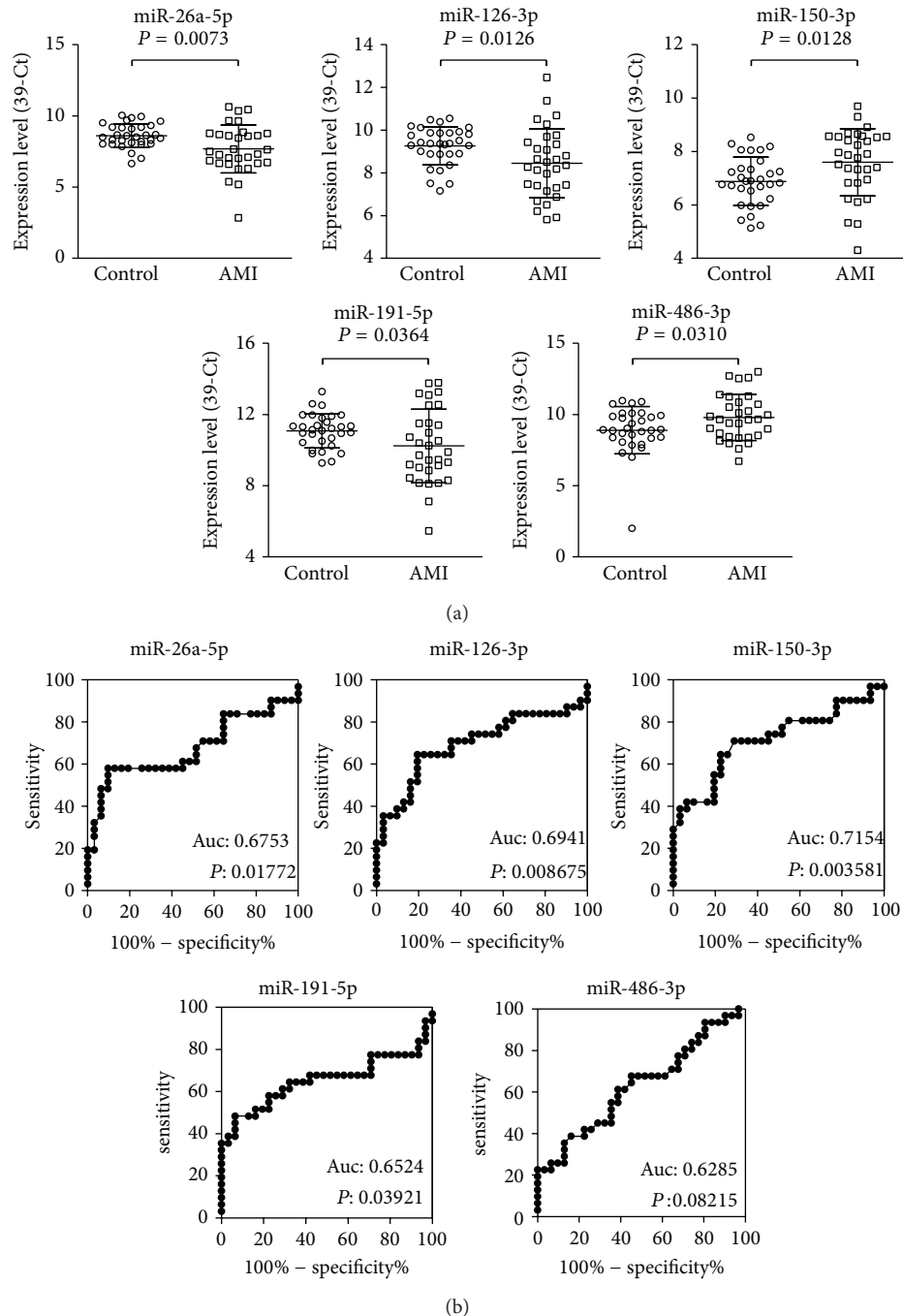


FIGURE 2: Expression levels and predictive power of five candidate miRNAs in the healthy controls and acute myocardial infarction (AMI) patients. (a) Expression levels of 5 candidate miRNAs in serum samples from 31 healthy controls and 31 AMI patients. Ct values generated from RT-qPCR were normalized to the spiked-in synthetic miRNA and then converted to 39-Ct. Data are presented as mean \pm SD. P values were calculated using the *t*-test. (b) ROC analysis using expression levels of individual miRNAs in healthy controls and AMI samples.

was determined by calculating the Δ Ct values between the upregulated and downregulated miRNAs. The expression ratios of six different combinations between the 2 upregulated and 3 downregulated miRNAs were then evaluated for their diagnostic accuracy using ROC analysis (Figure 3(a)).

Remarkably, all six different expression ratios had much better predictive power than individual miRNAs with AUC

P values less than 0.0001 (Table 4). Five of the six expression ratios showed an AUC greater than 0.8. The expression ratio between miR-486-3p and miR-191-5p showed the best predictive power, with an AUC of 0.863 and 95% confidence interval of 0.765 to 0.961. The optimal cutoff value was 2.58 with a sensitivity of 83.87% and a specificity of 83.33% (Figure 3(b)). Although the sample size was small, this study provides

TABLE 3: Validation of differentially expressed serum miRNAs in patients with acute myocardial infarction.

miRNA name	AMI (mean \pm SD)	Ctrl. (mean \pm SD)	Fold-change (AMI versus Ctrl.)	<i>t</i> -test <i>P</i> value	ROC AUC	ROC <i>P</i> value
miRNA upregulated in AMI						
miR-486-3p	9.79 \pm 1.61	8.89 \pm 1.66	1.87	0.0310	0.6285	0.0822
miR-150-3p	7.60 \pm 1.25	6.88 \pm 0.91	1.64	0.0128	0.7154	0.0036
miRNA downregulated in AMI						
miR-26a-5p	7.68 \pm 1.68	8.61 \pm 0.84	−1.90	0.0073	0.6753	0.0177
miR-191-5p	10.23 \pm 2.07	11.08 \pm 0.96	−1.80	0.0364	0.6524	0.0392
miR-126-3p	8.45 \pm 1.61	9.27 \pm 0.89	−1.76	0.0126	0.6941	0.0087

Ctrl.: control; AMI: acute myocardial infarction; ROC: receiver operator characteristics; and AUC: area under the curve.

strong support for the notion that circulating miRNAs may be used as diagnostic markers. More importantly, these data clearly demonstrated the superior differentiating power of miRNA ratios rather than single miRNA levels as biomarkers for the diagnosis of AMI.

4. Discussion

miRNAs represent an abundant group of small noncoding RNAs that regulate gene expression and affect physiological processes such as development, cell proliferation, and cell death [37, 38]. miRNAs may respond to damage in cardiovascular diseases, such as in acute responses to ischemia [17, 19–21], in chronic stages such as hypertrophy [39–44], and in heart failure [37, 44–48]. Studies of miRNAs in cardiovascular diseases have mostly been based on tissues of disease models [41, 44, 45, 49] and transgenic mice [39, 40, 44, 46]. The possibility of using miRNAs as a novel myocardial biomarker has been previously raised [50]; however, studies on the detection of blood miRNAs in AMI patients are limited [23]. One study showed that miR-208 was significantly increased after isoproterenol-induced myocardial injury [35], and another study demonstrated that circulating miR-1 was a potential novel biomarker for AMI [24].

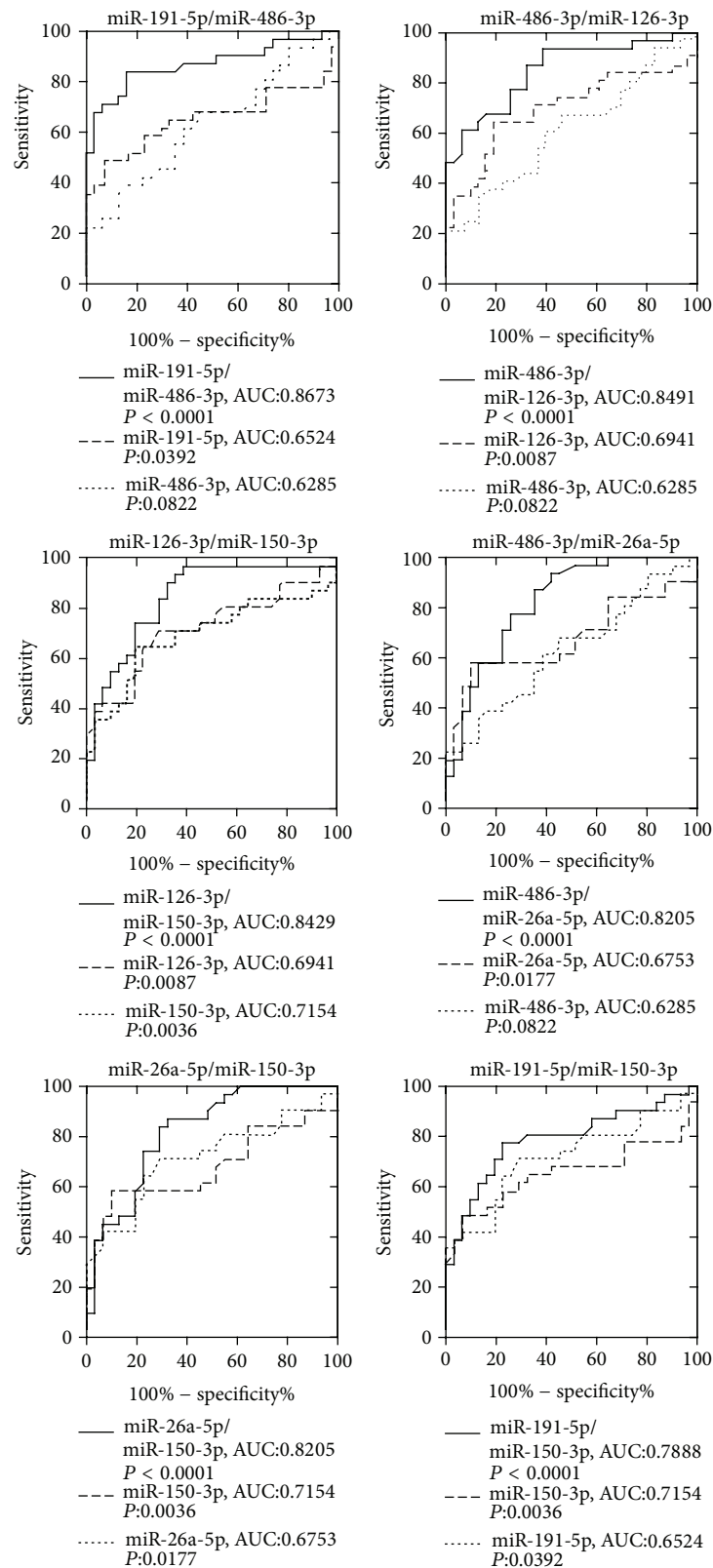
In our profiling study, we confirmed the increased expression of miR-1 and miR-208 in AMI serum. In addition, we identified several circulating miRNAs whose expression was even more profoundly altered in AMI patients. Two of the most significantly upregulated miRNAs observed in the AMI samples were miR-486-3p and miR-150-3p. Similar to miR-1 and miR-133, miR-486 is a muscle-enriched miRNA [51]. Recent studies have found that miR-486 is controlled by three transcription factors known to regulate muscle growth and homeostasis, including SRF, MRTF-A, and MyoD [51]. The observation that miR-486 is downregulated in Duchenne's muscular dystrophy [52] and in denervation-induced muscle atrophy [51] further supports that miR-486 is a critical regulator for muscle growth. Small et al. showed that miR-486 directly targets phosphatase and tensin homolog (PTEN) and Foxo1a to enhance the PI3 K/AKT signaling in muscle cells [51]. Overexpression of miR-486 reduces the protein level of PTEN and Foxo1a and enhances PI3 K/AKT signaling, eventually leading to muscle hypertrophy [51]. PI3 kinase is a known regulator of skeletal muscle hypertrophy and

atrophy [53]. As left ventricular hypertrophy often precedes AMI [54], the increase of miR-486 in the plasma of AMI patients may reflect an underlying cardiac hypertrophy associated with these AMI patients. Recent studies have shown that pharmacologic inhibition of PI3 K gamma promotes infarct resorption and prevents adverse cardiac remodeling after myocardial infarction in mice [55]. It is possible that pharmacologic inhibitors blocking the PI3 K/AKT signaling may also provide benefit for AMI patients with increased miR-486 level.

miR-150 is highly expressed in immune cells, including B- and T-lymphocytes, and has been shown to regulate the proliferation and differentiation of myeloid and lymphoid cells [56]. Recently, dysregulated expression of miR-150 has been reported in cardiac tissues from AMI patients [25, 57], consistent with our observation that plasma miR-150-3p levels were upregulated in the AMI samples. miR-150 has been shown to aggravate H₂O₂-induced cardiac myocyte injury by downregulating c-Myb gene [58], a gene involved in regulating the differentiation of myogenic progenitor cells. These results suggest that miR-150 may participate in H₂O₂-mediated gene regulation and functional modulation in cardiac myocytes.

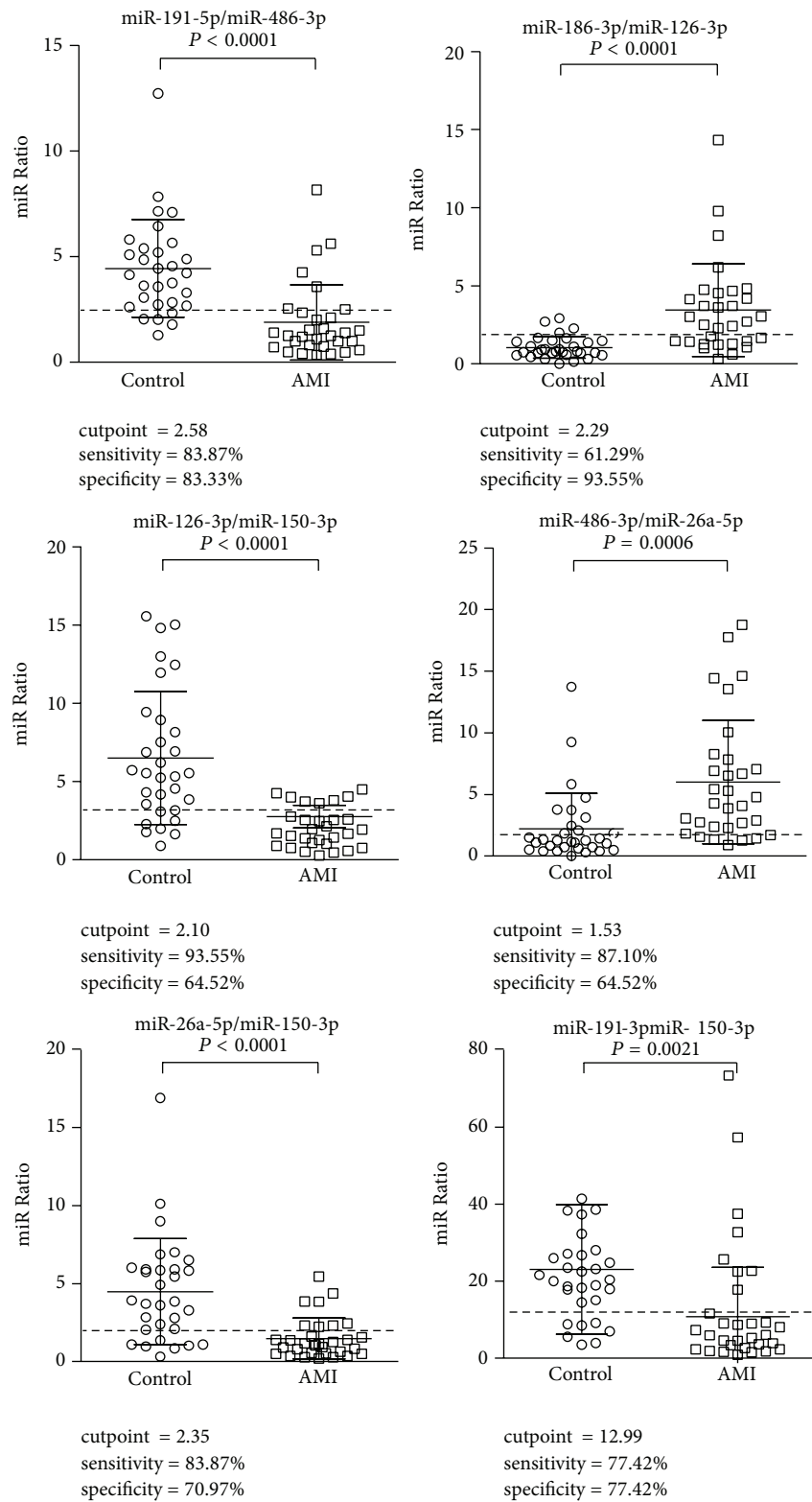
The profiling analysis revealed that a large number of miRNAs are downmodulated in AMI, including miR-126 and miR-26. The most significantly downregulated miRNA was the endothelial cell-specific miR-126, which promotes angiogenesis in response to angiogenic growth factors, such as vascular endothelial growth factor or basic fibroblast growth factor, by repressing negative regulators of signal transduction pathways and inflammation [45, 59–63]. Previously, Jakob et al. reported a pronounced loss of miR-126 in angiogenic early outgrowth cells (EOCs, CD34⁺) in patients with chronic heart failure [45]. The authors observed that miR-126 mimic transfection increased the capacity of angiogenic EOCs from patients with CHF to improve cardiac neovascularization and function. Recently, Qiang et al. also reported that dysregulated miR-126 in endothelial progenitor cells is associated with the prognosis of chronic heart failure patients [64]. These results suggest that administration of miR-126 may rescue endothelial cell function and offer a potential therapeutic approach.

In this study, we observed a significantly reduced miR-26 level in AMI samples. Zhang et al. recently found that



(a)

FIGURE 3: Continued.



(b)

FIGURE 3: Predictive power and expression ratios between two candidate serum miRNAs in the healthy controls and acute myocardial infarction (AMI) patients. (a) ROC analysis using expression ratios between two miRNAs (control $N = 31$, AMI $N = 31$ patients). (b) Expression ratios of miRNA combinations in AMI and control samples. Data are presented as mean \pm SD. P values were calculated using the t -test.

TABLE 4: Receiver operator characteristic curve analysis of miRNA ratios in the prediction of acute myocardial infarction.

Combined miRNAs	AMI (mean ± SD)	Ctrl. (mean ± SD)	<i>t</i> -test <i>P</i> value	ROC AUC	AUC 95% CI	ROC <i>P</i> value	Sensitivity	Specificity
miR-191-5p/miR-486-3p	1.89 ± 1.78	4.42 ± 2.31	1.02E – 05	0.8629	0.7648 to 0.9610	<0.0001	83.87%	83.33%
miR-486-3p/miR-126-3p	3.46 ± 2.96	1.06 ± 0.71	4.66E – 05	0.8491	0.7531 to 0.9451	<0.0001	61.29%	93.55%
miR-126-3p/miR-150-3p	2.77 ± 4.04	6.52 ± 4.24	7.0E – 04	0.8429	0.7423 to 0.9434	<0.0001	93.59%	64.52%
miR-486-3p/miR-26a-5p	6.00 ± 5.03	2.23 ± 2.88	0.0006	0.8205	0.7160 to 0.9250	<0.0001	77.42%	74.19%
miR-26a-5p/miR-150-3p	1.50 ± 1.34	4.50 ± 3.41	2.49E – 05	0.8205	0.7166 to 0.9244	<0.0001	83.87%	70.97%
miR-191-5p/miR-150-3p	10.77 ± 12.84	23.01 ± 16.87	0.0021	0.7888	0.6718 to 0.9058	<0.0001	77.42%	77.42%

Ctrl.: control; AMI: acute myocardial infarction; ROC: receiver operator characteristics; and AUC: area under the curve.

miR-26 is significantly reduced in a rat cardiac hypertrophy model and may regulate physiological structural changes of rat hearts by targeting glycogen synthase kinase 3 β (GSK3 β) [65]. The authors suggested that overexpression of miR-26 or suppression of GSK3 β may represent a promising therapeutic strategy. Although no previous study has linked miR-191 to cardiovascular functions, the expression ratio between miR-191 and miR-486 may serve as a potential serum biomarker for AMI patients in our study.

The major limitation of the current study is that we could not record the exact onset time of STEMI in our patients. A difference in AMI onset could contribute to the variation of serum miRNA levels among these patients. However, our data are mostly compatible with the previous AMI studies [1, 6, 19, 23, 24].

5. Conclusion

In conclusion, we found that the serum level of five miRNAs, including miR-486-3p, miR-191-5p, miR-126-3p, miR-26a-5p, and miR-150-3p, were significantly different in the AMI patients compared to the healthy controls. ROC analysis using the expression ratio of miR-486-3p and miR-191-5p showed an area under the serum concentration time curve of 0.867. Our findings implicate that serum miRNAs may be used as potential diagnostic biomarkers for STEMI.

Conflict of Interests

The authors declare that there is no conflict of interests regarding the publication of this paper.

Acknowledgments

Dr. Chu's research was supported by the Taiwan National Health Research Institutes (NHRI), Taiwan (Grants NHRI-EX91-9108SC, NHRI-EX92-9108SC, NHRI-EX-93-9108SC, NHRI-EX94-9108SC, NHRI-EX95-9108SC, and NHRI-EX96-9627SI), and Grants CMRPG32057 from Chang Gung Memorial Hospital and NSC 94-2089-B-188-888, 94-2314-B-182-071, and 95-2314-B-182-021 (Pao-Hsien Chu) from the National Sciences Council, Taiwan.

References

- [1] P. T. O'Gara, F. G. Kushner, D. D. Ascheim et al., "2013 ACCF/AHA guideline for the management of ST-elevation myocardial infarction: a report of the American College of Cardiology Foundation/American Heart Association Task Force on Practice Guidelines," *Circulation*, vol. 127, no. 4, pp. e362–e425, 2013.
- [2] F. A. Masoudi, R. O. Bonow, R. G. Brindis et al., "ACC/AHA 2008 statement on performance measurement and reperfusion therapy: a report of the ACC/AHA Task Force on Performance Measures (Work group to address the challenges of performance measurement and reperfusion therapy)," *Circulation*, vol. 118, no. 24, pp. 2649–2661, 2008.
- [3] J. S. Alpert, K. Thygesen, E. Antman, and J. P. Bassand, "Myocardial infarction redefined—a consensus document of The Joint European Society of Cardiology/American College of Cardiology Committee for the redefinition of myocardial infarction," *Journal of the American College of Cardiology*, vol. 36, no. 3, pp. 959–969, 2000.
- [4] H. V. Anderson, R. E. Shaw, R. G. Brindis et al., "Relationship between procedure indications and outcomes of percutaneous coronary interventions by American College of Cardiology/American Heart Association Task Force Guidelines," *Circulation*, vol. 112, no. 18, pp. 2786–2791, 2005.
- [5] E. Braunwald, E. M. Antman, J. W. Beasley et al., "ACC/AHA guideline update for the management of patients with unstable angina and non-ST-segment elevation myocardial infarction—2002: summary article: a report of the American College of Cardiology/American Heart Association Task Force on Practice Guidelines (Committee on the Management of Patients with Unstable Angina)," *Circulation*, vol. 106, no. 14, pp. 1893–1900, 2002.
- [6] A. Deten, H. C. Volz, W. Briest, and H.-G. Zimmer, "Differential cytokine expression in myocytes and non-myocytes after myocardial infarction in rats," *Molecular and Cellular Biochemistry*, vol. 242, no. 1-2, pp. 47–55, 2003.
- [7] M. Nian, P. Lee, N. Khaper, and P. Liu, "Inflammatory cytokines and postmyocardial infarction remodeling," *Circulation Research*, vol. 94, no. 12, pp. 1543–1553, 2004.
- [8] M. Bujak and N. G. Frangogiannis, "The role of TGF- β signaling in myocardial infarction and cardiac remodeling," *Cardiovascular Research*, vol. 74, no. 2, pp. 184–195, 2007.
- [9] P. Anversa and B. Nadal-Ginard, "Myocyte renewal and ventricular remodeling," *Nature*, vol. 415, no. 6868, pp. 240–243, 2002.
- [10] M. Dobaczewski, C. Gonzalez-Quesada, and N. G. Frangogiannis, "The extracellular matrix as a modulator of the inflammatory and reparative response following myocardial infarction," *Journal of Molecular and Cellular Cardiology*, vol. 48, no. 3, pp. 504–511, 2010.
- [11] C. E. Grueter, E. van Rooij, B. A. Johnson et al., "A cardiac MicroRNA governs systemic energy homeostasis by regulation of MED13," *Cell*, vol. 149, no. 3, pp. 671–683, 2012.
- [12] R. A. Boon, K. Iekushi, S. Lechner et al., "MicroRNA-34a regulates cardiac ageing and function," *Nature*, vol. 495, no. 7439, pp. 107–110, 2013.
- [13] H. Kasuga, M. Fukuyama, A. Kitazawa, K. Kontani, and T. Katada, "The microRNA miR-235 couples blast-cell quiescence to the nutritional state," *Nature*, vol. 497, no. 7450, pp. 503–506, 2013.
- [14] J. W. Kornfeld, C. Baitzel, A. C. Konner et al., "Obesity-induced overexpression of miR-802 impairs glucose metabolism through silencing of Hnf1b," *Nature*, vol. 494, no. 7435, pp. 111–115, 2013.
- [15] S. J. Song, L. Poliseno, M. S. Song et al., "MicroRNA-antagonism regulates breast cancer stemness and metastasis via TET-family-dependent chromatin remodeling," *Cell*, vol. 154, no. 2, pp. 311–324, 2013.
- [16] H. Hasuwa, J. Ueda, M. Ikawa, and M. Okabe, "miR-200b and miR-429 function in mouse ovulation and are essential for female fertility," *Science*, vol. 341, no. 6141, pp. 71–73, 2013.
- [17] A. Bonauer, G. Carmona, M. Iwasaki et al., "MicroRNA-92a controls angiogenesis and functional recovery of ischemic tissues in mice," *Science*, vol. 324, no. 5935, pp. 1710–1713, 2009.
- [18] S. Rane, M. He, D. Sayed et al., "Downregulation of MiR-199a derepresses hypoxia-inducible factor-1 α and sirtuin 1 and recapitulates hypoxia preconditioning in cardiac myocytes," *Circulation Research*, vol. 104, no. 7, pp. 879–886, 2009.

- [19] S. Dong, Y. Cheng, J. Yang et al., "MicroRNA expression signature and the role of MicroRNA-21 in the early phase of acute myocardial infarction," *The Journal of Biological Chemistry*, vol. 284, no. 43, pp. 29514–29525, 2009.
- [20] Y. Cheng, P. Zhu, J. Yang et al., "Ischaemic preconditioning-regulated miR-21 protects heart against ischaemia/reperfusion injury via anti-apoptosis through its target PDCD4," *Cardiovascular Research*, vol. 87, no. 3, pp. 431–439, 2010.
- [21] X. Wang, H. Zhu, X. Zhang et al., "Loss of the miR-144/451 cluster impairs ischaemic preconditioning-mediated cardioprotection by targeting Rac-1," *Cardiovascular Research*, vol. 94, no. 2, pp. 379–390, 2012.
- [22] J. N. Zhu, R. Chen, Y. H. Fu et al., "Smad3 inactivation and MiR-29b upregulation mediate the effect of carvedilol on attenuating the acute myocardium infarction-induced myocardial fibrosis in rat," *PLoS One*, vol. 8, no. 9, Article ID e75557, 2013.
- [23] G.-K. Wang, J.-Q. Zhu, J.-T. Zhang et al., "Circulating microRNA: a novel potential biomarker for early diagnosis of acute myocardial infarction in humans," *European Heart Journal*, vol. 31, no. 6, pp. 659–666, 2010.
- [24] J. Ai, R. Zhang, Y. Li et al., "Circulating microRNA-1 as a potential novel biomarker for acute myocardial infarction," *Biochemical and Biophysical Research Communications*, vol. 391, no. 1, pp. 73–77, 2010.
- [25] Y. Devaux, M. Vausort, G. P. McCann et al., "MicroRNA-150: a novel marker of left ventricular remodeling after acute myocardial infarction," *Circulation: Cardiovascular Genetics*, vol. 6, no. 3, pp. 290–298, 2013.
- [26] R. Recchioni, F. Marcheselli, F. Olivieri, S. Ricci, A. D. Procopio, and R. Antonicelli, "Conventional and novel diagnostic biomarkers of acute myocardial infarction: a promising role for circulating microRNAs," *Biomarkers*, vol. 18, no. 7, pp. 547–558, 2013.
- [27] V. Koberle, B. Kronenberger, T. Pleli et al., "Serum microRNA-1 and microRNA-122 are prognostic markers in patients with hepatocellular carcinoma," *European Journal of Cancer*, vol. 49, no. 16, pp. 3442–3449, 2013.
- [28] L. A. Selth, S. L. Townley, A. G. Bert et al., "Circulating microRNAs predict biochemical recurrence in prostate cancer patients," *British Journal of Cancer*, vol. 109, no. 3, pp. 641–650, 2013.
- [29] S.-C. Shen, W.-J. Ho, S.-C. Wu et al., "Peripheral vascular endothelial dysfunction in glaucomatocyclitic crisis: a preliminary study," *Investigative Ophthalmology and Visual Science*, vol. 51, no. 1, pp. 272–276, 2010.
- [30] P. H. Chu, C. W. Chiang, L. A. Hsu, K. H. Lin, N. J. Cheng, and C. T. Kuo, "Low prevalence of coronary arterial disease in Chinese adults with mitral stenosis," *Chang Gung Medical Journal*, vol. 24, no. 2, pp. 97–102, 2001.
- [31] C.-H. Tang, C.-S. Wu, T.-H. Lee et al., "Preeclampsia-eclampsia and the risk of stroke among peripartum in Taiwan," *Stroke*, vol. 40, no. 4, pp. 1162–1168, 2009.
- [32] H.-C. Chen, G.-H. Chen, Y.-H. Chen et al., "MicroRNA deregulation and pathway alterations in nasopharyngeal carcinoma," *British Journal of Cancer*, vol. 100, no. 6, pp. 1002–1011, 2009.
- [33] C. Chen, D. A. Ridzon, A. J. Broomer et al., "Real-time quantification of microRNAs by stem-loop RT-PCR," *Nucleic Acids Research*, vol. 33, no. 20, p. e179.9, 2005.
- [34] T. D. Schmittgen, E. J. Lee, and J. Jiang, "High-throughput real-time PCR," *Methods in Molecular Biology*, vol. 429, pp. 89–98, 2008.
- [35] X. Ji, R. Takahashi, Y. Hiura, G. Hirokawa, Y. Fukushima, and N. Iwai, "Plasma miR-208 as a biomarker of myocardial injury," *Clinical Chemistry*, vol. 55, no. 11, pp. 1944–1949, 2009.
- [36] M. Avissar, B. C. Christensen, K. T. Kelsey, and C. J. Marsit, "MicroRNA expression ratio is predictive of head and neck squamous cell carcinoma," *Clinical Cancer Research*, vol. 15, no. 8, pp. 2850–2855, 2009.
- [37] E. van Rooij, W. S. Marshall, and E. N. Olson, "Toward microRNA-based therapeutics for heart disease: the sense in antisense," *Circulation Research*, vol. 103, no. 9, pp. 919–928, 2008.
- [38] E. M. Small, R. J. A. Frost, and E. N. Olson, "MicroRNAs add a new dimension to cardiovascular disease," *Circulation*, vol. 121, no. 8, pp. 1022–1032, 2010.
- [39] Z. P. Huang, J. Chen, H. Y. Seok et al., "MicroRNA-22 regulates cardiac hypertrophy and remodeling in response to stress," *Circulation Research*, vol. 112, no. 9, pp. 1234–1243, 2013.
- [40] A. Ucar, S. K. Gupta, J. Fiedler et al., "The miRNA-212/132 family regulates both cardiac hypertrophy and cardiomyocyte autophagy," *Nature Communications*, vol. 3, article 1078, 2012.
- [41] J. Ganesan, D. Ramanujam, Y. Sassi et al., "MiR-378 controls cardiac hypertrophy by combined repression of mitogen-activated protein kinase pathway factors," *Circulation*, vol. 127, no. 21, pp. 2097–2106, 2013.
- [42] C. E. Winbanks, C. Beyer, A. Hagg, H. Qian, P. V. Sepulveda, and P. Gregorevic, "miR-206 represses hypertrophy of myogenic cells but not muscle fibers via inhibition of HDAC4," *PLoS One*, vol. 8, no. 9, Article ID e73589, 2013.
- [43] P. A. Da Costa Martins and L. J. De Windt, "MicroRNAs in control of cardiac hypertrophy," *Cardiovascular Research*, vol. 93, no. 4, pp. 563–572, 2012.
- [44] S. Heymans, M. F. Corsten, W. Verhesen et al., "Macrophage MicroRNA-155 promotes cardiac hypertrophy and failure," *Circulation*, vol. 128, no. 13, pp. 1420–1432, 2013.
- [45] P. Jakob, C. Doerries, S. Briand et al., "Loss of angiomiR-126 and 130a in angiogenic early outgrowth cells from patients with chronic heart failure: role for impaired in vivo neovascularization and cardiac repair capacity," *Circulation*, vol. 126, no. 25, pp. 2962–2975, 2012.
- [46] E. Dirx, M. M. Gladka, L. E. Philippen et al., "Nfat and miR-25 cooperate to reactivate the transcription factor Hand2 in heart failure," *Nature Cell Biology*, vol. 15, no. 11, pp. 1282–1293, 2013.
- [47] T. Seeger, F. Haffez, A. Fischer et al., "Immunosenescence-associated microRNAs in age and heart failure," *European Journal of Heart Failure*, vol. 15, no. 4, pp. 385–393, 2013.
- [48] A. J. Tijssen, Y. M. Pinto, and E. E. Creemers, "Non-cardiomyocyte microRNAs in heart failure," *Cardiovascular Research*, vol. 93, no. 4, pp. 573–582, 2012.
- [49] R. D. Bagnall, T. Tsoutsman, R. E. Shephard, W. Ritchie, and C. Semsarian, "Global microRNA profiling of the mouse ventricles during development of severe hypertrophic cardiomyopathy and heart failure," *PLoS One*, vol. 7, no. 9, Article ID e44744, 2012.
- [50] K. B. Margulies, "MicroRNAs as novel myocardial biomarkers," *Clinical Chemistry*, vol. 55, no. 11, pp. 1897–1899, 2009.
- [51] E. M. Small, J. R. O'Rourke, V. Moresi et al., "Regulation of PI3-kinase/Akt signaling by muscle-enriched microRNA-486," *Proceedings of the National Academy of Sciences of the United States of America*, vol. 107, no. 9, pp. 4218–4223, 2010.
- [52] M. S. Alexander, J. C. Casar, N. Motohashi et al., "Regulation of DMD pathology by an ankyrin-encoded miRNA," *Skeletal Muscle*, vol. 1, article 27, 2011.

- [53] D. J. Glass, "PI3 kinase regulation of skeletal muscle hypertrophy and atrophy," *Current Topics in Microbiology and Immunology*, vol. 346, pp. 267–278, 2010.
- [54] C. A. Larsson, B. Daka, B. Gullberg, L. Rastam, and U. Lindblad, "Clusters of AMI risk factors and their association with left ventricular hypertrophy: a population-based study within the Skaraborg Project, Sweden," *International Journal of Cardiology*, vol. 168, no. 6, pp. 5416–5421, 2013.
- [55] I. M. Seropian, A. Abbate, S. Toldo et al., "Pharmacologic inhibition of phosphoinositide 3-kinase gamma (pi3kg) promotes infarct resorption and prevents adverse cardiac remodeling after myocardial infarction in mice," *Journal of Cardiovascular Pharmacology*, vol. 56, no. 6, pp. 651–658, 2010.
- [56] E. Tsitsiou and M. A. Lindsay, "microRNAs and the immune response," *Current Opinion in Pharmacology*, vol. 9, no. 4, pp. 514–520, 2009.
- [57] Y. Devaux, M. Vausort, G. P. McCann et al., "A panel of 4 microRNAs facilitates the prediction of left ventricular contractility after acute myocardial infarction," *PLoS One*, vol. 8, no. 8, Article ID e70644, 2013.
- [58] X. Li, M. Kong, D. Jiang, J. Qian, Q. Duan, and A. Dong, "MicroRNA-150 aggravates H₂O₂-induced cardiac myocyte injury by down-regulating c-myc gene," *Acta Biochimica et Biophysica Sinica*, vol. 45, no. 9, pp. 734–741, 2013.
- [59] C. Urbich, A. Kuehnbacher, and S. Dimmeler, "Role of microRNAs in vascular diseases, inflammation, and angiogenesis," *Cardiovascular Research*, vol. 79, no. 4, pp. 581–588, 2008.
- [60] J. E. Fish, M. M. Santoro, S. U. Morton et al., "miR-126 regulates angiogenic signaling and vascular integrity," *Developmental Cell*, vol. 15, no. 2, pp. 272–284, 2008.
- [61] T. Donnem, K. Lonvik, K. Eklo et al., "Independent and tissue-specific prognostic impact of miR-126 in nonsmall cell lung cancer," *Cancer*, vol. 117, no. 14, pp. 3193–3200, 2011.
- [62] N. Zhu, D. Zhang, H. Xie et al., "Endothelial-specific intron-derived miR-126 is down-regulated in human breast cancer and targets both VEGFA and PIK3R2," *Molecular and Cellular Biochemistry*, vol. 351, no. 1-2, pp. 157–164, 2011.
- [63] E. Jusufovic, M. Rijavec, D. Keser et al., "let-7b and miR-126 are down-regulated in tumor tissue and correlate with microvessel density and survival outcomes in non—small—cell lung cancer," *PLoS One*, vol. 7, no. 9, Article ID e45577, 2012.
- [64] L. Qiang, L. Hong, W. Ningfu, C. Huaihong, and W. Jing, "Expression of miR-126 and miR-508-5p in endothelial progenitor cells is associated with the prognosis of chronic heart failure patients," *International Journal of Cardiology*, vol. 168, no. 3, pp. 2082–2088, 2013.
- [65] Z. H. Zhang, J. Li, B. R. Liu et al., "MicroRNA-26 was decreased in rat cardiac hypertrophy model and may be a promising therapeutic target," *Journal of Cardiovascular Pharmacology*, vol. 62, no. 3, pp. 312–319, 2013.

Research Article

Exploitation of a Very Small Peptide Nucleic Acid as a New Inhibitor of miR-509-3p Involved in the Regulation of Cystic Fibrosis Disease-Gene Expression

**Felice Amato,^{1,2} Rossella Tomaiuolo,^{1,2} Fabrizia Nici,³ Nicola Borbone,³
Ausilia Elce,^{1,2,4} Bruno Catalanotti,³ Stefano D'Errico,³ Carmine Marco Morgillo,³
Giuseppe De Rosa,³ Laura Mayol,³ Gennaro Piccialli,³
Giorgia Oliviero,³ and Giuseppe Castaldo^{1,2}**

¹ *Dipartimento di Medicina Molecolare e Biotecnologie Mediche, Via Pansini 5, 80131 Napoli, Italy*

² *CEINGE-Biotecnologie Avanzate, 80131 Napoli, Italy*

³ *Dipartimento di Farmacia, Università degli Studi di Napoli Federico II, Via D. Montesano 49, 80131 Napoli, Italy*

⁴ *Università Telematica Pegaso, 80143 Napoli, Italy*

Correspondence should be addressed to Giorgia Oliviero; golivier@unina.it

Received 6 December 2013; Accepted 18 March 2014; Published 15 April 2014

Academic Editor: Daniela De Stefano

Copyright © 2014 Felice Amato et al. This is an open access article distributed under the Creative Commons Attribution License, which permits unrestricted use, distribution, and reproduction in any medium, provided the original work is properly cited.

Computational techniques, and in particular molecular dynamics (MD) simulations, have been successfully used as a complementary technique to predict and analyse the structural behaviour of nucleic acids, including peptide nucleic acid- (PNA-) RNA hybrids. This study shows that a 7-base long PNA complementary to the seed region of miR-509-3p, one of the miRNAs involved in the posttranscriptional regulation of the CFTR disease-gene of Cystic Fibrosis, and bearing suitable functionalization at its N- and C-ends aimed at improving its resistance to nucleases and cellular uptake, is able to revert the expression of the luciferase gene containing the 3'UTR of the gene in A549 human lung cancer cells, in agreement with the MD results that pointed at the formation of a stable RNA/PNA heteroduplex notwithstanding the short sequence of the latter. The here reported results widen the interest towards the use of small PNAs as effective anti-miRNA agents.

1. Introduction

In the last twelve years a new group of endogenous, small, noncoding fragments of RNA, 18–25 nucleotides in length, named microRNAs (miRNAs) emerged for its ability to suppress the gene expression at posttranscriptional level [1, 2]. To date more than 1,400 miRNAs have been identified. MicroRNAs regulate the gene expression by annealing with the complementary mRNAs, thus preventing their translation or inducing their degradation [3, 4]. Although miRNAs usually recognize the 3'UTR many of them are capable of binding the 5'UTR or even coding regions of target mRNAs. Due to the small number of constituting nucleobases, each miRNA can recognize one or many mRNAs and each mRNA can be the target of many miRNAs. The result of this

network of interactions is the coregulatory role of miRNAs on the translation/degradation of one or more mRNAs [5]. Despite the potential occurrence of off-target effects, it is emerging that the modulation of specific miRNAs represents a new approach to achieve the control of gene expression. Potential applications of miRNA inhibitors (antimiR) range from diagnostics to regulation of important proteins involved in numerous cancers [6]. A number of human diseases have been associated with a deregulation of specific miRNAs [7–12]. Among these is the genetic disease Cystic Fibrosis (CF). CF is the most common lethal genetic disorder among Caucasians with one in every 3,000 newborns affected. CF is due to mutations in the CFTR gene encoding the CFTR chloride channel expressed by most epithelial cells [13]. The CF phenotype typically includes the altered sweat test, pancreatic

insufficiency, and pulmonary infections that gradually lead to respiratory insufficiency. To date more than 1,900 mutations of CF gene have been described, and a set of miRNAs inhibiting the CFTR expression at the posttranscriptional level has been described [14]. Furthermore, our group has shown that mutations in the 3'UTR of the CFTR gene may have a pathogenic effect by enhancing the affinity for the miR-509-3p miRNA [15].

The approaches to downregulate a specific miRNA essentially use oligonucleotide (ON) analogues which being complementary to miRNAs are able to reduce or inhibit their activity. For this purpose a number of ribose modified ONs, usually bearing a phosphorothioate backbone, have recently been used. Interesting results have been obtained by using 2'-O-methyl-ribonucleotides [16, 17] and other 2'-modified ONs [18, 19]. In addition, locked nucleic acids (LNAs) have shown interesting activity [20, 21] especially when used in combination with unmodified DNA monomers. Recently, several studies have demonstrated that the DNA mimics named peptide nucleic acids (PNAs) can be effectively used as anti-miRNA [22–24]. In the PNAs a 2-aminoethyl-glycine polymer replaces the ribose-phosphate DNA backbone [25]. PNA molecules are resistant to protease and nuclease degradation and recognize with a high affinity complementary fragments of DNA or RNA [26]. Many studies have been performed on the binding capability of PNAs and on the topological way in which they can recognize nucleic acids in single strand, duplex, or quadruplex arrangements to form heteroduplex, heterotriplex, and heteroquadruplex complexes [27–31] or to act as quadruplex ligands, respectively [32, 33]. The anti-miRNA activity of a PNA can occur in the nucleus by targeting the pre-miRNA or in the cytoplasm by binding the pre-miRNA and/or the mature miRNA [17]. In both cases it is necessary that the PNA can pass through the cell membrane and also through the nuclear membrane for the former case. The main drawback in the use of PNAs as intracellular probes lies in the poor water solubility when their length exceeds the 12–14 bases. Furthermore, the cellular uptake behaviour of a PNA is not easily predictable because it is mostly dependent on the PNA base composition and the overall lipophilicity. Recent studies report on the feasibility of a miRNA regulation approach by using unmodified PNAs and PNAs conjugated with peptides or hydrophilic groups [34, 35].

PNA having a poly-lysine tail display increased water solubility and cellular uptake [23, 24]. In addition, negatively charged PNAs can be obtained by synthesizing PNA-DNA hybrid strands or by attaching negative groups to the PNA monomers [34, 36]. In the last case, cationic lipids can be used as transfection reagents.

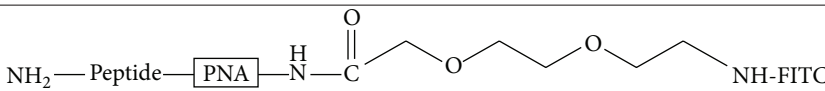
We recently reported that some anionic PNAs, synthesized by our group, are a potential treatment for CF by targeting the miR-509-3p involved in the regulation of CF disease-gene expression [37]. In that study we synthesized a 14-base long PNA fully complementary to the 5'-end of miR-509-3p and carrying a tetrapeptide tail containing two serine phosphates at its C-terminus and a fluorescein group at its N-terminus (PNA1, Table 1). We demonstrated, by *in vitro* studies on A549 cell lines, that the serine phosphate tail represents

a suitable conjugation to improve both the water solubility and the cellular uptake of a PNA molecule. Hybridization studies on PNA1 in the presence of miR-509-3p, performed by UV and CD spectroscopies and by electrophoretic mobility shift assay (EMSA), prove that the anionic peptide tail does not hamper the formation of the miR-509-3p/PNA1 heteroduplex. Finally, by reverting the expression of the luciferase gene containing the 3'UTR of the CFTR gene, we also demonstrated that PNA1 is able to recognize miR-509-3p in A549 cells. In continuing our studies on the Cystic Fibrosis and on the control of the related miR-509-3p miRNA, we decided to test the capability of the short 7-mer PNA2 (Table 1), bearing the same functionalization of PNA1 and complementary to the seed region of miR-509-3p, to bind this miRNA. Our interest towards shorter PNA anti-miRNAs was triggered by the consideration that the synthesis of longer PNAs (14–16 bases long) is an expensive and not an easily achievable task, especially when the PNA is conjugated to peptide tails and/or labelled at both ends. In addition, a recent study has reported that a very short LNA (8 bases long) was able to recognize and silence a family of miRNAs with no off-target effects [38]. Furthermore, experimental and computational evidence for different types of miRNA target sites demonstrated that probes with as few as seven base pairs of complementarity to the 5'-end of miRNAs are sufficient to confer regulation *in vivo* and are used in biologically relevant targets [5, 39]. The synthesis of PNA2 was preceded by a molecular modelling study aimed at evaluating the structural behaviour of the goal seven bases long miR-509-3p/PNA2 heteroduplex in comparison with that of the longer miR-509-3p/PNA1 heteroduplex. The stability and the structure of the miR-509-3p/PNA2 duplex were evaluated by molecular modelling and by UV, CD, and EMSA analyses. We here anticipate that PNA2, notwithstanding its reduced length, was still able to recognize miR-509-3p in A549 cells where it reverted the expression of the luciferase gene containing the 3'UTR of the CFTR gene.

2. Materials and Methods

2.1. Synthesis of miR-509-3p and PNAs (Table 1). The miR-509-3p mimic (2'-OMe modified) was synthesized and purified by the oligonucleotide synthesis facility at CEINGE-Biotecnologie Avanzate (Naples, Italy). The 4-methyl-benzhydrylamine-resin (MBHA resin, 0.4 mmol/g), all Fmoc/Boc protected monomers, and the 2-(2-(fluorenylmethoxycarbonylamino)ethoxy) ethoxyacetic (AEEA) spacer-linker were purchased from Link Technologies. Fmoc-L-Ser(PO(OBzl)OH)-OH building block, 2-(1-H-benzotriazol-1-yl)-1,1,3,3-tetramethyluronium hexafluorophosphate (HBTU), 2-(1-H-7-azabenzotriazole-1-yl)-1,1,3,3-tetramethyluronium hexafluorophosphate (HATU), and 1-hydroxybenzotriazole (HOBt) were purchased from Novabiochem. The following abbreviations are used: trifluoroacetic acid (TFA), dimethylformamide (DMF), dichloromethane (DCM), N,N-diisopropylethylamine (DIPEA), N-methylpyrrolidone (NMP), 1,8-diazabicyclo(5,4,0)undec-7-ene (DBU), and 2-(6-hydroxy-3-oxo-3H-xanthen-9-yl)-5-isothiocyanate-benzoic acid (FITC).

TABLE 1: Structures and sequences of miR-509-3p and PNA1-3. PNA sequences are written from C- to N-terminus.



miRNA		U	G	A	U	U	G	G	U	A	C	G	U	C	U	G	U	G	G	U	A	G
PNA1	G-S(P)-S(p)-G-a	c	t	a	a	c	c	a	t	g	c	a	g	a	Linker-FITC							
PNA2	G-S(P)-S(p)-G-a	c	t	a	a	c	c	Linker-FITC														
PNA3	G-S(P)-S(p)-G-t	t	t	t	t	t	t															

PNA2 and PNA3 were synthesized using the Fmoc-solid-phase strategy. The MBHA resin (50 mg, 0.02 mmol), after swelling in DCM (30 min) and DMF washings, was treated with a solution of 20% piperidine (2 mL) in DMF for 10 min. After washings in DMF, the resin was reacted with Fmoc-Gly (5 eq., in NMP 0.25 M), HATU (3.6 eq. in DMF 0.2 M), and DIPEA (5 eq.)/lutidine (6 eq.) for 1 h at room temperature. During the peptide and PNA synthesis the Fmoc group was removed by a treatment with a 5% DBU in DMF solution (5 min). In the case of Fmoc-Ser amino acids the basic treatment was prolonged (20 min). Couplings of Fmoc-L-Ser(PO(OBzl)OH)-OH were achieved using the following conditions: Fmoc-Ser monomer (8 eq. in NMP 0.4 M), HATU (8 eq. in DMF 0.4 M), and DIPEA (8 eq.)/lutidine (12 eq.) for 15 h at room temperature. PNA monomers and AEEA-COOH linker were reacted using the following conditions: monomer building block (8 eq. in NMP 0.4 M), HATU (8 eq. in DMF 0.4 M), and DIPEA (8 eq.)/lutidine (12 eq.) for 4 h at room temperature.

For the coupling with the fluorescent group the FITC monomer (5 eq., 0.2 M) was dissolved in DMF/DIPEA (2.5 : 97.5 v/v) and the solution was added to the resin, which was gently shaken in the dark for 15 h. The resin was finally treated with TFA/anisole/ethanedithiol (9 : 0.5 : 0.5; v/v/v) for 3.5 h and the products were precipitated with cold diethyl ether. The precipitates were recovered by centrifugation and following two washings with diethyl ether were dissolved in water and lyophilized. The PNA2 and PNA3 were obtained with a 48–50% overall yield (94–95% medium yield for each coupling).

The purifications were performed by HPLC using a RP-18 column (Merck, RT 250–10 5 μm) eluted with a linear gradient from 10% to 90% of eluent B in eluent A in 30 min. Eluent A: 0.1% TFA in water; eluent B: 0.1% TFA in acetonitrile. For these purifications the UV/VIS detector was set at 495 nm corresponding to the maximum of absorption of FITC. The collected yellow fractions were lyophilized and stored at –20°C in the dark.

The structures of PNA2 and PNA3 were confirmed by MALDI-TOF mass spectrometry on a Bruker Autoflex I instrument using α-cyano-4-hydroxycinnamic acid, 10 mg/mL in acetonitrile-3% aqueous TFA (1:1, v/v) as the matrix.

PNA2 m/z calculated 2812, found 2813 [M + H]⁺.

PNA3 m/z calculated 2864, found 2865 [M + H]⁺.

2.2. Molecular Modelling. The initial structures of the heteroduplexes formed by miR-509-3p with PNA1 and PNA2 were built by using the NMR structure of the 6-mer RNA(GAGUUC)/PNA(GAACTC) heteroduplex (PDB ID = 176D) [43]. Starting from the lowest energy NMR structure, one nucleotide was added aligning a duplicate of the reference structure on the PNA backbone. Once the 7-mer heteroduplex was obtained, the bases were mutated to match the PNA2 sequence. Watson-Crick canonical pairs were then refined using distance restraints on the first seven bases of miR-509-3p/PNA2 heteroduplex. The same procedure was used to build the miR-509-3p/PNA1 heteroduplex, starting from the refined structure of miR509-3P/PNA2 heteroduplex.

The equilibration of the systems and production of MD simulations were performed using the Amber 12 suite of programs [44, 45]. The Leap module of Ambertools13 was used to create parameter and topology files for the MD simulations using the ff99SB force field for RNA and standard amino acids [44, 45]. For PNAs parameterization we used the Sanders et al. force field for PNA [46] downloaded from the RESP and ESP charge database (R.E.D.D.B. <http://q4md-forcefieldtools.org/REDDB> Project ID = F93) [47], whereas the parameters for serine phosphate were taken from reference [48]. TIP3P water molecules were added with a minimum spacing of 10.0 Å from the box edges to the RNA:PNA molecules and Na⁺ counterions were added to each system to reach the neutralization of the system.

The geometry of the system was minimized in four steps as follows: (1) optimization of hydrogen atoms (500 steps of steepest descent and 4,500 steps of conjugate gradient); (2) optimization of water molecules and counterions (2,000 steps of steepest descent and 8,000 steps of conjugate gradient); (3) further optimization of hydrogen atoms, water molecules, and counterions (3,500 steps of steepest descent and 11,500 steps of conjugate gradient); (4) final optimization of the whole system (2,500 steps of steepest descent and 8,500 steps of conjugate gradient). Thermalization of the system was performed in four steps of 60 ps, increasing the temperature from 10 to 298 K. Concomitantly, interstrand distance restraints were applied to the RNA:PNA heteroduplex to preserve all base pairs canonical Watson-Crick bond, allowing 0.1 Å movement from the equilibrium bond distance (either closer or farther). Thus, the force constant applied during thermalization was set to 32 kcal mol⁻¹ Å⁻² and was gradually reduced in the next step to 10 kcal mol⁻¹ Å⁻² and subsequently decreased by increments of 5 kcal mol⁻¹ Å⁻²

in the next stages. Then, an additional step of 250 ps was performed in order to equilibrate the system density at constant pressure (1 bar) and temperature (298 K). Finally, an extended trajectory covering was run using a time step of 2 fs. SHAKE was used for those bonds containing hydrogen atoms in conjunction with periodic boundary conditions at constant pressure and temperature, particle mesh Ewald was used for the treatment of long range electrostatic interactions, and a cutoff of 9 Å was used for nonbonded interactions.

All production simulations were repeated in triplicate with random seeding for initial velocities and extended to 20 ns. In order to further assay the stability of the RNA:PNA heteroduplexes, we extended one run of PNA2 up to 50 ns, for a total simulation time of 90 ns for PNA2 and 60 ns for PNA1. The structural features were determined using the Curves+ software package [40], and visualization of trajectories was performed in VMD [41], while the trajectory analyses were performed using Ambertools13.

2.3. Preparation of miRNA/PNA Heteroduplexes (Annealing). The miR-509-3p/PNA heteroduplexes (1:1.5 or 1:5) were formed by heating the mixture of the samples dissolved in 100 mM KCl, 10 mM K_2HPO_4 , at 90°C for 5 min and slowly cooling at room temperature for 12 h. The amount of each PNA sample was estimated by quantitative UV at 80°C using the following molar extinction coefficients: PNA1 $\epsilon = 149.6 \text{ mL } \mu\text{mol}^{-1} \text{ cm}^{-1}$, PNA2 $\epsilon = 69.7 \text{ mL } \mu\text{mol}^{-1} \text{ cm}^{-1}$, PNA3 $\epsilon = 61.6 \text{ mL } \mu\text{mol}^{-1} \text{ cm}^{-1}$, and miR-509-3p $\epsilon = 205.0 \text{ mL } \mu\text{mol}^{-1} \text{ cm}^{-1}$.

2.4. UV and UV Melting Studies. The UV spectra were recorded on a Jasco V-530 UV spectrophotometer equipped with a Peltier-type temperature control system (model PTC-348WI). Thermal denaturation experiments were carried out in the temperature range 5–90°C by monitoring the absorbance at 260 nm at the heating rate of 0.5°C/min. The apparent T_m was estimated from the maximum in the first derivative of the melting profile.

2.5. CD Studies. CD spectra were recorded with a Jasco J-715 spectropolarimeter equipped with a Peltier Thermostat Jasco ETC-505T using 0.1 cm path length cuvettes and calibrated with an aqueous solution of 0.06% d-10-(1)-camphorsulfonic acid at 290 nm. The molar ellipticity $[\Theta]$ ($\text{deg cm}^2 \text{ dmol}^{-1}$) was calculated from the following equation: $[\Theta] = [\Theta]_{\text{obs}}/10lC$, where $[\Theta]_{\text{obs}}$ is the ellipticity (mdeg), C is the oligonucleotide molar concentration, and l is the optical path length of the cell (cm). CD measurements (220–320 nm) were carried out at a scan rate of 100 nm/min with a 2 nm bandwidth. The concentration of miR-509-3p/PNA2 and miR-509-3p was $1.0 \times 10^{-5} \text{ M}$. The spectra were signal-averaged over at least three scans and baseline was corrected by subtracting the buffer spectrum.

2.6. Cell Line, Construct, and Transfections. A549 human lung carcinoma cells were purchased from ATCC (Manassas, USA). Cells were maintained in Dulbecco's modified Eagle's medium (Gibco Invitrogen, USA) with 10% heat inactivated

fetal bovine serum (HyClone, USA) without the addition of antibiotics. Luciferase construct bearing the 3'UTR of CFTR gene [15] was used as miR-509-3p sensitive. Transfection of A549 cells with miRNA-mimics (Qiagen, Germany, EU) or PNA was performed with Attractene Transfection Reagent (Qiagen) as previously reported [37]. Briefly, cells seeded in 96-well plates were cotransfected with the luciferase reporter constructs and the miR-509-3p mimic. 24 h after, the cells were transfected with anti-miR-509-3p PNA. The transfection efficiency ($\approx 80\%$) was assessed by measuring the percentage of fluorescent cells relative to the total number of cells. The luciferase activity level was measured 24 h after transfection using the Dual-Glo Luciferase Assay System (Promega Corporation). The relative reporter activity was obtained by normalization to the Renilla luciferase activity.

2.7. Electrophoretic Mobility Shift Assay. The miR-509-3p mimic (2'OMe-modified) was synthesized by the oligonucleotide synthesis facility at CEINGE-Biotecnologie Avanzate (Naples, Italy). As previously reported [37], the miRNA and PNA were annealed in 1X NEBuffer 2 (50 mM NaCl, 10 mM Tris-HCl, 10 mM $MgCl_2$, 1 mM DTT, and pH 7.9 at 25°C) for 2 h at room temperature. All the reactions were loaded into 20% polyacrylamide gels in 0.5X Tris-Borate-EDTA (TBE) buffer and run at 140 V for 3 h. The fluorescence signal was acquired placing the wet gel directly on the plate of the Typhoon 8600 scanner.

3. Results and Discussion

With the aim of evaluating the feasibility of our hypothesis of shortening the PNA1 molecule to achieve a more synthetically affordable PNA targeted against miR-509-3p that preserves the hybridization properties of the parent PNA1, PNA2 was designed by deleting all the PNA1 bases that were not complementary to the “seed region” of miR-509-3p (i.e. the first seven bases at its 5' end, considered the most important target to achieve the anti-miRNA activity). As previously done for PNA1 [37], to improve the water solubility and the cellular uptake of PNA2 we decided to add the negatively charged tetrapeptide G-S(P)-S(P)-G at the C-end, whereas the fluorescent AEEA linker-FITC was added at the N-end to assess the cellular localization of PNA2. Before proceeding to the in-lab synthesis of PNA2, we estimated the stability and the conformational features of the goal miR-509-3p/PNA2 heteroduplex by means of computational techniques and compared the results with those of the correspondent heteroduplex formed with the PNA1. Computational techniques, and in particular molecular dynamics (MD) simulations, have been successfully used as complementary technique to predict and analyse the structural behaviour of nucleic acids, including PNA-RNA hybrids [46, 49, 50].

3.1. Molecular Dynamics Simulations. The miR-509-3p/PNA2 and miR-509-3p/PNA1 heteroduplexes were built starting from the NMR structure of the RNA (GAGUUC)/PNA(GAACTC) duplex (PDB-ID 176D)

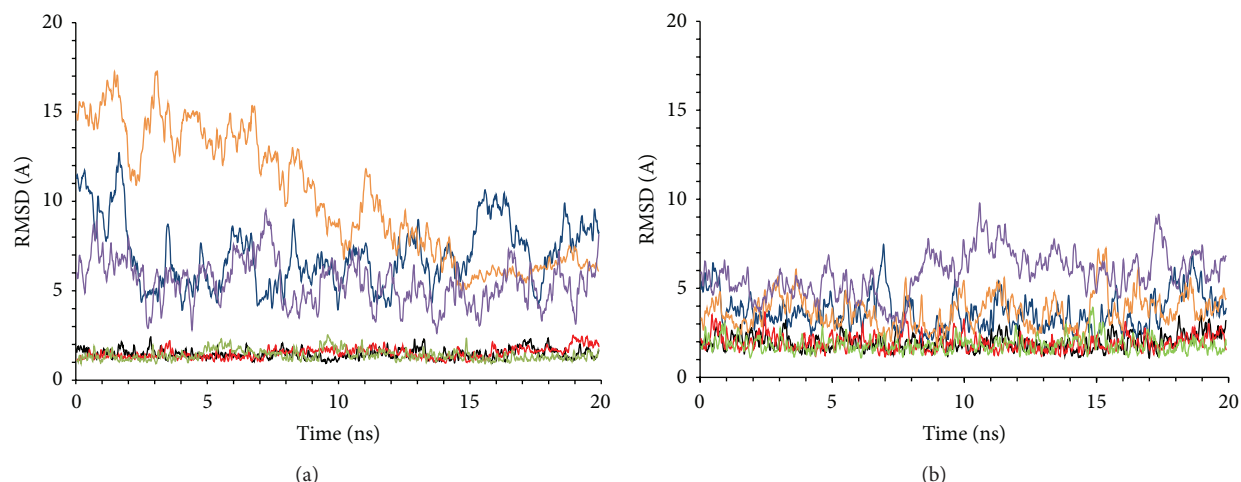


FIGURE 1: Root-mean-square deviation in the three MD runs on miR-509-3p/PNA2 (a) and miR-509-3p/PNA1 (b) heteroduplexes. Superimpositions were made on the MD-averaged structures for each trajectory taking into account the whole structure (blue, orange, and purple) or only the duplex region (black, red, and green).

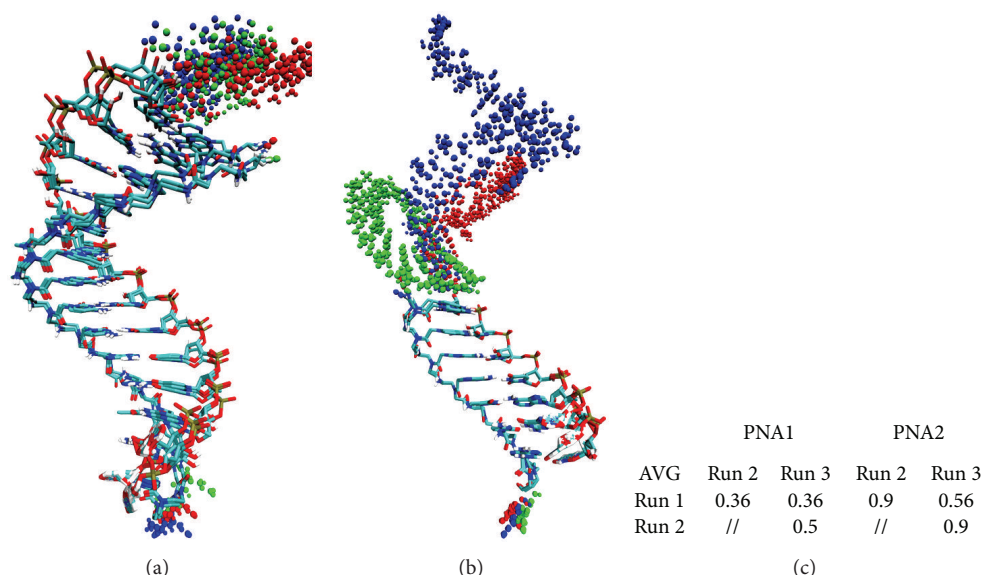


FIGURE 2: Superimposition of the MD average structures of miR-509-3p/PNA1 complex (a) and of miR-509-3p/PNA2 complex (b). Duplexes regions are represented in licorice coloured by atom type (carbon in cyan, oxygen in red, nitrogen in blue, phosphate in brown, and hydrogen in white). The miR-509-3p single strand regions are represented in spheres coloured by MD run (blue, run 1; green, run 2; red, run 3). (c) RMSD in Å, calculated on phosphates in the duplexes regions, among the average structures of the MD runs.

[43] as described in Materials and Methods. Each system was firstly analysed by means of three runs of 20 ns molecular dynamics in order to better sample the conformational behaviour of the complexes. Secondly, in order to further assay the stability of the miR-509-3p/PNA2 duplex, we extended one run of miR-509-3p/PNA2 up to 50 ns, for a total simulation time of 90 ns for miR-509-3p/PNA2 and 60 ns for miR-509-3p/PNA1.

The macroscopic properties of the systems, such as temperature, pressure, volume, density, and energy, were fairly constant during the whole simulation for both of the systems (data not shown). As expected, the analysis of

the RMSD in the trajectories of miR-509-3p/PNA2 and miR-509-3p/PNA1 complexes showed high flexibility of the single stranded miRNA segment (Figure 1). On the contrary, the behaviour of the region of miR-509-3p hybridized with PNAs was characterized by low RMSD values and low fluctuations, thus indicating the presence of a stable secondary structure (Figure 1).

Moreover, the comparison of the average structures obtained from each trajectory (Figure 2) revealed the convergence of the trajectories as shown by the low RMSD values in the duplex region of both complexes with PNA1 and PNA2 (>0.5 Å and >0.9 Å, resp.).

TABLE 2: Comparison of backbone torsion angles and helicoidal parameters for average structures of each run after 20 ns MD simulation. Highlighted in bold are values for structure obtained by averaging all the three runs. Standard deviation is reported in brackets.

(a)							
Duplex name	Helicoidal parameters						
	Twist (°)	Roll (°)	Tilt (°)	Inclination (°)	H.Ris (°)	H.Twi (°)	Groove width (Å)
PNA:RNA_NMR ^a	30.1 (4)	4.9 (4.3)	1.0 (3.3)	9.0 (2.7)	2.98 (0.2)	30.6 (4.2)	6.1 (0.5)
PNA:RNA_MD ^b	23.7; 23.2						
A-RNA ^c	32	12	2.8	15.8	3.3		3.8
PNA2 AVG tot	24.5 (1.1)	6.5 (1.6)	1 (0.9)	14.2 (0.6)	2.79 (0.10)	25.3 (1.1)	6.8 (0.6)
PNA1 AVG tot	24.9 (2.8)	5.7 (2.2)	0.9 (1.3)	13 (1.1)	2.77 (0.16)	25.5 (2.9)	6.8 (0.5)

(b)							
	Torsional PNA angles (in degrees)						
	N4-C5	C5-C	C-N1	C2-C3	C3-N4	N4-C7	χ
PNA:RNA_NMR ^a	-84.9	80	105.7	66	-100.1	9.1	50.6
PNA2	-79.9	125.2	78.6	70.4	-103	-2.9	78
PNA1	-81.3	129	131.5	69.5	-103.3	-2.1	78.5

(c)							
	Torsional RNA angles (in degrees)						
	α	β	γ	δ	ϵ	ζ	χ
PNA:RNA_NMR ^a	-68.4	111.75	58.4	78.5	-148.7	-72.5	-104.5
A-RNA ^c	-52	175	42	79	-146	-75	-157
miR20a ^d	-99.1	162.6	73.1	88.7	-138	-119.4	-147.6
PNA2 AVG tot	-84.4	172.8	81.3	79.2	-160.4	-70.3	-159.5
PNA1 AVG tot	-88.8	145.8	85.5	81.8	-161.1	-70.9	-158.7

^aCalculated on the average of the 10 NMR structures of PDB structure 176D; ^bfrom [40]; ^cfrom [41]; ^dfrom [42].

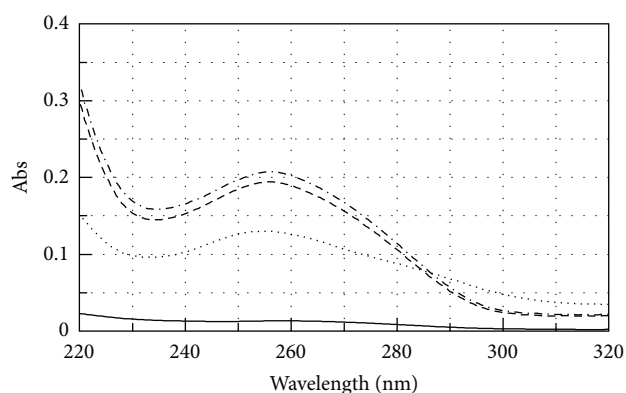


FIGURE 3: UV spectra of miR-509-3p (dashed line), PNA2 (solid line), miR-509-3p/PNA2 mixture (1:1.5) (dotted line), and the arithmetical sum (dashed-dotted line).

The analysis of the helicoidal parameters and torsion angles (Table 2) demonstrated that both miRNA/PNA duplexes could be described as A-type double helix with few noticeable deviations from the canonical structure. In particular, the lower step-averaged twist values reported in Table 2 indicated a slight unwinding of the RNA/PNA helices with respect to canonical A-RNA structures, in agreement

with what was previously observed in other MD simulations of RNA/PNA duplexes [43, 49]. The lower roll and tilt values observed in the MD run pointed at an expansion of the major groove. Finally, the analysis of torsion angles reported in Table 2 highlighted the strong similarity between the two duplexes. Taken together, the MD results indicated that both heteroduplexes assumed a conformation resembling the canonical A-type RNA helix rather than the experimentally determined NMR structure. Moreover, the torsion angles of RNA segments in miR-509-3p/PNA2 and miR-509-3p/PNA1 duplexes showed values very similar to those adopted by miR20a in the 4F3T crystal structure [42] suggesting that PNA2 and PNA1 could easily interact with the AGO-miRNA complex, not requiring any conformational adaptations. On the basis of the positive indications coming from the MD studies, we synthesised the PNA2 molecule and studied its ability to recognize the 2'-OMe mimic of miR-509-3p by CD, UV, and EMSA studies and evaluated its ability to restore the expression of the luciferase gene containing the 3'UTR of the CFTR gene in the presence of miR-509-3p.

3.2. Synthesis of PNA2 and PNA3. PNA2 and PNA3, chosen as the negative control and bearing the same functionalization of PNA2, were synthesized using the standard Fmoc-solid-phase strategy on the Rink-amide resin following the

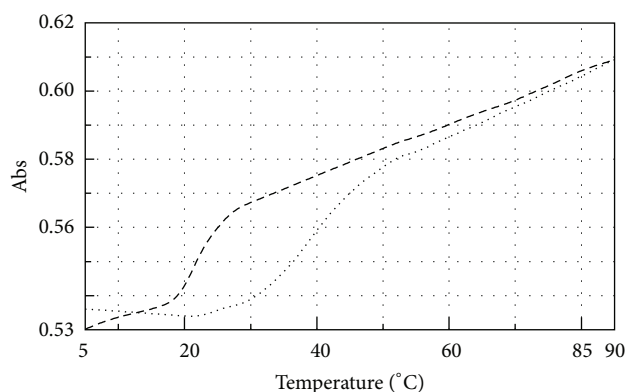


FIGURE 4: UV melting profile of miR-509-3p alone (dashed line) and miR-509-3p/PNA2 mixture (1:1.5 dotted line).

previously reported synthetic approach [37]. The sequences and the complete structures of PNA2 and PNA3 are shown in Table 1.

3.3. UV and UV Melting Studies. The miR-509-3p/PNA2 complex, prepared as described in Materials and Methods, was analysed by UV spectroscopy in the temperature range of 25–90°C. The data showed for the miR-509-3p/PNA2 complex a lower value of absorbance than the arithmetic sum of each component alone (Figure 3), thus evidencing that heteroduplex stacking interactions between the miRNA strand and the PNA2 had occurred. The UV melting experiments performed on the miR-509-3p/PNA2 mixture (1:1.5 ratio) showed a sigmoidal profile, which was indicative for the heteroduplex/single strands transition (Figure 4). The calculated apparent melting temperature of the miRNA/PNA2 heteroduplex was 40°C. The UV melting profile of the sole PNA2 did not show any significant variation in the A_{260} value in 10–70°C (data not shown), whereas, the UV melting of the sole miR-509-3p, in the same experimental conditions, showed a sigmoidal profile with an apparent melting temperature of 26°C, which could be attributed to the melting of poorly stable secondary structures of the miRNA. This data suggests that PNA2 is able to form a complex with miR-509-3p provided with the thermal stability required for *in vivo* experiments.

3.4. Circular Dichroism Spectra Analyses. To further confirm the formation of the miR-509-3p/PNA2 heteroduplex complex, circular dichroism (CD) spectra were registered for the miR-509-3p, PNA2, and their 1:1.5 mixture after the annealing procedure (Figure 5). In particular, the miR-509-3p/PNA2 mixture showed the typical CD profile of antiparallel RNA/PNA heteroduplexes, characterized by maxima at around 260 and 220 nm and minima at around 235 and 196 nm, thus confirming the capability of the PNA2 to form a heteroduplex with the miR-509-3p miRNA.

3.5. EMSA Results. The recognition phenomena between the miR-509-3p and the FITC-labelled PNA2 were also

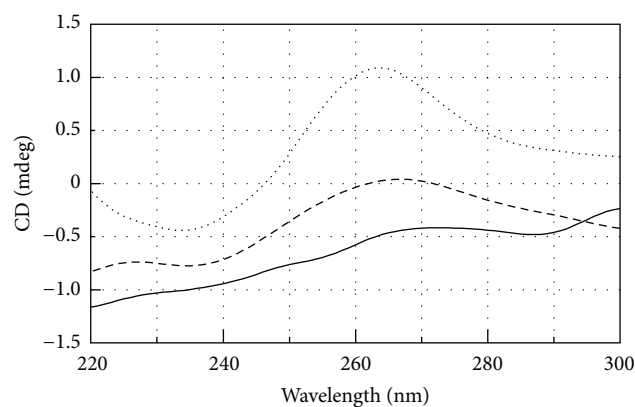


FIGURE 5: CD spectra of miR-509-3p alone (dashed line), PNA2 alone (solid line), and miR-509-3p/PNA2 mixture (1:1.5) (dotted line).

studied by electrophoretic mobility shift assay (Figure 6(a)). To allow the visualization of miR-509-3p alone, the gel was also visualized after the EtBr staining (Figure 6(b)). The superimposition of FITC and EtBr stained gels is shown in Figure 6(c). The electrophoretic mobility of PNA2 alone (lanes 1) was slower than that of miR-509-3p alone (lane 2). When miR-509-3p and PNA2 were mixed in the molar ratios of 1:1.5 and 1:5 (lanes 3 and 4, resp.) we observed the appearance of a new band, corresponding to the miR-509-3p/PNA2 complex, which was upshifted relative to the bands of the two components alone. The formation of the miR-509-3p/PNA2 complex was further confirmed by the disappearance of the band of the free miR-509-3p in the miRNA/PNA2 1:5 complex (lane 4, Figures 6(b) and 6(c)). The EMSA data further corroborated the CD evidence about the ability of PNA2 to form a stable complex in the presence of miR-509-3p miRNA.

3.6. Biological Activity. Once the ability of PNA2 to form a stable heteroduplex with miR-509-3p was demonstrated, we examined its potential of being a miR-509-3p inhibitor in a biological context. For this purpose we tested the ability of PNA2 to revert the reduction of luciferase activity induced by the transfection of the 2'-OMe mimic of miR-509-3p in A549 cells. As shown in Figure 7 the transfection of PNA2, but not of PNA3, was able to rescue the luciferase activity in a dose-dependent manner. In this experiment A549 cells were first transfected with the pLuc-CFTR-3'UTR plasmid (a reporter luciferase construct sensitive to the miR-509-3p mimic action due to the presence of the 3'UTR of the CFTR gene) and with miR-509-3p miRNA. As expected, the transfection of the miR-509-3p reduced the luciferase activity down to 40%. The luciferase activity was rescued after the transfection of the PNA2 in a dose-dependent manner. In these experiments the commercially available Attractene cationic lipid transfection reagent was used. The fluorescent microscopy image of the A549 cells taken 24 h after the transfection with PNA2 (Figure 8) confirmed the PNA2 uptake by the cells.

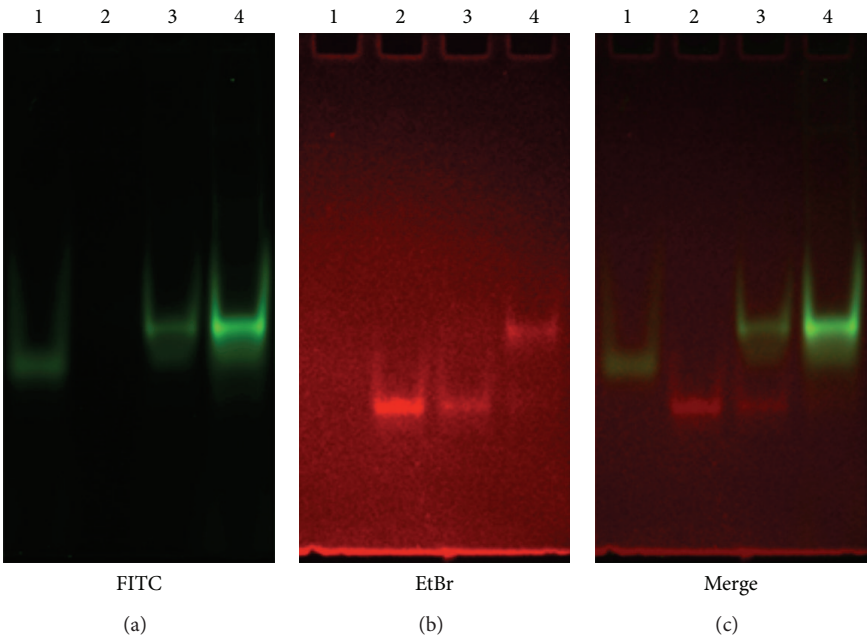


FIGURE 6: EMSA of PNA2 alone (lanes 1), miR-509-3p alone (lanes 2), miR-509-3p/PNA2 1:1.5 (lanes 3), and miR-509-3p/PNA2 1:5 (lanes 4) visualized by FITC (a) or EtBr (b) staining. The superimposition of FITC and EtBr stained gels is shown in (c).

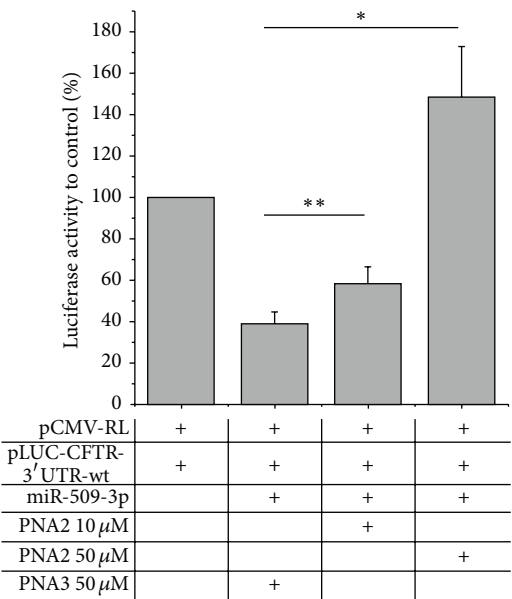


FIGURE 7: Inhibition of miR-509-3p effect by PNA2. Different doses of PNA2 were transfected in A549 cells. A significant inhibition of miR-509-3p was observed using PNA2 in a dose-dependent manner. * P values < 0.02, ** P values < 0.002. The 7-mer poly-thymine PNA3 had no effect on miR-509-3p.

4. Conclusions

Previously, we showed that the activity of the miR-509-3p miRNA, one of miRNAs involved in the posttranscriptional

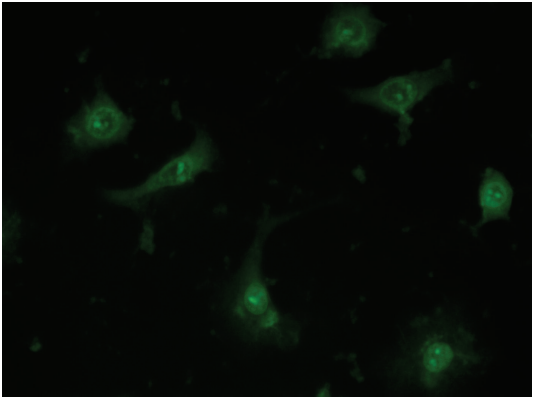


FIGURE 8: Representative uptake of FITC-labelled PNA2 by A549 cells.

regulation of CFTR gene of CF and CF-RD, could be inhibited through the use of the 14-mer PNA1 fully complementary to the first fourteen bases of miR-509-3p [37]. With this study, we demonstrate that the activity of miR-509-3p can be inhibited even with the use of a PNA as short as seven bases long targeting exclusively the seed region of the miRNA. This finding, probably due to the higher affinity of PNAs over RNAs towards the complementary RNA strand, further widens the interest towards the use of peptide nucleic acids as effective anti-miRNA agents, considering the number of advantages in terms of cost and time saving in the synthesis of the PNAs or for what attains their cellular uptake.

Conflict of Interests

The authors declare that there is no conflict of interests regarding the publication of this paper.

Acknowledgments

This work was financially supported by “Progetto FARO 2011” (Finanziamento per l’Avvio di Ricerche Originali) and PRIN Grant 2009 from the Italian Ministero dell’Università e della Ricerca. The authors are grateful to Dr. Luisa Cuorvo for her technical assistance.

References

- [1] L. He and G. J. Hannon, “MicroRNAs: small RNAs with a big role in gene regulation,” *Nature Reviews Genetics*, vol. 5, no. 7, pp. 522–531, 2004.
- [2] S. Griffiths-Jones, H. K. Saini, S. van Dongen, and A. J. Enright, “miRBase: tools for microRNA genomics,” *Nucleic Acids Research*, vol. 36, no. 1, pp. D154–D158, 2008.
- [3] M. Selbach, B. Schwanhäusser, N. Thierfelder, Z. Fang, R. Khanin, and N. Rajewsky, “Widespread changes in protein synthesis induced by microRNAs,” *Nature*, vol. 455, no. 7209, pp. 58–63, 2008.
- [4] Q. Jing, S. Huang, S. Guth et al., “Involvement of microRNA in AU-rich element-mediated mRNA instability,” *Cell*, vol. 120, no. 5, pp. 623–634, 2005.
- [5] J. Brennecke, A. Stark, R. B. Russell, and S. M. Cohen, “Silencing of microRNA families by seed-targeting tiny LNAs,” *Nature Genetics*, vol. 43, pp. 371–378, 2011.
- [6] G. Castaldo, F. Lembo, and R. Tomaiuolo, “Molecular diagnostics: between chips and customized medicine,” *Clinical Chemistry and Laboratory Medicine*, vol. 48, no. 7, pp. 973–982, 2010.
- [7] A. G. Bader, D. Brown, and M. Winkler, “The promise of microRNA replacement therapy,” *Cancer Research*, vol. 70, no. 18, pp. 7027–7030, 2010.
- [8] S. Costinean, N. Zanesi, Y. Pekarsky et al., “Pre-B cell proliferation and lymphoblastic leukemia/high-grade lymphoma in μ -miR155 transgenic mice,” *Proceedings of the National Academy of Sciences of the United States of America*, vol. 103, no. 18, pp. 7024–7029, 2006.
- [9] A. Rodriguez, E. Vigorito, S. Clare et al., “Requirement of bic/microRNA-155 for normal immune function,” *Science*, vol. 316, no. 5824, pp. 608–611, 2007.
- [10] P. N. Brown and H. Yin, “PNA-based microRNA inhibitors elicit anti-inflammatory effects in microglia cells,” *Chemical Communications*, vol. 49, pp. 4415–4417, 2013.
- [11] S. Ullah, P. John, and A. Bhatti, “MicroRNAs with a role in gene regulation and in human diseases,” *Molecular Biology Reports*, 2013.
- [12] Y. Li and K. V. Kowdley, “MicroRNAs in common human diseases,” *Genomics Proteomics Bioinformatics*, vol. 10, pp. 246–253, 2012.
- [13] I. McIntosh and G. R. Cutting, “Cystic fibrosis transmembrane conductance regulator and the etiology and pathogenesis of cystic fibrosis,” *FASEB Journal*, vol. 6, no. 10, pp. 2775–2782, 1992.
- [14] A. E. Gillen, N. Gosalia, S.-H. Leir, and A. Harris, “microRNA regulation of expression of the cystic fibrosis transmembrane conductance regulator gene,” *Biochemical Journal*, vol. 438, no. 1, pp. 25–32, 2011.
- [15] F. Amato, M. Seia, S. Giordano et al., “Gene mutation in microRNA target sites of CFTR gene: a novel pathogenetic mechanism in cystic fibrosis?” *PLoS ONE*, vol. 8, Article ID e60448, 2013.
- [16] E. van Rooij, A. L. Purcell, and A. A. Levin, “Developing MicroRNA therapeutics,” *Circulation Research*, vol. 110, no. 3, pp. 496–507, 2012.
- [17] E. van Rooij and E. N. Olson, “MicroRNA therapeutics for cardiovascular disease: opportunities and obstacles,” *Nature Reviews Drug Discovery*, vol. 11, pp. 860–872, 2012.
- [18] K. J. Rayner, C. C. Esau, F. N. Hussain et al., “Inhibition of miR-33a/b in non-human primates raises plasma HDL and lowers VLDL triglycerides,” *Nature*, vol. 478, no. 7369, pp. 404–407, 2011.
- [19] C. Esau, S. Davis, S. F. Murray et al., “miR-122 regulation of lipid metabolism revealed by in vivo antisense targeting,” *Cell Metabolism*, vol. 3, no. 2, pp. 87–98, 2006.
- [20] J. Elmén, M. Lindow, S. Schütz et al., “LNA-mediated microRNA silencing in non-human primates,” *Nature*, vol. 452, no. 7189, pp. 896–899, 2008.
- [21] R. E. Lanford, E. S. Hildebrandt-Eriksen, A. Petri et al., “Therapeutic silencing of microRNA-122 in primates with chronic hepatitis C virus infection,” *Science*, vol. 327, no. 5962, pp. 198–201, 2010.
- [22] E. Brognara, E. Fabbri, F. Aimi et al., “Peptide nucleic acids targeting miR-221 modulate p27Kip1 expression in breast cancer MDA-MB-231 cells,” *International Journal of Oncology*, vol. 41, pp. 2119–2127, 2012.
- [23] A. G. Torres, M. M. Fabani, E. Vigorito et al., “Chemical structure requirements and cellular targeting of microRNA-122 by peptide nucleic acids anti-miRs,” *Nucleic Acids Research*, vol. 40, no. 5, pp. 2152–2167, 2012.
- [24] M. M. Fabani, C. Abreu-Goodger, D. Williams et al., “Efficient inhibition of miR-155 function in vivo by peptide nucleic acids,” *Nucleic Acids Research*, vol. 38, no. 13, pp. 4466–4475, 2010.
- [25] P. E. Nielsen, M. Egholm, R. H. Berg, and O. Buchardt, “Sequence-selective recognition of DNA by strand displacement with thymine-substituted polyamide,” *Science*, vol. 254, no. 5037, pp. 1497–1500, 1991.
- [26] M. Pooga, T. Land, T. Bartfai, and Ü. Langel, “PNA oligomers as tools for specific modulation of gene expression,” *Biomolecular Engineering*, vol. 17, no. 6, pp. 183–192, 2001.
- [27] X. Zhang, T. Ishihara, and D. R. Corey, “Strand invasion by mixed base PNAs and a PNA-peptide chimera,” *Nucleic Acids Research*, vol. 28, no. 17, pp. 3332–3338, 2000.
- [28] S. A. Kushon, J. P. Jordan, J. L. Seifert, H. Nielsen, P. E. Nielsen, and B. A. Armitage, “Effect of secondary structure on the thermodynamics and kinetics of PNA hybridization to DNA hairpins,” *Journal of the American Chemical Society*, vol. 123, no. 44, pp. 10805–10813, 2001.
- [29] R. Besch, C. Giovannangeli, T. Schuh, C. Kammerbauer, and K. Degitz, “Characterization and quantification of triple helix formation in chromosomal DNA,” *Journal of Molecular Biology*, vol. 341, no. 4, pp. 979–989, 2004.
- [30] P. E. Nielsen, “Peptide Nucleic Acids (PNA) in chemical biology and drug discovery,” *Chemistry and Biodiversity*, vol. 7, no. 4, pp. 786–804, 2010.
- [31] J. Amato, M. I. Stellato, E. Pizzo et al., “PNA as a potential modulator of COL7A1 gene expression in dominant dystrophic

- epidermolysis bullosa: a physico-chemical study," *Molecular BioSystems*, 2013.
- [32] J. Amato, G. Oliviero, E. de Pauw, and V. Gabelica, "Hybridization of short complementary PNAs to G-quadruplex forming oligonucleotides: an electrospray mass spectrometry study," *Biopolymers*, vol. 91, no. 4, pp. 244–255, 2009.
- [33] J. Amato, B. Pagano, N. Borbone et al., "Targeting G-Quadruplex structure in the human c-Kit promoter with short PNA sequences," *Bioconjugate Chemistry*, vol. 22, no. 4, pp. 654–663, 2011.
- [34] M. Gaglione, G. Milano, A. Chambery, L. Moggio, A. Romanelli, and A. Messere, "PNA-based artificial nucleases as antisense and anti-miRNA oligonucleotide agents," *Molecular BioSystems*, vol. 7, no. 8, pp. 2490–2499, 2011.
- [35] A. Manicardi, E. Fabbri, T. Tedeschi et al., "Cellular uptakes, biostabilities and anti-miR-210 activities of chiral arginine-PNAs in leukaemic K562 cells," *ChemBioChem*, vol. 13, pp. 1327–1337, 2012.
- [36] M. Egholm, O. Buchardt, L. Christensen et al., "PNA hybridizes to complementary oligonucleotides obeying the Watson-Crick hydrogen-bonding rules," *Nature*, vol. 365, no. 6446, pp. 566–568, 1993.
- [37] F. Amato, R. Tomaiuolo, N. Borbone et al., "Design, synthesis and biochemical investigation, by in vitro luciferase reporter system, of peptide nucleic acids as new inhibitors of miR-509-3p involved in the regulation of cystic fibrosis disease-gene expression," *MedChemComm*, 2013.
- [38] S. Obad, C. O. dos Santos, A. Petri et al., "Silencing of microRNA families by seed-targeting tiny LNAs," *Nature Genetics*, vol. 43, no. 4, pp. 371–380, 2011.
- [39] D. M. Patrick, R. L. Montgomery, X. Qi et al., "Stress-dependent cardiac remodeling occurs in the absence of microRNA-21 in mice," *Journal of Clinical Investigation*, vol. 120, no. 11, pp. 3912–3916, 2010.
- [40] R. Lavery, M. Moakher, J. H. Maddocks, D. Petkeviciute, and K. Zakrzewska, "Conformational analysis of nucleic acids revisited: curves+," *Nucleic Acids Research*, vol. 37, no. 17, Article ID gkp608, pp. 5917–5929, 2009.
- [41] W. Humphrey, A. Dalke, and K. Schulten, "VMD: visual molecular dynamics," *Journal of Molecular Graphics*, vol. 14, no. 1, pp. 33–38, 1996.
- [42] E. Elkayam, C.-D. Kuhn, A. Tocilj et al., "The structure of human argonaute-2 in complex with miR-20a," *Cell*, vol. 150, pp. 100–110, 2012.
- [43] S. C. Brown, S. A. Thomson, J. M. Veal, and D. G. Davis, "NMR solution structure of a peptide nucleic acid complexed with RNA," *Science*, vol. 265, no. 5173, pp. 777–780, 1994.
- [44] V. Hornak, R. Abel, A. Okur, B. Strockbine, A. Roitberg, and C. Simmerling, "Comparison of multiple amber force fields and development of improved protein backbone parameters," *Proteins: Structure, Function and Genetics*, vol. 65, no. 3, pp. 712–725, 2006.
- [45] D.A. Case, T.A. Darden, T.E. Cheatham III et al., "AMBER 12," University of California, 2012.
- [46] J. M. Sanders, M. E. Wampole, C.-P. Chen et al., "Effects of hypoxanthine substitution in peptide nucleic acids targeting KRAS2 oncogenic mRNA molecules: theory and experiment," *The Journal of Physical Chemistry B*, 2013.
- [47] F.-Y. Dupradeau, C. Cézard, R. Lelong et al., "R.E.D.D.B.: a database for RESP and ESP atomic charges, and force field libraries," *Nucleic Acids Research*, vol. 36, no. 1, pp. D360–D367, 2008.
- [48] J. W. Craft Jr. and G. B. Legge, "An AMBER/DYANA/MOLMOL phosphorylated amino acid library set and incorporation into NMR structure calculations," *Journal of Biomolecular NMR*, vol. 33, no. 1, pp. 15–24, 2005.
- [49] R. Soliva, E. Sherer, F. J. Luque, C. A. Laughton, and M. Orozco, "Molecular dynamics simulations of PNA-DNA and PNA-RNA duplexes in aqueous solution," *Journal of the American Chemical Society*, vol. 122, no. 25, pp. 5997–6008, 2000.
- [50] J. Panecka, C. Mura, and J. Trylska, "Molecular dynamics of potential rRNA binders: single-stranded nucleic acids and some analogues," *Journal of Physical Chemistry B*, vol. 115, no. 3, pp. 532–546, 2011.

Research Article

Rapid Degradation of Hfq-Free RyhB in *Yersinia pestis* by PNPase Independent of Putative Ribonucleolytic Complexes

Zhongliang Deng,^{1,2} Zizhong Liu,² Yujing Bi,² Xiaoyi Wang,² Dongsheng Zhou,² Ruifu Yang,² and Yanping Han²

¹ Department of Sanitary Inspection, School of Public Health, University of South China, Hengyang, Hunan 421001, China

² State Key Laboratory of Pathogen and Biosecurity, Beijing Institute of Microbiology and Epidemiology, Beijing 100071, China

Correspondence should be addressed to Ruifu Yang; ruifuyang@gmail.com and Yanping Han; yanpinghan@gmail.com

Received 26 December 2013; Revised 10 March 2014; Accepted 15 March 2014; Published 10 April 2014

Academic Editor: Ammad Ahmad Farooqi

Copyright © 2014 Zhongliang Deng et al. This is an open access article distributed under the Creative Commons Attribution License, which permits unrestricted use, distribution, and reproduction in any medium, provided the original work is properly cited.

The RNA chaperone Hfq in bacteria stabilizes sRNAs by protecting them from the attack of ribonucleases. Upon release from Hfq, sRNAs are preferably degraded by PNPase. PNPase usually forms multienzyme ribonucleolytic complexes with endoribonuclease E and/or RNA helicase RhlB to facilitate the degradation of the structured RNA. However, whether PNPase activity on Hfq-free sRNAs is associated with the assembly of RNase E or RhlB has yet to be determined. Here we examined the roles of the main endoribonucleases, exoribonucleases, and ancillary RNA-modifying enzymes in the degradation of *Y. pestis* RyhB in the absence of Hfq. Expectedly, the transcript levels of both RyhB1 and RyhB2 increase only after inactivating PNPase, which confirms the importance of PNPase in sRNA degradation. By contrast, the signal of RyhB becomes barely perceptible after inactivating of RNase III, which may be explained by the increase in PNPase levels resulting from the exemption of *pnp* mRNA from RNase III processing. No significant changes are observed in RyhB stability after deletion of either the PNPase-binding domain of RNase E or *rhlB*. Therefore, PNPase acts as a major enzyme of RyhB degradation independent of PNPase-containing RNase E and RhlB assembly in the absence of Hfq.

1. Introduction

Small regulatory RNAs (sRNAs) function as posttranscriptional regulators by altering translation or stability of the target mRNA, which increases their applicability in different physiological processes in bacteria [1]. The RNA chaperone Hfq is hypothesized to facilitate the access of sRNAs to their mRNA targets and stabilize sRNAs by protecting them from the attack of RNase E [2]. Given that the increasing amount of available information on sRNA-induced mRNA decay is accumulating [3–6], the sRNA degradation processes and RNases that catalyze such activities must be investigated. The multienzyme assembly of RNA degradosome is important for mRNA decay and processing in *Escherichia coli*. RNase E and polynucleotide phosphorylase (PNPase) are two major components of the RNA degradation process [7, 8]. RNase E is also responsible for the rapid degradation of sRNAs and competes with Hfq in accessing the same RNA

sequences [9–11]. Hfq recruits RNase E by directly interacting with the RhlB-recognition region, which is hypothesized to cause the coupled cleavage of mRNA and sRNA [6, 12]. PNPase plays the protective role in the RNase E-dependent degradation in the presence of Hfq [13, 14]. Recent studies show that Hfq has a limited access to RNAs under wild-type conditions considering the dynamic interactions of Hfq with sRNAs [15–17]. A transient Hfq-free state of sRNAs may also be observed. A recent study shows that sRNAs are preferably degraded by the major exoribonuclease PNPase upon release from Hfq [14]. PNPase usually cooperates with RNase E in RNA degradation complexes [18]. RNA helicase RhlB usually facilitates RNA degradation by manipulating RNA structure and remodeling ribonucleoprotein complexes in the presence or absence of RNase E [19]. However, the relationship between the PNPase activity in Hfq-free sRNAs and RNA degradation complexes remains unknown.

TABLE 1: Bacterial strains used in this study.

Strains	Relevant characteristics	Sources or reference
WT	Wild-type strain 201	[24]
Δhfq	hfq^-	[25]
$\Delta hfq::hfq$	$hfq^-::pACYC184-hfq$	[25]
Δrnc	rnc^-	This study
$\Delta hfq-rne_{910}$	$hfq^- rne_{910-1061aa}^-$	This study
$\Delta hfq-rng$	$hfq^- rng^-$	This study
$\Delta hfq-rnc$	$hfq^- rnc^-$	This study
$\Delta hfq-pnp$	$hfq^- pnp^-$	This study
$\Delta hfq-rnb$	$hfq^- rnb^-$	This study
$\Delta hfq-rnr$	$hfq^- rnr^-$	This study
$\Delta hfq-pcnB$	$hfq^- pcnB^-$	This study
$\Delta hfq-rhlB$	$hfq^- rhlB^-$	This study
$\Delta hfq-rnc-rne_{910}$	$hfq^- rnc^- rne_{910-1061aa}^-$	This study
$\Delta hfq-rnc-rng$	$hfq^- rnc^- rng^-$	This study
$\Delta hfq-rnc-pnp$	$hfq^- rnc^- pnp^-$	This study
$\Delta hfq-rnc-rnb$	$hfq^- rnc^- rnb^-$	This study
$\Delta hfq-rnc-rnr$	$hfq^- rnc^- rnr^-$	This study
$\Delta hfq-rnc-rhlB$	$hfq^- rnc^- rhlB^-$	This study

The well-characterized sRNA RyhB was used as a model sRNA for this study. RyhB is an Hfq-binding sRNA that maintains iron homeostasis in bacteria [20, 21]. Besides Hfq, RyhB also becomes very stable when the overall mRNA transcription is stalled in *E. coli* [6]. Two RyhB homologs possessing the conserved core and *rho* sequences in *E. coli* [20] have also been characterized in *S. typhimurium* [22]. RyhB1 and RyhB2 are upregulated in the infected lungs of mice upon intranasal inoculation of *Yersinia pestis*, which indicates that they may serve as important functions during *Y. pestis* pathogenesis. The stability of RyhB1 and RyhB2 is differentially Hfq-dependent in *Y. pestis* grown under nutrient-limiting conditions [23]. This study constructs single or combined *hfq* mutant strains that lack various RNases or ancillary enzymes and monitors the expression level and degradation speeds of RyhB to investigate the effect of these enzymes on the degradation of Hfq-free RyhB.

2. Materials and Methods

2.1. Bacterial Strains and Growth Conditions. All strains are derivatives of *Y. pestis* strain 201, a newly established biovar, the *Microtus* [24]. Table 1 shows the bacterial strains that are used in this study. Except for the RNase E mutants, all mutant strains were constructed by replacing the entire gene with an antibiotic cassette via λ -Red homologous recombination. RNase E is essential for viability in bacteria, but deleting the C-terminal half (CTH) of this enzyme is not lethal [26]. The CTH after the 910th containing putative PNPase-binding site (1190-1221aa corresponding to 1021-1061aa in *E. coli* RNase E) [26] was deleted and designated as *rne*₉₁₀. Bacteria were grown to midexponential phase ($A_{620} \approx 1.0$) in BHI medium at 26°C. Iron depletion was induced by adding 100 μ M 2',2'-dipyridyl (DIP) for 20 min. Antibiotics were added

when needed at the following concentrations: 34 μ g/mL chloramphenicol, 50 μ g/mL kanamycin, 100 μ g/mL ampicillin, 20 μ g/mL gentamicin, and 20 μ g/mL streptomycin.

2.2. RNA Extraction and Northern Blotting Analysis. Pure bacterial cultures were mixed with RNAprotect Bacteria Reagent (Qiagen) to minimize RNA degradation. The total RNA was then extracted from *Y. pestis* using TRIzol Reagent (Invitrogen). Northern blotting analysis was performed by using a DIG Northern Starter Kit (Roche) according to the manufacturer's protocol described by Beckmann et al. [27]. RNA samples (3 μ g) were denatured at 70°C for 5 min, separated on 6% polyacrylamide-7M urea gel, and transferred onto Hybond N⁺ membranes (GE) via electroblotting. The membranes were UV-crosslinked and prehybridized for 1 hr, and 3'-end DIG-labeled RNA oligonucleotides were added. The membranes were then hybridized overnight at 68°C in a DIG Easy Hyb. RNA was immunologically detected and scanned according to the instructions. Multiple exposures to X-ray film were taken to achieve the desired signal strength.

2.3. RNA Half-Life Determination. Bacteria grown to exponential phase were treated with 250 μ g/mL rifampicin for RNA half-life determination. Culture samples were collected at 0, 5, 10, 20, 30, and 60 min and were subject to RNA extraction and Northern blotting. Films were scanned and RNA band intensity was measured using Quantity One software. The intensities were plotted and RNA half-lives were calculated using the slope from each plot.

2.4. Quantitative RT-PCR. Total RNA was isolated from different *Y. pestis* strains grown to exponential growth phase ($OD_{620} = 1.2$) in BHI by using Trizol Reagent (Invitrogen). DNA contaminants were removed by using DNA-free Kit

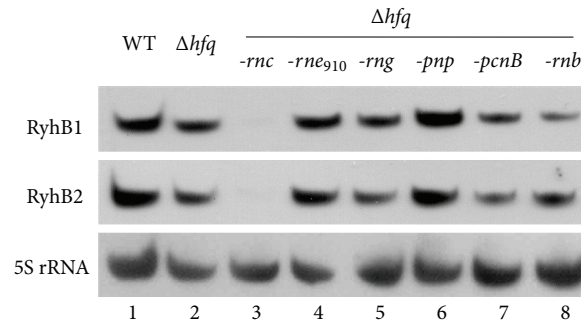


FIGURE 1: Effects of RNases and an ancillary RNA-modifying enzyme on the transcriptional level of *Y. pestis* RyhB1 and RyhB2 in the Δhfq background. RyhB1 and RyhB2 were detected by Northern blotting using 5 μ g of total RNA extracted from *Y. pestis* grown to exponential phase in BHI medium upon treatment with 100 μ M DIP treatment for 20 min. 5S rRNA was used as a negative control. Lanes 1–8 represent WT (lane 1), *hfq* mutant (lane 2), double mutants lacking *hfq*, and another gene encoding either endoribonucleases (RNase E₉₁₀, RNase G) (lanes 4 and 5), exoribonucleases (RNase III, PNPase, and RNase II) (lanes 3, 6, and 8), or ancillary RNA-modifying enzyme (polyA polymerase) (lane 7).

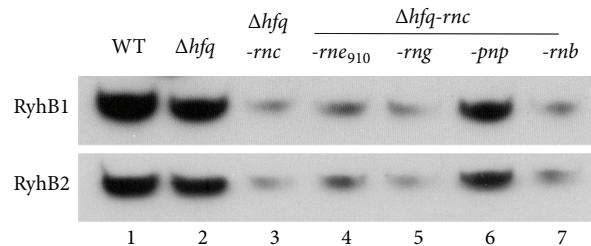


FIGURE 2: Effects of various ribonucleases on the transcriptional level of RyhB1 and RyhB2 upon inactivation of Hfq and RNase III. RyhB1 and RyhB2 were detected by Northern blotting using 5 μ g of total RNA extracted from *Y. pestis* grown to exponential phase in BHI medium upon treatment with 100 μ M DIP treatment for 20 min. Lanes 1–7 represent WT (lane 1), *hfq* mutant (lane 2), *hfq-rnc* double mutants (lane 3) and triple mutants lacking *hfq*, *rnc*, and another gene encoding RNase E₉₁₀ (lane 4), RNase G (lane 5), PNPase (lane 6), or RNase II (lane 7).

(Ambion), and the cDNA was converted by using random hexamer primers with the Superscript II system (Invitrogen). Real-time PCR was performed in duplicate for each RNA preparation by using the LightCycler system (Roche) with an appropriate dilution of cDNA as a template. Negative controls without reverse transcriptase enzyme were included in all experiments. Relative quantitative analysis across different cDNA templates was performed by using LightCycler 480 software (Bio-Rad) with the 16S rDNA as the normalized gene.

3. Results and Discussion

3.1. Influence of RNases and Ancillary RNA-Modifying Enzymes on the Regulation of Hfq-Free RyhB. BHI was selected as the growth medium for bacterial culture because some mutants that were constructed in this study experienced a slow growth upon inoculation into TMH medium, which pose a challenge to our experiments.

The expressions of RyhB1 and RyhB2 were monitored in multiple *hfq* mutants that lacked major RNases or ancillary RNA-modifying enzymes to validate the influence of

endoribonucleases, exoribonucleases, and ancillary RNA-modifying enzymes on RyhB regulation in *Y. pestis* without Hfq (Figure 1). The expression levels of RyhB1 and RyhB2 slightly increased (~1.8-fold) upon the deletion of PNPase, but no obvious changes were observed in the RNase E truncate and deletion strains of RNase G (*rng*), RNase II (*rnb*), or polyA polymerase (*pcnB*). In contrast, RyhB was rarely detected in the double mutants that lacked Hfq and RNase III (*rnc*).

The *rne* (910-1221aa), *rng*, *pnp*, and *rnb* genes were deleted from the double deletion mutant that lacked Hfq and RNase III to determine which RNases account for the degradation of RyhB1 and RyhB2, respectively (Figure 2). RyhB in the *hfq-rnc-pnp* mutant reached a similar amount of that in the *hfq* mutant, which indicates that PNPase was the main contributor in the degradation of Hfq-free RyhB [14].

The degradation of Hfq-free RyhB by PNPase tends to occur in stationary phase rather than exponential phase in *E. coli* [14]. However, the inactivation of PNPase in this study increased the RyhB levels in *Y. pestis* grown to exponential phase. Therefore, PNPase may degrade the Hfq-free RyhB in different growth-phase-dependent manners in *E. coli* and in *Y. pestis*. However, such discrepancy may also be due

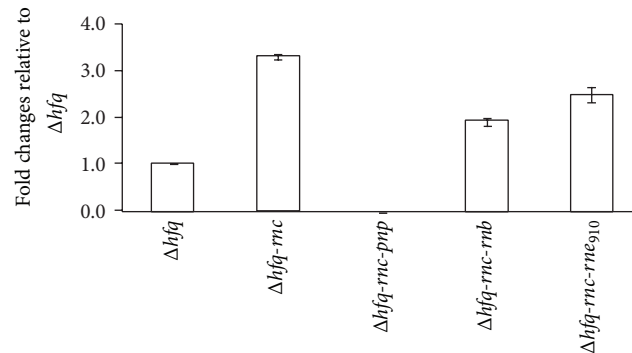


FIGURE 3: Expression levels of the *pnp* mRNA in multiple mutants of *Y. pestis* by using quantitative PCR. RNA samples were prepared from various mutants lacking Hfq and other ribonucleases grown to exponential phase in BHI medium. The relative abundance of the *pnp* mRNA was accessed by real-time PCR.

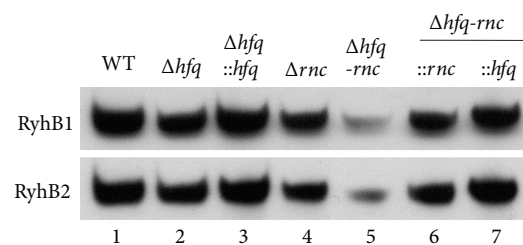


FIGURE 4: Effects of Hfq and RNase III on the transcriptional level of RyhB1 and RyhB2 in *Y. pestis*. Total RNAs were extracted from WT, *hfq/rnc* single or double mutants, and their complementary strains and then were subject to Northern blotting analysis.

to the different sample timing that was used in these two experiments. It would be helpful to make it clear if more time-point samplings are included in these experiments.

3.2. The RNase-III-Inactivation-Induced mRNA Level Increase of PNPase May Be Partially Responsible for the Degradation of Hfq-Free RyhB. Few amounts of *micA* could be also detected in the *hfq-rnc* double mutant of *E. coli* [14]. Andrade et al. explained this phenomenon as an impairment of RNase III activity that was caused by the decreased duplex in the absence of Hfq. However, this impairment cannot explain the obvious difference in RyhB expression between *hfq* and *hfq-rnc* double mutant. RNase III can alter gene expression by cleaving dsRNA or by binding without cleaving RNA [28]. RNase III has been proved to involve in the autoregulation of PNPase in *E. coli* by cleaving the 5' end of *pnp* mRNA [29]. However, the unprocessed *pnp* mRNA is accumulated and can be translated into polynucleotide phosphorylase in *E. coli rnc* mutant [29]. To determine if the inactivation of RNase III affected the expression of PNPase, quantitative PCR was performed to estimate the relative amounts of *pnp* mRNA in different mutants (Figure 3). The *pnp* gene was upregulated from 1.9- to 3.3-fold in *hfq-rnc* double and triple mutants than in the *hfq* mutant, which further confirmed that PNPase was the main exoribonuclease responsible for the degradation of *Y. pestis* RyhB in the absence of *hfq*. The RNase-III-inactivation-induced upregulation of PNPase could be partially responsible for the decreased expression of

RyhB (Figure 2). However, the effects of RNase III on RyhB stability could not be determined through other means.

3.3. PNPase Activity on RyhB in the Absence of RNase III Is Dependent on the State of Hfq Binding. RNase III affects the stability of the Hfq-dependent sRNA, *MicA*, in *Salmonella* [30]. The expression patterns of single and double mutants of *rnc* and *hfq* were compared via Northern blotting to examine the effects of RNase III and Hfq inactivation on the rapid degradation of RyhB. RyhB was rarely detected after inactivating both RNase III and Hfq. However, the amount of RyhB could reach modest levels in the *rnc* and *hfq* single mutants as well as in the complementary strains that carried the corresponding plasmids. Therefore, the PNPase activity on RyhB in the absence of RNase III depends on the state of Hfq binding (Figure 4). RyhB was rapidly degraded by the increased levels of PNPase in the absence of Hfq because of the RNase III inactivation.

3.4. Rapid Degradation of Hfq-Free RyhB by PNPase Is Independent of the PNPase-Containing RNase E or RhlB Assembly. RyhB1 was rapidly degraded, but RyhB2 retained its stability in the absence of *Y. pestis hfq* grown in TMH medium [23]. In *Y. pestis hfq* mutant grown in BHI medium, RyhB1 obtained a 22.8 min half-life whereas RyhB2 obtained a 54.3 min half-life (Figure 5). Although the Hfq-dependent stabilities of *Y. pestis* RyhB1 and RyhB2 remained different in this study, RyhB1 showed a significantly higher stability in bacterial cells that were grown in rich media (with $a > 20$ min half-life) than

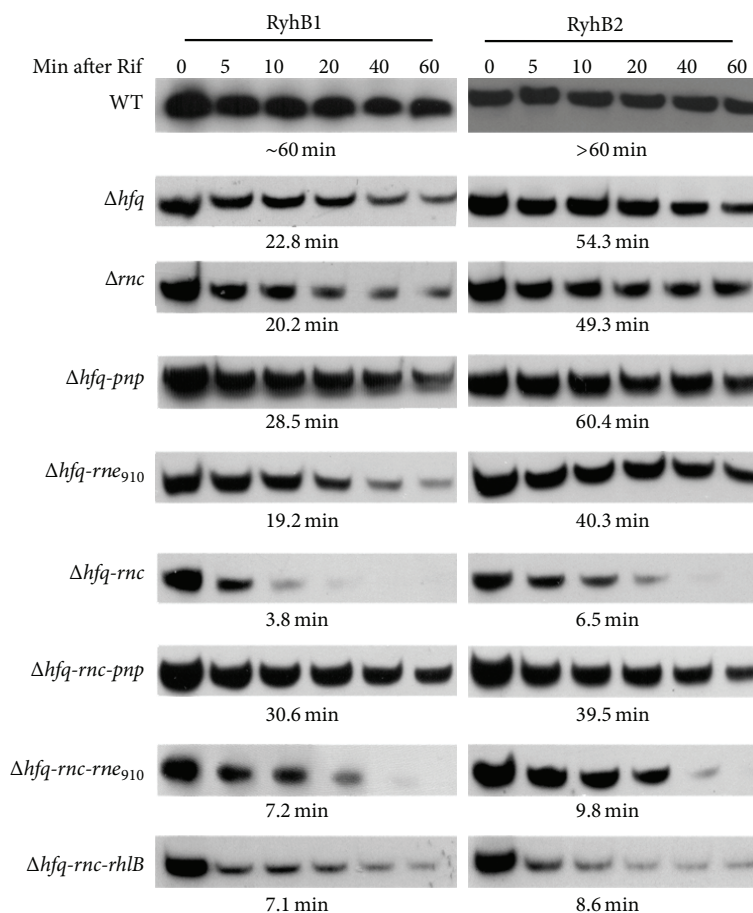


FIGURE 5: Effects of various RNases or ancillary RNA-modifying enzymes on RyhB stability in Hfq-lacking *Y. pestis*. Various mutants grown to exponential phase were treated with 250 μ g/mL of rifampicin. Culture samples were collected at 0, 5, 10, 20, 40, and 60 min and were subject to RNA extraction and Northern blotting, respectively.

in bacterial cells that were grown in minimal media (with ~8 min half-life). The half-lives of both RyhB1 and RyhB2 exceeded 60 min in a WT strain that was grown exponentially in BHI medium (data not shown), which indicated that the nutrition conditions would influence the stability of *Y. pestis* RyhB in the absence of Hfq.

The half-lives of RyhB in the *hfq-pnp* double mutant were investigated to verify the effects of PNPase on the degradation of Hfq-free RyhB (Figure 5). The stability of RyhB slightly increased in the *hfq-pnp* double mutant rather than in the *hfq* single mutant, which confirmed the role of PNPase in the degradation of Hfq-free RyhB. The *rnc* deletion mutation produced insignificant effects on the stability of RyhB with half-lives of 20.2 min and 49.3 min (Figure 5). However, the 14 min decrease in the half-life of RyhB2 in the *hfq-rne₉₁₀* double mutant remains unclear. The half-lives of RyhB dramatically reduced to 3.8 min and 6.5 min in the *hfq-rnc* double mutant, whereas the deletion of the *pnp* gene increased the half-life of RyhB to >30 min (Figure 5). Therefore, the RNase-III-induced PNPase increase might be responsible for the RyhB degradation in the absence of Hfq, and the PNPase served as the main enzyme in the degradation of Hfq-free RyhB.

PNPase usually forms multienzyme ribonucleolytic complexes with RNase E and/or RNA helicase RhlB during the degradation of the structured RNA [31, 32]. RNase E serves as a “scaffolding” protein of RNA degradosome that contains the binding sites of three major degradosome components, namely, PNPase, DEAD-box helicase RhlB, and enolase [8, 33]. RhlB facilitates the formation of single stranded RNA, which helps PNPase to engage in the 3' to 5' exoribonucleolytic degradation of RNA [15]. PNPase directly interacts with RhlB by forming the transient complex, which is not dependent on the formation of the degradosome [34]. Therefore, this study tries to determine if RNase E degradosome is involved in PNPase activity on Hfq-free RyhB. Given that the deletion of the *rne* gene in the encoding of RNase E is lethal, an *rne* mutant without PNP-binding domain was constructed in this study to produce an RNase E protein that was unassociated with PNPase.

The Northern blotting analysis revealed that the mutation of *rne* and *rhlB* had a > 7 min half-life in the *hfq-rnc* mutant, but its stability was substantially lower than that upon PNPase inactivation (Figure 5). Therefore, the PNPase-containing degradosome or exosome plays minor roles in Hfq-free RyhB decay, and PNPase might be involved in these

processes by itself or through other unknown mechanisms. Therefore, the degradation of Hfq-free sRNAs is far more complex than what was previously expected. An extended analysis should be performed to check if these results could be applied to other sRNAs.

Conflict of Interests

The authors declare that there is no conflict of interests regarding the publication of this paper.

Authors' Contribution

Zhongliang Deng and Zizhong Liu contributed equally to this work.

Acknowledgments

This study was funded by the National Natural Science Foundation of China (31171248) and the National Basic Research Program of China (2014CB744405).

References

- [1] G. Storz, J. Vogel, and K. M. Wassarman, "Regulation by small RNAs in bacteria: expanding frontiers," *Molecular Cell*, vol. 43, no. 6, pp. 880–891, 2011.
- [2] T. Morita and H. Aiba, "RNase E action at a distance: degradation of target mRNAs mediated by an Hfq-binding small RNA in bacteria," *Genes and Development*, vol. 25, no. 4, pp. 294–298, 2011.
- [3] K. J. Bandyra, N. Said, V. Pfeiffer, M. W. Gorna, J. Vogel, and B. F. Luisi, "The seed region of a small RNA drives the controlled destruction of the target mRNA by the endoribonuclease RNase E," *Molecular Cell*, vol. 47, pp. 943–953, 2012.
- [4] K. Prévost, G. Desnoyers, J.-F. Jacques, F. Lavoie, and E. Massé, "Small RNA-induced mRNA degradation achieved through both translation block and activated cleavage," *Genes and Development*, vol. 25, no. 4, pp. 385–396, 2011.
- [5] A. J. Carpousis, "Degradation of targeted mRNAs in *Escherichia coli*: regulation by a small antisense RNA," *Genes and Development*, vol. 17, no. 19, pp. 2351–2355, 2003.
- [6] E. Massé, F. E. Escorcia, and S. Gottesman, "Coupled degradation of a small regulatory RNA and its mRNA targets in *Escherichia coli*," *Genes and Development*, vol. 17, no. 19, pp. 2374–2383, 2003.
- [7] A. J. Carpousis, "The RNA degradosome of *Escherichia coli*: an mRNA-degrading machine assembled on RNase E," *Annual Review of Microbiology*, vol. 61, pp. 71–87, 2007.
- [8] J. A. R. Worrall, M. Góna, N. T. Crump et al., "Reconstitution and analysis of the multienzyme *Escherichia coli* RNA degradosome," *Journal of Molecular Biology*, vol. 382, no. 4, pp. 870–883, 2008.
- [9] I. Moll, T. Afonyushkin, O. Vytvytska, V. R. Kabardin, and U. Bläsi, "Coincident Hfq binding and RNase E cleavage sites on mRNA and small regulatory RNAs," *RNA*, vol. 9, no. 11, pp. 1308–1314, 2003.
- [10] K. S. Frohlich, K. Papenfort, A. Fekete, and J. Vogel, "A small RNA activates CFA synthase by isoform-specific mRNA stabilization," *The EMBO Journal*, vol. 32, pp. 2963–2979, 2013.
- [11] M. Folichon, V. Arluison, O. Pellegrini, E. Huntzinger, P. Régnier, and E. Hajnsdorf, "The poly(A) binding protein Hfq protects RNA from RNase E and exoribonucleolytic degradation," *Nucleic Acids Research*, vol. 31, no. 24, pp. 7302–7310, 2003.
- [12] Y. Ikeda, M. Yagi, T. Morita, and H. Aiba, "Hfq binding at RhlB-recognition region of RNase E is crucial for the rapid degradation of target mRNAs mediated by sRNAs in *Escherichia coli*," *Molecular Microbiology*, vol. 79, no. 2, pp. 419–432, 2011.
- [13] N. de Lay and S. Gottesman, "Role of polynucleotide phosphorylase in sRNA function in *Escherichia coli*," *RNA*, vol. 17, no. 6, pp. 1172–1189, 2011.
- [14] J. M. Andrade, V. Pobre, A. M. Matos, and C. M. Arraiano, "The crucial role of PNPase in the degradation of small RNAs that are not associated with Hfq," *RNA*, vol. 18, no. 4, pp. 844–855, 2012.
- [15] P.-H. Lin and S. Lin-Chao, "RhlB helicase rather than enolase is the β -subunit of the *Escherichia coli* polynucleotide phosphorylase (PNPase)-exoribonucleolytic complex," *Proceedings of the National Academy of Sciences of the United States of America*, vol. 102, no. 46, pp. 16590–16595, 2005.
- [16] A. Fender, J. Elf, K. Hampel, B. Zimmermann, and E. G. H. Wagner, "RNAs actively cycle on the Sm-like protein Hfq," *Genes and Development*, vol. 24, no. 23, pp. 2621–2626, 2010.
- [17] K. Moon and S. Gottesman, "Competition among Hfq-binding small RNAs in *Escherichia coli*," *Molecular Microbiology*, vol. 82, no. 6, pp. 1545–1562, 2011.
- [18] A. J. Carpousis, "The *Escherichia coli* RNA degradosome: structure, function and relationship in other ribonucleolytic multienzyme complexes," *Biochemical Society Transactions*, vol. 30, no. 2, pp. 150–155, 2002.
- [19] G.-G. Liou, H.-Y. Chang, C.-S. Lin, and S. Lin-Chao, "Dead box RhlB RNA helicase physically associates with exoribonuclease PNPase to degrade double-stranded RNA independent of the degradosome-assembling region of RNase E," *Journal of Biological Chemistry*, vol. 277, no. 43, pp. 41157–41162, 2002.
- [20] E. Massé and S. Gottesman, "A small RNA regulates the expression of genes involved in iron metabolism in *Escherichia coli*," *Proceedings of the National Academy of Sciences of the United States of America*, vol. 99, no. 7, pp. 4620–4625, 2002.
- [21] T. A. Geissmann and D. Touati, "Hfq, a new chaperoning role: binding to messenger RNA determines access for small RNA regulator," *The EMBO Journal*, vol. 23, no. 2, pp. 396–405, 2004.
- [22] G. Padalon-Brauch, R. Hershberg, M. Elgrably-Weiss et al., "Small RNAs encoded within genetic islands of *Salmonella typhimurium* show host-induced expression and role in virulence," *Nucleic Acids Research*, vol. 36, no. 6, pp. 1913–1927, 2008.
- [23] Z. Deng, X. Meng, S. Su et al., "Two sRNA RyhB homologs from *Yersinia pestis* biovar microtus expressed in vivo have differential Hfq-dependent stability," *Research in Microbiology*, vol. 163, pp. 413–418, 2012.
- [24] D. Zhou, Z. Tong, Y. Song et al., "Genetics of metabolic variations between *Yersinia pestis* biovars and the proposal of a new biovar, microtus," *Journal of Bacteriology*, vol. 186, no. 15, pp. 5147–5152, 2004.
- [25] J. Geng, Y. Song, L. Yang et al., "Involvement of the post-transcriptional regulator Hfq in *Yersinia pestis* virulence," *PLoS ONE*, vol. 4, no. 7, Article ID e6213, 2009.
- [26] A. Leroy, N. F. Vanzo, S. Sousa, M. Dreyfus, and A. J. Carpousis, "Function in *Escherichia coli* of the non-catalytic part of RNase E: role in the degradation of ribosome-free mRNA," *Molecular Microbiology*, vol. 45, no. 5, pp. 1231–1243, 2002.

- [27] B. M. Beckmann, A. Grünweller, M. H. W. Weber, and R. K. Hartmann, "Northern blot detection of endogenous small RNAs (~14 nt) in bacterial total RNA extracts," *Nucleic Acids Research*, vol. 38, no. 14, p. e147, 2010.
- [28] D. Drider and C. Condon, "The continuing story of endoribonuclease III," *Journal of Molecular Microbiology and Biotechnology*, vol. 8, no. 4, pp. 195–200, 2005.
- [29] C. Portier, L. Dondon, M. Grunberg-Manago, and P. Régnier, "The first step in the functional inactivation of the *Escherichia coli* polynucleotide phosphorylase messenger is a ribonuclease III processing at the 5' end," *The EMBO Journal*, vol. 6, no. 7, pp. 2165–2170, 1987.
- [30] S. C. Viegas, I. J. Silva, M. Saramago, S. Domingues, and C. M. Arraiano, "Regulation of the small regulatory RNA MicA by ribonuclease III: a target-dependent pathway," *Nucleic Acids Research*, vol. 39, no. 7, pp. 2918–2930, 2011.
- [31] V. R. Kabardin, D. Singh, and S. Lin-Chao, "Composition and conservation of the mRNA-degrading machinery in bacteria," *Journal of Biomedical Science*, vol. 18, no. 1, article 23, 2011.
- [32] I. J. Silva, M. Saramago, C. Dressaire, S. Domingues, S. C. Viegas, and C. M. Arraiano, "Importance and key events of prokaryotic RNA decay: the ultimate fate of an RNA molecule," *Wiley Interdisciplinary Reviews*, vol. 2, no. 6, pp. 818–836, 2011.
- [33] L. Dominguez-Malfavon, L. D. Islas, B. F. Luisi, R. Garcia-Villegas, and J. Garcia-Mena, "The assembly and distribution in vivo of the *Escherichia coli* RNA degradosome," *Biochimie*, vol. 95, no. 11, pp. 2034–2041, 2013.
- [34] S. Lin-Chao, N.-T. Chiou, and G. Schuster, "The PNPase, exosome and RNA helicases as the building components of evolutionarily-conserved RNA degradation machines," *Journal of Biomedical Science*, vol. 14, no. 4, pp. 523–532, 2007.

Research Article

Synthesis and Gene Silencing Properties of siRNAs Containing Terminal Amide Linkages

Maria Gaglione,¹ M. Emilia Mercurio,¹ Nicoletta Potenza,¹ Nicola Mosca,¹ Aniello Russo,¹ Ettore Novellino,² Sandro Cosconati,¹ and Anna Messere¹

¹ *Dipartimento Scienze e Tecnologie Ambientali, Biologiche e Farmaceutiche, Seconda Università degli Studi di Napoli, Via Vivaldi 43, 81100 Caserta, Italy*

² *Dipartimento di Chimica Farmaceutica e Tossicologica, Università "Federico II," Via D. Montesano 49, 80131 Napoli, Italy*

Correspondence should be addressed to Sandro Cosconati; sandro.cosconati@unina2.it and Anna Messere; anna.messere@unina2.it

Received 10 December 2013; Accepted 23 January 2014; Published 26 March 2014

Academic Editor: Daniela De Stefano

Copyright © 2014 Maria Gaglione et al. This is an open access article distributed under the Creative Commons Attribution License, which permits unrestricted use, distribution, and reproduction in any medium, provided the original work is properly cited.

The active components of the RNAi are 21 nucleotides long dsRNAs containing a 2 nucleotide overhang at the 3' end, carrying 5'-phosphate and 3'-hydroxyl groups (siRNAs). Structural analysis revealed that the siRNA is functionally bound at both ends to RISC. Terminal modifications are considered with interest as the introduction of chemical moieties interferes with the 3' overhang recognition by the PAZ domain and the 5'-phosphate recognition by the MID and PIWI domains of RISC. Herein, we report the synthesis of modified siRNAs containing terminal amide linkages by introducing hydroxyethylglycine PNA (*heg*PNA) moieties at 5', and at 3' positions and on both terminals. Results of gene silencing studies highlight that some of these modifications are compatible with the RNAi machinery and markedly increase the resistance to serum-derived nucleases even after 24 h of incubation. Molecular docking simulations were attained to give at atomistic level a clearer picture of the effect of the most performing modifications on the interactions with the human Argonaute 2 PAZ, MID, and PIWI domains. This study adds another piece to the puzzle of the heterogeneous chemical modifications that can be attained to enhance the silencing efficiency of siRNAs.

1. Introduction

RNA interference (RNAi) has come into the limelight in the antisense world following the discoveries of Mello and colleagues [1] that double-stranded RNAs (dsRNAs) can elicit potent degradation of targeted mRNA sequences in *C. elegans* and in mammalian cells [2, 3]. The active components of the RNAi are small interfering RNAs (siRNAs), 21-22 nucleotides long dsRNA. These short species are naturally produced by Dicer-mediated cleavage of larger dsRNAs and they contain a 2 nucleotide (nt) overhang at the 3' end, a 5' phosphate and a 3'-hydroxyl group [2, 4]. Synthetic siRNAs can also be introduced into cells in order to experimentally activate RNAi [2]. siRNA duplexes with 5'-hydroxyl ends are rapidly phosphorylated in cells by the cellular kinase Clp1 [5], then the siRNA strand with the thermodynamically less stable 5' end is preferentially incorporated as the guiding or antisense

strand (AS) in the RNA-induced silencing complex (RISC) [6], while the passenger or sense strand (SS) of the siRNA duplex is cleaved by the human Argonaute 2 protein (hAgo 2) and liberated from the complex [7]. The selection of the guide strand is then based on the thermodynamic stability of the siRNA duplex ends, the strand that is always the one whose 5' end is less tightly paired to its complement. When the siRNA is fully base paired, the local thermodynamic difference (thermodynamic asymmetry) between the two 5' ends favors assembly into RISC of the strand with the lower internal stability at 5' end.

The Argonaute proteins are, indeed, core components of RISC and are made up by PAZ, Mid, and PIWI domains. X-ray structural analysis [8, 9] revealed that the siRNA is bound at both ends: the 5' end to the MID domain with some contributions from the PIWI domain and the 3' end to the PAZ domain. The seed sequence is located in

a narrow portion of the RNA binding groove. Endogenous pre-microRNAs, transcribed by cellular RNA polymerase II as single-stranded hairpin-loop RNAs, are also cleaved by Dicer to yield microRNA (miRNA) duplexes. These molecules are further processed as described for the siRNAs and incorporated in RISC by association of their guide strand to hAgo 2. Mature miRNAs play crucial roles in the regulation of gene expression during development and cell differentiation [10]. In addition, recent studies indicate that they are important regulators of virus-host interactions [11, 12].

Given its reliability and ease of use, RNAi has become the most widely used technology in functional genomics studies *in vitro* and in several model organisms. Nevertheless, to translate this potential into a broad new family of therapeutics, it is necessary to optimize the efficacy of the RNA-based drugs [13]. It might be possible to achieve this optimization using chemical modifications that improve, just like for antisense oligonucleotides (ASOs) [14], their *in vivo* stability, cellular delivery, biodistribution, pharmacokinetic, potency, and specificity [15]. In this respect, a rational design of effective chemically modified siRNA must consider as a general principle that the two strands of siRNA function differently and as practical hint that the nucleotides are different according to positions and nature. The 3' and 5' ends of siRNAs are critical determinants of their capacity to interfere with the unwinding of the duplex, of the incorporation of the siRNA into RISC, and of the rate of target cleavage and product release. The modifications in the terminal positions are considered with interest because the introduction of chemical moieties in these regions interferes with 3' overhang recognition by the PAZ domain [8, 16] and 5'-phosphate recognition by the MID domain of RISC [17, 18].

Peptide Nucleic Acids (PNAs) are oligonucleotide mimics in which the sugar-phosphate backbone has been replaced by a pseudo-peptide backbone [19]. When used in antisense constructs, PNA confers chemical and enzymatic stability and high affinity towards complementary DNA and RNA [19, 20]. Nonetheless, PNA have limited solubility and tendency to aggregate and are not easily internalized into cells, whereas oligonucleotide PNA (ON-PNA) chimeras are molecules with high solubility and increased capacity to cross biological membranes as compared to canonical PNA. Chimeric molecules in which tracts of DNA are bound to N and/or C terminus of PNA have been widely reported [21–31]. Differently from DNA-PNA chimeras, not many studies have been conducted on RNA-PNA chimeras. So far, few results have been reported for the use of RNA-PNA chimeras in RNAi, even if the advantage of mixing peptide and nucleic acids bonds has been demonstrated [27, 32–34].

In this paper we describe the synthesis of modified siRNAs containing terminal amide linkages (Figure 1). RNA-5'-PNA-OH (siRNA 2–4, Table 1) and RNA-5'-PNA-O-phosphate (siRNA 8–10, Table 1) were synthesized with the aim to study the impact of hydroxyethylglycine backbone (*heg*PNA) on silencing activity. The effect of *heg*PNA on both 5' and 3' ends of the siRNAs was also investigated by synthesizing PNA-3'-RNA-5'-PNA-OH (siRNA 5–7, Table 1) and PNA-3'-RNA-5'-PNA-O-phosphate (siRNA 11–13, Table 1).

Modified siRNAs containing *heg*PNA at 5' and at 3', 5' ends were then compared with chimeric 3'-PNA-OH siRNAs (siRNA 17–19, Table 1). At last, we introduced a new modification into siRNA consisting of a *heg*PNA monomer inserted at 5' end of RNA domain by phosphodiester linkage and having at the C-terminus a methylamide function (herein referred as “5'-capped” siRNAs, 14–16 in Table 1). The biostability of 2–19 was investigated through incubation in 100% fetal bovine serum (FBS), revealing that PNA moieties on both strands of the siRNA markedly increase the resistance to serum-derived nucleases. Gene silencing studies performed in HeLa cells highlighted that the amide linkage is compatible with the RNAi machinery when placed at 3' end of siRNA, in some cases improving its performances. On the other hand, amide linkage dramatically decreased the interference activity when located at 5' or at both 3' and 5' regions of siRNAs. Interestingly, “5'-capped” siRNAs partially restored the interfering effect. Finally, molecular docking simulations were engaged to give a picture of the interactions of the most performing modifications with the hAgo 2 protein.

2. Materials and Methods

2.1. Materials and Apparatus. SynBase CPG solid supports loading 0.040 and 0.10 meq g⁻¹, 2'-OTBDMS-RNA phosphoramidite, PNA monomers, and standard RNA-synthesis reagents (Acetonitrile external wash (wash A), Amidite diluent, Activator solution, Cap A, Cap B, Acetonitrile wash B, Oxidizer) were purchased from Link Technologies (Lanarkshire, Scotland). Standard PNA-synthesis reagents (PyBop activator, HOBt, Base solution, Cap solution, Piperidine, Deblock solution, DMF, wash B) were from Novabiochem. DMF external wash (wash A, 0.01% H₂O) was from LabScan. All other reagents and solvents were from Sigma-Aldrich. Solid phase synthesis was performed on an ABI Expedite 8909 oligo synthesizer using standard and modified protocols. HPLC chromatographic analyses and purifications were performed on Nucleogel SAX (Macherey-Nagel, 1000-8/46) and RP-18 (Waters, C-18, 3.9 × 300 mm) columns using a Waters 600 Controller, equipped with the diode array detector Waters 996 and with Millennium software. For column chromatography, silica gel 60 (0.040–0.063 mm) from Merck was used. Centrifugations were performed on a Z 200 A Hermle centrifuge. Samples were lyophilized by FD4 Freeze Dryer (Heto Lab Equipment). All conjugates were analyzed by MALDI TOF mass spectrometry using a MALDI-TOF micro MX (Waters Co., Manchester, UK), equipped with a pulsed nitrogen laser ($\lambda = 337$ nm). All measurements were performed using the negative detection mode. All spectra were processed and analyzed using the MassLynx 4.1 software (Waters, Milford, MA USA). LC ESI-MS analyses were performed on a MSQ mass spectrometer (ThermoElectron, Milan, Italy) equipped with an ESI source operating at 3 kV needle voltage ($T = 320^\circ\text{C}$) and with a complete Surveyor HPLC system, comprising a MS pump, an autosampler, and a PDA detector. All buffers were prepared from highly purified Milli Q water and made RNase-free by treatment with DEPC (diethylpyrocarbonate) (Sigma Aldrich). UV measurements

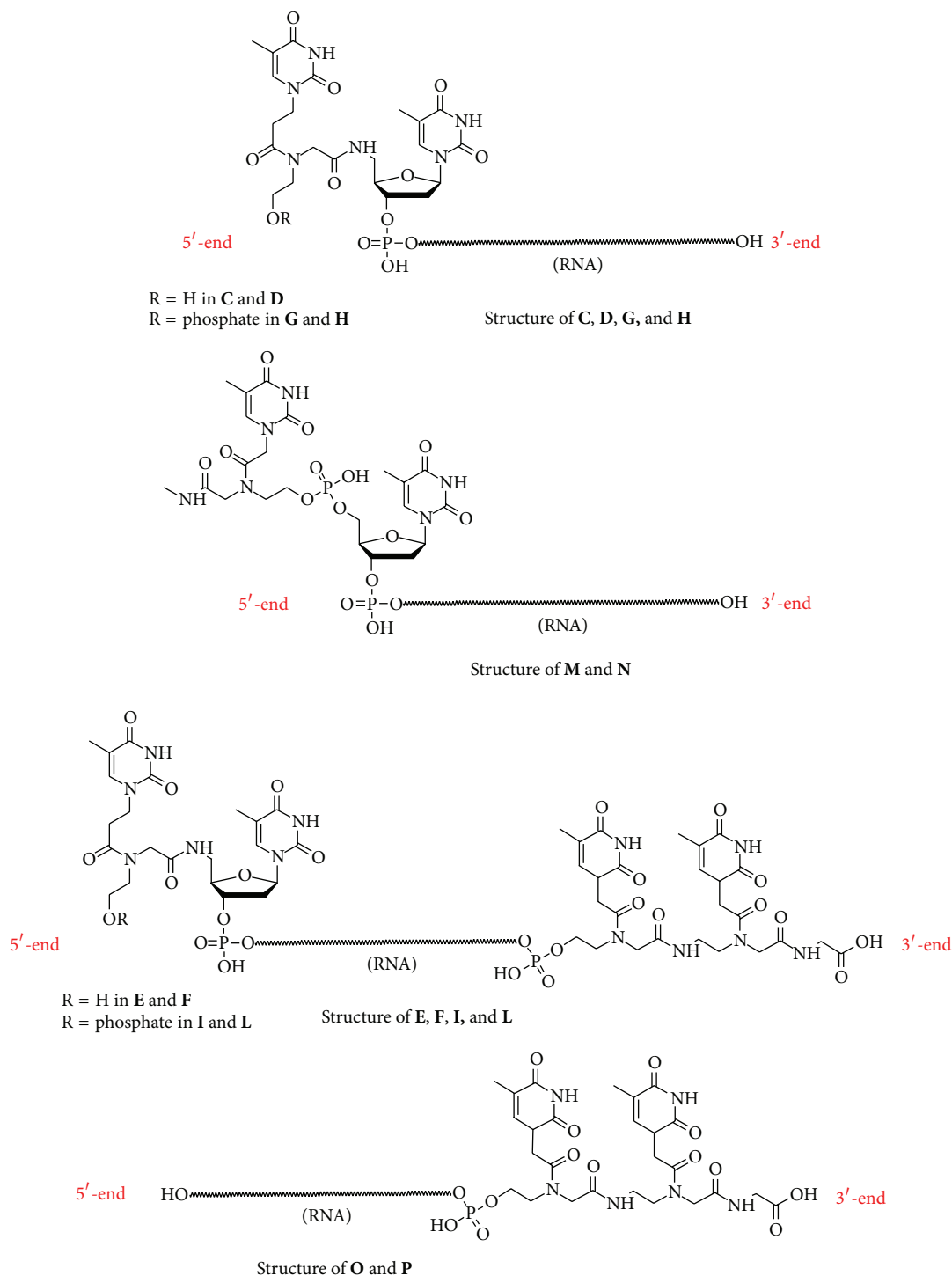


FIGURE 1: Structure of the RNA oligomers forming modified siRNAs 2–19.

and melting curves of duplexes ($1.0 \mu\text{M}$) were acquired on a Jasco V-550 spectrophotometer equipped with a Jasco ETC-505T Peltier temperature programmer using a 1 cm path-length quartz cell (Hellma). The concentrations were estimated spectrophotometrically at 90°C using the following additive molar extinction coefficient $\epsilon^{260} (\text{L cm}^{-1} \text{mol}^{-1})$, $T = 8800$, $A = 15400$, $C = 7200$, $G = 11500$, and $U = 9900$ for the

natural nucleobases and $t = 8600$ for the PNA monomers. Oligomers were suspended in RNase-free annealing buffer (100 mM potassium acetate, 30 mM Hepes-KOH, pH = 7.4, and 2 mM magnesium acetate) and equimolar ratios of the sense and antisense strands were annealed to form the duplexes to a final concentration of $25 \mu\text{M}$ by incubation at 90°C for 1 min and gradually cooling to room temperature.

TABLE 1

	siRNA sequence	siRNAs	Tm °C	Δ
a	AS 3'TTGCAUGC GCCUUAUGAAGCU5'	siRNA 1 wt	76	—
b	SS 5'CGUACGCGGAAUACUUCGATT3'			
C	3'TTGCAUGC GCCUUAUGAAGCT ^{NHCO₂OH} 5'	siRNA 2	65	-11
b	5'CGUACGCGGAAUACUUCGATT3'			
a	3'TTGCAUGC GCCUUAUGAAGCU5'	siRNA 3	65	-11
D	5' ^{OH} _t ^{CONH} -TCGUACGCGGAAUACUUCGATT3'			
C	3'TTGCAUGC GCCUUAUGAAGCT ^{NHCO₂OH} 5'	siRNA 4	65	-11
D	5' ^{OH} _t ^{CONH} -TCGUACGCGGAAUACUUCGATT3'			
E	3' <i>tt</i> GCAUGC GCCUUAUGAAGCT ^{NHCO₂OH} 5'	siRNA 5	66	-10
b	5'CGUACGCGGAAUACUUCGATT3'			
a	3'TTGCAUGC GCCUUAUGAAGCU5'	siRNA 6	66	-10
F	5' ^{OH} _t ^{CONH} -TCGUACGCGGAAUACUUCGATT3'			
E	3' <i>tt</i> GCAUGC GCCUUAUGAAGCT ^{NHCO₂OH} 5'	siRNA 7	66	-10
F	5' ^{OH} _t ^{CONH} -TCGUACGCGGAAUACUUCGATT3'			
G	3'TTGCAUGC GCCUUAUGAAGCT ^{NHCO₂OP} 5'	siRNA 8	67	-9
b	5'CGUACGCGGAAUACUUCGATT3'			
a	3'TTGCAUGC GCCUUAUGAAGCU5'	siRNA 9	66	-10
H	5' ^{PO₃} _t ^{CONH} -TCGUACGCGGAAUACUUCGATT3'			
G	3'TTGCAUGC GCCUUAUGAAGCT ^{NHCO₂OP} 5'	siRNA 10	67	-9
H	5' ^{PO₃} _t ^{CONH} -TCGUACGCGGAAUACUUCGATT3'			
I	3' <i>tt</i> GCAUGC GCCUUAUGAAGCT ^{NHCO₂OP} 5'	siRNA 11	66	-10
b	5'CGUACGCGGAAUACUUCGATT3'			
a	3'TTGCAUGC GCCUUAUGAAGCU5'	siRNA 12	68	-8
L	5' ^{PO₃} _t ^{CONH} -TCGUACGCGGAAUACUUCGATT3'			
I	3' <i>tt</i> GCAUGC GCCUUAUGAAGCT ^{NHCO₂OP} 5'	siRNA 13	66	-10
L	5' ^{PO₃} _t ^{CONH} -TCGUACGCGGAAUACUUCGATT3'			
M	3'TTGCAUGC GCCUUAUGAAGCT _t ^{CONHCH₃} 5'	siRNA 14	70	-6
b	5'CGUACGCGGAAUACUUCGATT3'			
a	3'TTGCAUGC GCCUUAUGAAGCU5'	siRNA 15	68	-8
N	5' ^{CH₃NHCO₂} _t -TCGUACGCGGAAUACUUCGATT3'			
M	3'TTGCAUGC GCCUUAUGAAGCT _t ^{CONHCH₃} 5'	siRNA 16	70	-6
N	5' ^{CH₃HNCO₂} _t -TCGUACGCGGAAUACUUCGATT3'			
O	3' <i>tt</i> GCAUGC GCCUUAUGAAGCU5'	siRNA 17	76	—
b	5'CGUACGCGGAAUACUUCGATT3'			
a	3'TTGCAUGC GCCUUAUGAAGCU5'	siRNA 18	76	—
P	5'CGUACGCGGAAUACUUCGATT3'			
O	3' <i>tt</i> GCAUGC GCCUUAUGAAGCU5'	siRNA 19	76	—
P	5'CGUACGCGGAAUACUUCGATT3'			

Melting curves were recorded at 260 nm using a heating rate of 0.5°C/min, a slit of 2 nm, and a response of 0.2 s. T_m values were obtained from the maxima of the first derivatives of the melting curves. Circular Dichroism spectra of the siRNA samples (1.0 μM) were recorded at 15°C using a 1 cm quartz cell in the Jasco J-815 spectropolarimeter equipped with a PFD-425S thermal controller unit. ³¹P NMR spectrum was recorded at 161.98 MHz on a Bruker WM-400 spectrometer using 85% H₃PO₄ as external standard.

2.2. General Procedures for RNA Oligomers Synthesis. All oligomers were synthesized on ABI Expedite 8909 oligo

synthesizer by using standard and modified protocols (1 μM scale), 2'-OTBDMS-RNA phosphoramidite monomers, and standard RNA synthesis reagents. Unmodified RNAs **a** and **b** were prepared on SynBase CPG solid support (CPG-OH, loading 0.04 meq g⁻¹) (a: calculated mass 6646.1, found 6645.9; b: calculated mass 6669.1, found 6667.8).

The RNA oligomers **C** and **D** were synthesized using last coupling monomer 5'-MMT-amino-T phosphoramidite. After deprotection (2% DCA in DCM), the 5'-amino group of oligomer was coupled to 2-(N-(2-((4-methoxyphenyl)diphenylmethoxy)ethyl)-2-(5-methyl-2,4-dioxo-3,4-dihydropyrimidin-1(2H)-yl)acetamido) acetic acid (0.2 M in

DMF) [35] by using a solution 0.2 M HATU in DMF, 0.2 M DIPEA, and 0.3 M lutidine in DMF. The coupling cycle was carried out by a procedure slightly modified with respect to the standard PNA synthesis protocols in the steps of washing and deblocking as described here: (1) washing with 2.5 mL of (ACN/DMF) (1:1, v/v); (2) coupling 20 minutes; (3) washing with 2.5 mL of ACN/DMF (1:1, v/v); (4) capping with 5% of acetic anhydride and 6% of 2,6-lutidine in DMF, 2.0 mL; (5) washing with 2.5 mL of ACN/DMF (1:1, v/v) and 2.5 mL of DMF; (6) deblocking with a solution of dichloroacetic acid (2%) in ACN; (7) washing with 2.5 mL of DMF and 5 mL of ACN (C: calculated mass 6910.2, found 6910.0; D: calculated mass 7240.4, found 7238.0).

The RNA oligomers **E** and **F** were grown on the support **VIII**, following the same procedures described for the 5' terminal modification of the oligomers **C** and **D** (E: calculated mass 6958.9, found 6957.7; F: calculated mass 7288.1, found 7286.9).

The RNA oligomers **G** and **H** were prepared after solid phase phosphorylation of the oligomers **C** and **D**. The phosphorylation reaction was achieved by using a solution 0.1 M of chemical phosphorylation reagent [36] in ACN with 0.3 M BTT in ACN. The oxidation was achieved by treatment with $I_2/H_2O/Py$ (G: calculated mass 6990.2, found 6988.9; H: calculated mass 7320.3, found 7319.1).

The RNA oligomers **I** and **L** were synthesized on support **VIII**, following the same procedures described for 5' terminal couplings and phosphorylation of the oligomers **G** and **H** (I: calculated mass 7038.9, found 7037.7; L: calculated mass 7368.1, found 7366.9).

The RNA oligomers **M** and **N** were prepared on standard SynBase CPG support, by introducing derivative **X** as last coupling monomer. The last coupling was carried out on automated synthesizer with a 0.1 M solution of derivative **X** in ACN (double coupling) and by using 0.3 M BTT in ACN, as activating solution. All succeeding procedures followed the standard protocol for RNA synthesis (M: calculated mass 7004.1, found 7002.8; N: calculated mass 7334.3, found 7333.1).

The RNA oligomers **O** and **P** were grown on support **VIII**, following the standard protocol for RNA synthesis (O: calculated mass 6693.8, found 6692.6; P: calculated mass 6716.8, found 6715.0).

2.3. Synthesis of Derivative VI. 572 mg of SynBase CPG solid supports (CPG-OH, high loading 0.10 meq g⁻¹) were functionalized with 297 mg (1.0 mmol) of Fmoc-Gly-OH using PyBOP (520 mg, 1.0 mmol) and HOBt (153 mg, 1.0 mmol) as activating agents in dry DMF (6 mL). The mixture was kept at r. t. for 16 h under shaking. The support was filtered and washed with DMF and Et₂O and then dried under reduced pressure, thus obtaining support **III** (0.089 mmol/g, 89% coupling yield). The yield of incorporation of the glycine residue was calculated by quantitative UV measurements (301 nm) of the fluorene derivative released by piperidine/DMF (1:4, v/v) treatment of weighed amounts of support. Gly-linking support was washed with pyridine and then treated with acetic anhydride

in pyridine (6.0 mL, 2:3, v/v, 1 h, r.t.) to block the unreacted hydroxy groups. After deblocking of amino function of supported glycine by a solution of piperidine in DMF (20%), 2-(N-(2-((4-methoxyphenyl)diphenylmethoxy)ethyl)-2-(5-methyl-2,4-dioxo-3,4-dihydropyrimidin-1(2H)-yl)acetamido) acetic acid (0.2 M in DMF) [35] was coupled by a solution 0.2 M HATU in DMF, 0.2 M DIPEA, and 0.3 M lutidine in DMF. The coupling cycle was carried out by a slightly modified procedure consisting of the following steps: (1) washing with 2.5 mL of (ACN/DMF) (1:1, v/v); (2) coupling 20 minutes; (3) washing with 2.5 mL of ACN/DMF (1:1, v/v); (4) capping with 5% of acetic anhydride and 6% of 2,6-lutidine in DMF, 2.0 mL; (5) washing with 2.5 mL of ACN/DMF (1:1, v/v) and 2.5 mL of DMF; (6) deblocking with a solution of dichloroacetic acid (2%) in DCA; (7) washing with 2.5 mL of DMF and 5 mL of ACN (0.089 meq g⁻¹, 100% coupling yield). The phosphorylation reaction was achieved (0.088 meq g⁻¹, 99% coupling yield) by using a solution 0.1 M of chemical phosphorylation reagent in ACN with 0.3 M BTT in ACN. The oxidation was achieved by treatment with $I_2/H_2O/Py$. After ammonium hydroxide treatment and purification by C18 Sep-Pak columns eluted by water/ACN (7:3, v:v) derivative **VI** was isolated and characterized (ESI-MS: m/z = 940.267 [M-2H⁺+2Na⁺], calculated for C₄₁H₄₉N₆O₁₅P: 896.30; ³¹P NMR δ : 1.846).

2.4. Functionalization of the CPG Resin: Support VIII. Fmoc-Gly-OH (60 mg, 0.2 mmol), PyBop (104 mg, 0.2 mmol), and HOBt (30 mg, 0.2 mmol) in dry DMF (5.0 mL) were added to CPG-OH resin (500 mg, 0.04 meq g⁻¹ of hydroxy groups), previously washed with DMF. The mixture was kept at r.t. with shaking for 24 h. The support was filtered and washed with DMF and Et₂O and then dried under reduced pressure, thus providing functionalized CPG (0.035 mmol/g, 89% coupling yield). The yield of incorporation of the glycine residue was calculated by quantitative UV measurements (301 nm) of the fluorene derivative released by piperidine/DMF (1:4, v/v) treatment of weighed amounts of support. Gly-linking support was washed with pyridine and then treated with acetic anhydride in pyridine (6.0 mL, 2:3, v/v, 10 min, r.t.) to block the unreacted hydroxy groups. After deblocking of amino function of supported glycine by a solution of piperidine in DMF (20%), N-(Thymin-1-ylacetyl)-N-(2-Fmoc-aminoethyl)glycine (53 mg, 0.2 mmol) was reacted in DMF and in presence of HATU (76 mg, 0.2 mmol) and DIPEA (52 μ L, 0.3 mmol) for 1 h at r.t. with shaking. The coupling yields, measured as previously described, were 90% (0.031 mmol/g). A capping procedure was carried out, after washing with DMF, by the addition of acetic anhydride in pyridine (2:3, v/v, 1 h, r.t.). After deblocking of amino function of supported PNA by a solution of piperidine in DMF (20%), 2-(N-(2-((4-methoxyphenyl)diphenylmethoxy)ethyl)-2-(5-methyl-2,4-dioxo-3,4-dihydropyrimidin-1(2H)-yl)acetamido) acetic acid [35] (0.2 M in DMF) was coupled by a solution 0.2 M HATU in DMF, 0.2 M DIPEA, and 0.3 M lutidine in DMF. The coupling cycle was carried out by a slightly modified procedure consisting in the following

steps: (1) washing with 2.5 mL of (ACN/DMF) (1:1, v/v); (2) coupling 20 minutes; (3) washing with 2.5 mL of ACN/DMF (1:1, v/v); (4) capping with 5% of acetic anhydride and 6% of 2,6-lutidine in DMF, 2.0 mL; (5) washing with 2.5 mL of ACN/DMF (1:1, v/v) and 2.5 mL of DMF. The obtained support **VIII** resulted in 0.031 meq g^{-1} (100% coupling yield) as judged by quantitative UV measurements (478 nm) of the MMT cation released by dichloroacetic acid (2%) in DCM treatment of weighed amounts of **VIII**.

2.5. Synthesis of Derivative X. Methyl ester derivative of *hegPNA IX* (0.50 g; 1.67 mmol) was dissolved in anhydrous DCM (15 mL). Anhydrous DIEA (0.63 mL, 3.69 mmol) and 2-cyanoethyl-N,N-diisopropylphosphoramidochloridite (0.24 mL; 1.10 mmol) were added to this solution. After 1 h the solvent was evaporated *in vacuo* and the residue dissolved in EtOAc and washed four times with brine. The organic phase was dried and evaporated *in vacuo*. The residue was purified by column chromatography on silica gel using DCM/EtOAc/N₃Et, (49.5:49.5:1, v:v:v) as the eluent. 0.65 g (78% yield) of derivative **X** was obtained (³¹P-NMR (CDCl₃) δ : 146.0, 146.7).

2.6. Cell Cultures, Transfections, and Luciferase Assay. HeLa cells were grown at 37°C, 5% CO₂ in Dulbecco's modified Eagle's medium supplemented with 10% fetal bovine serum (FBS) (EuroClone), 100 units mL⁻¹ penicillin, and 100 mg mL⁻¹ streptomycin (EuroClone). The day before transfection, cells were trypsinized, diluted in the appropriate amount of growth medium without antibiotics, and transferred to 12-well plates (1 mL per well) such that they were 80–90% confluent at the time of transfection. Cotransfections of reporter plasmids (per well 1 μ g pGL2-control, encoding the firefly *Photinus pyralis* luciferase and 0.05 μ g pRL-TK, encoding *Renilla reniformis* luciferase, Promega) and 10 nM siRNAs were carried out with Lipofectamine2000 (Invitrogen) as described by the manufacturer. Luciferase activities were monitored 2 days after transfection using Dual-Luciferase Reporter Assay System (Promega) according to the manufacturer's protocol. The firefly luciferase activity was normalized to the Renilla luciferase activity and the uninhibited activity (plasmids encoding the luciferases cotransfected with unrelated siRNA as control) was set to 1. Data represent mean normalized luciferase activity from at least three experiments \pm s.d.

2.7. Stability of siRNAs in 100% FBS. 7.5 μ L of unmodified and modified siRNAs (20 μ M) were incubated with 75 μ L of FBS at 37°C. Aliquots of 22 μ L (40 pmoles) were withdrawn at different time points and immediately frozen. The solutions were then extracted with phenol and siRNAs were precipitated with ethanol. Samples were subjected to electrophoresis in 15% polyacrylamide-tris-borate-EDTA (TBE) under non-denaturing conditions and visualized by ethidium bromide staining. Equal amounts of siRNAs before serum incubation were extracted with phenol and loaded as controls. Gel images were captured by ChemiDoc XRS (Bio-Rad) and RNA electrophoretic bands were quantified by Image Lab software

(Bio-Rad). Signal intensity value of the intact siRNA was set at 1.

2.8. Molecular Docking. The miR-20a/hAgo 2 three-dimensional structure was downloaded from the Protein Data Bank (PDB code 4F3T) [9]. The co-crystal RNA present in this structure was used as template for the construction of the modified siRNAs featuring the modifications at the 5' and 3' end (viz. AS, antisense strand, of siRNAs **16** and **17**, resp.). SiRNA structures were built using the builder in the Maestro package of Schrodinger Suite 2010 and optimized using a version of MacroModel also included. The following parameters of energy minimization were used: OPLS2005 force field was used, water was used as an implicit solvent, and a maximum of 5000 iterations of the Polak-Ribier conjugate gradient minimization method was used with a convergence threshold of $0.01 \text{ kJ mol}^{-1} \text{ \AA}^{-1}$.

The new version of the docking program AutoDock4.2 (AD4) [37, 38], as implemented through the graphical user interface called AutoDockTools (ADT), was used to dock these siRNAs. The constructed compounds and the receptor structure were converted to AD4 format files using ADT generating automatically all other atom values. Since AD4 has a limit in the number of ligand rotatable bonds only the PNAs (viz. dTdT_a, dTdT_b, and dTdT_c) were free to rotate. The docking area was centered around the putative binding site (PAZ domain for **17** and MID domain for **16**). A set of grids of $90 \text{ \AA} \times 40 \text{ \AA} \times 75 \text{ \AA}$ with 0.375 \AA spacing was calculated around the docking area for the ligand atom types using AutoGrid4.2. For each ligand, 700 separate docking calculations were performed. Each docking calculation consisted of 25 million energy evaluations using the Lamarckian genetic algorithm local search (GALS) method. The GALS method evaluates a population of possible docking solutions and propagates the most successful individuals from each generation into the subsequent generation of possible solutions. A low-frequency local search according to the method of Solis and Wets is applied to docking trials to ensure that the final solution represents a local minimum. All dockings described in this paper were performed with a population size of 250, and 300 rounds of Solis and Wets local search were applied with a probability of 0.06. A mutation rate of 0.02 and a crossover rate of 0.8 were used to generate new docking trials for subsequent generations, and the best individual from each generation was propagated over the next generation. The docking results from each of the 700 calculations were clustered on the basis of root-mean square deviation (rmsd) (solutions differing by less than 3.0 \AA) between the cartesian coordinates of the atoms and were ranked on the basis of free energy of binding (ΔG_{AD4}). These lowest energy conformations were visually inspected for good chemical geometry. Because AD4 does not perform any structural optimization and energy minimization of the complexes found, a molecular mechanics/energy minimization (MM/EM) approach was applied to refine the AD4 output using the Schrodinger Suite 2010. The computational protocol applied consisted of the application of 100000 steps of the Polak-Ribière conjugate gradients (PRCG) or until the derivative convergence was

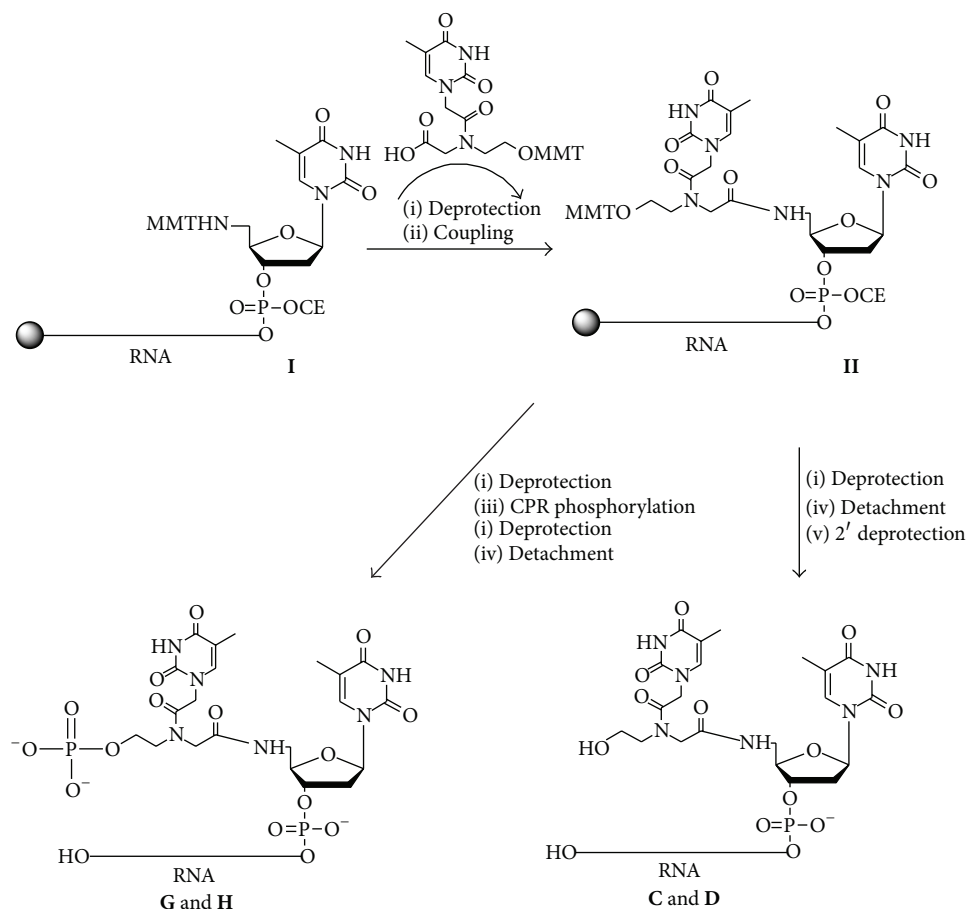


FIGURE 2: Assembling of the RNA oligomers **C**, **D**, **G**, and **H**. Reagents and conditions: (i) 2% DCA in DCM; (ii) 0.2 M HATU in DIPEA/DMF; (iii) 0.1 M CPR in ACN, 0.3 M BTT in ACN; (iv) NH_4OH , 50°C, 12 h; (v) $\text{Et}_3\text{N}\cdot 3\text{HF}$ in DMF 1:3 v/v, 65°C, 150 min.

0.05 kJ/mol. All complexes pictures were rendered employing the UCSF Chimera software [39].

3. Results

3.1. Chemistry

3.1.1. Synthesis of Unmodified siRNA 1 and Modified siRNAs 2–4. In the present work our attention was mainly focused on specific chemical modification at 5' region of the antisense and sense strands of siRNAs. In this respect, we decided to modify an siRNA targeting firefly luciferase mRNA [2] because of the possibility of testing it by an automated luciferase assay allowing an easy and accurate judgment of the gene silencing activity in cultured mammalian cells, thus comparing chemically modified siRNAs to the unmodified one. Unmodified RNA strands **a–b** in Table 1 (antisense 5'-UCGAAGUAUCCGCGUACGTT-3' and sense 5'-CGUACGCGGAUACUUCGATT-3') were synthesized following DNA/RNA fully automated protocols. The synthesis of the RNA-5'-PNA-OH **C–D** was carried out on CPG-OH support using commercially available 2'-O-TBDMS-3'-phosphoramidite ribonucleotides and

5'-MMT-NH-thymidine-3'-O-phosphoramidite. MMT-hydroxyethylglycine PNA monomers (MMT-O-PNA) were synthesized following reported procedures and characterized by ^1H and ^{13}C NMR spectroscopies [35]. The synthesis of the RNA tract was performed on a RNA synthesizer and 5'-MMT-NH-thymidine-3'-O-phosphoramidite was introduced as last coupling monomer to obtain support **I** (Figure 2). In order to incorporate the PNA monomer at 5' end of RNA sequence (support **II**, Figure 2), MMT-hydroxyethylglycine PNA monomer was coupled using PNA standard procedure (HATU in DIPEA/DMF).

After deblocking of the hydroxyl function by 2% DCA/DCM treatment, the oligomers were cleaved from the support by treatment with NH_4OH at 50°C overnight. The 2'-O-TBDMS protecting group was removed by $\text{Et}_3\text{N}\cdot 3\text{HF}$ and the resulting fully deprotected RNA oligomers **C** and **D** (Figure 2) were precipitated from ethanol, purified by anion exchange and RP-HPLC, and characterized by MALDI-TOF mass spectrometry. The MS-data confirmed the identity of the synthesized oligomers. Then, the oligomers **a**, **b**, **C**, and **D** were combined to form siRNAs **1–4** (Table 1) following the annealing procedure as described above.

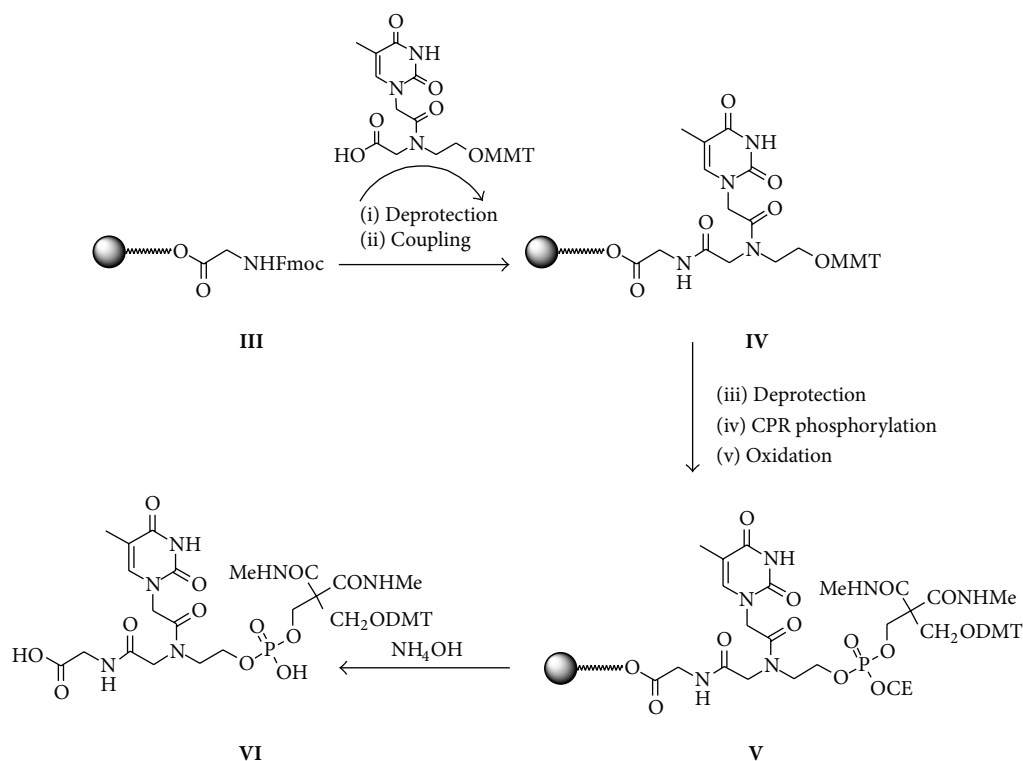


FIGURE 3: Solid phase synthesis of the derivative **VI**. Reagents and conditions: (i) 20% Piperidine in DMF; (ii) 0.2 M HATU in DMF, 0.2 M DIPEA, 0.3 M Lutidine in DMF; (iii) 2% DCA in DCM; (iv) 0.1 M CPR in ACN, 0.3 M BTT in ACN; (v) I_2/H_2O /pyridine.

3.1.2. Synthesis of Modified siRNAs 8–10: Solid Phase Chemical Phosphorylation. Chemical phosphorylation of the 5'-terminus of oligonucleotides is routinely achieved, with high yields using the CPR ([3-(4,4'-Dimethoxytrityloxy)-2,2-(N-methylamidocarbonyl)]-propyl-[(cyanoethyl)-(N,N-diisopropyl)]phosphoramidite) [36]. This method requires CPR introduced by coupling with phosphoramidite method. Aside from its inherent convenience, CPR also has the advantage over enzymatic methods in allowing immediate determination of the phosphorylation efficiency due to the presence of the DMT protecting group. The synthesis of the RNA-5'-PNA-O-phosphate **G–H** required a previous phase to study and optimize the chemical phosphorylation of *heg*PNA on solid phase. For this purpose, the chemical phosphorylation of *heg*PNA monomer was tested on CPG-OH support. The solid supports were functionalized with a Fmoc-Gly-OH as spacer using PyBop/HOBT as activating agents. The yield of glycine introduction, evaluated by spectrophotometric measurements of fluorene derivative, was 0.035 meq/g. CPG-Gly derivatized support was therefore functionalized with the MMT protected *heg*PNA monomer by PNA coupling procedure (HATU/DIPEA in DMF). After MMT removal, the OH function was chemically phosphorylated by using commercially available CPR. The CPG support gave good results in the phosphorylation reaction. In fact, the yields of phosphorylation on CPG support resulted 99% as calculated by the spectrophotometric measurements of DMT cation released after deprotection

of phosphate in DCA/DCM. After basic treatment for deprotection and detachment from support, PNA-O-phosphate derivative **VI** (Figure 3) was purified by RP-C18 cartridge and characterized by ^{31}P NMR and ESI-MS. On the basis of these results, CPG support was chosen to synthesize RNA-5'-PNA-O-phosphate **G–H** (Figure 2). The identity of full-length oligomers was confirmed by MALDI-TOF analysis. The oligomers **a**, **b**, **G**, and **H** (Figure 2) were combined to form siRNAs **8–10** (Table 1) following the annealing procedure as described above.

3.1.3. Synthesis of Modified siRNAs 5–7, 11–13, and 17–19. Modified 3',5'-PNA siRNAs were synthesized in order to study the effect of PNA on both 5' and 3' ends of siRNAs sense and antisense strands. The support **VIII** (Figure 4) was synthesized starting from CPG-OH support **VII** by reaction with Fmoc-amino and MMT-hydroxyethylglycine PNAs following procedures reported elsewhere [27]. After deprotection of OH function, the synthesis of RNA tract was performed using commercially available 2'-O-TBDMS-3'-O-phosphoramidite ribonucleotides on oligo synthesizer affording oligomers **O–P** (Table 1). To obtain the oligomers **E–F** and **I–L** (Table 1), the last couplings were done with 5'-MMT-NH-thymidine-3'-O-phosphoramidite and MMT-O-PNA monomer as described for **C–D** and **G–H**. Deprotection and cleavage of oligomers from support were carried out as described above. HPLC purification and MS-data confirmed

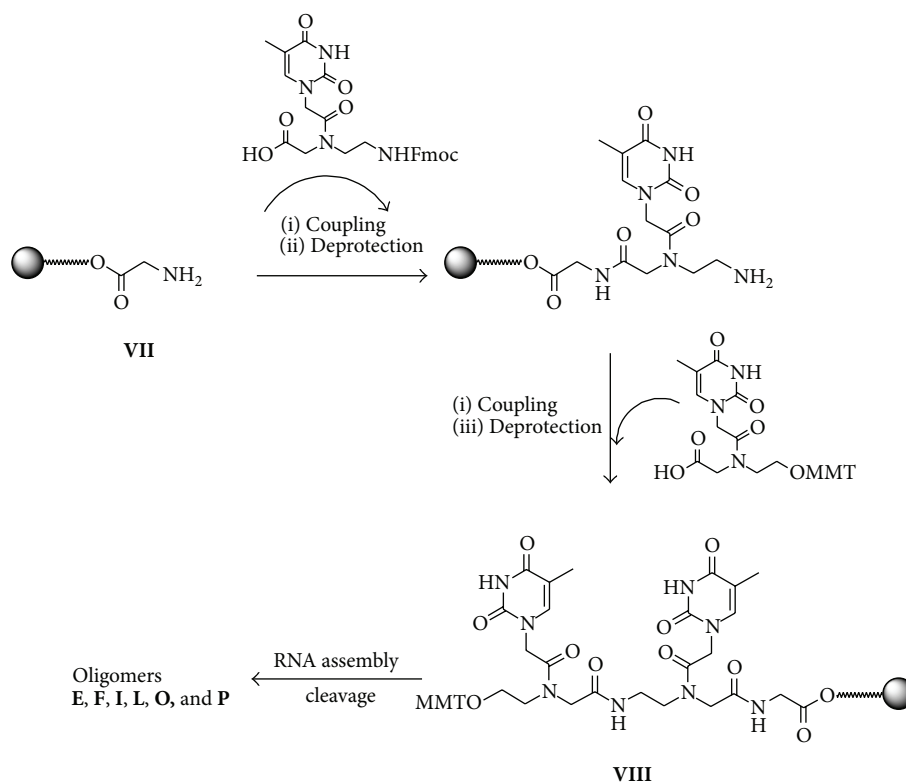


FIGURE 4: Synthesis of the support **VIII**. Reagents and conditions: (i) 0.2 M HATU in DIPEA/DMF; (ii) 20% Piperidine in DMF; (iii) 3%; DCA in DCM.

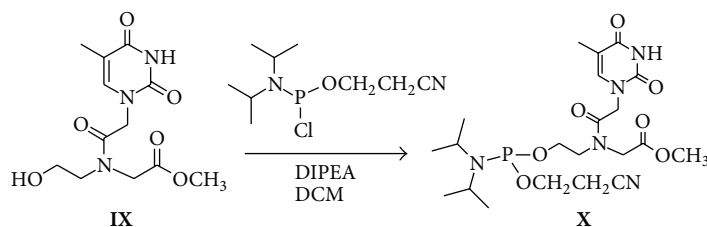


FIGURE 5: Synthesis of phosphoramidite PNA building block **X**.

the identities of chimeras **E-F**, **I-L**, and **O-P**. The siRNAs **5-7**, **11-13**, and **17-19** were assembled as described in Table 1 following the annealing procedure as described above.

3.1.4. Synthesis of the siRNAs 14-16. We synthesized a new set of siRNAs bearing at 5' end a PNA monomer linked by phosphodiester bridge and having the C-terminus as methylamide cap. For this purpose, phosphoramidite PNA building block **X** (Figure 5) was prepared by reaction of methyl ester derivative of *heg*PNA **IX** with 2-cianoethyl-N,N-diisopropylchlorophosphoramidite in dry DIPEA/DCM. After LC purification and ^{31}P NMR characterization, the PNA phosphoramidite derivative **X** was used as last coupling monomer to obtain the precursor of the oligomers **M-N**.

Methylamine treatment (33% in absolute ethanol) accomplished the deprotection and detachment of the oligomers

from the support as methylamide derivatives. Desilylation gave the RNA-5'-O-PNA-CONHCH₃ oligomers **M-N** (Table 1) that after purification and characterization by MALDI-TOF MS were combined with **a-b** to give the siRNAs **14-16** (Table 1) following the annealing procedure as described above.

3.2. Circular Dichroism Characterization of Native and Modified siRNAs. Although the conformational features alone do not warrant an interfering activity, a double-helical RNA-like A conformation is required for effective gene silencing. Indeed, the modified siRNAs **2-19** were all found to retain an RNA-like A conformation exhibiting CD spectra similar to those of the unmodified siRNA **1** with a typical positive shoulder at 280 nm and a large positive band at 260 nm. This behavior suggested that terminal amide linkages at 3'

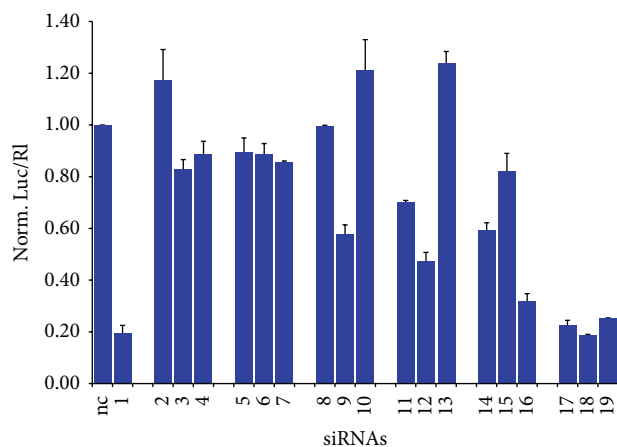


FIGURE 6: RNAi activity of native and modified siRNAs toward luciferase gene expression in HeLa cells. Small interfering RNAs were transfected at 10 nM concentration and luciferase activities were determined after 48 h. The firefly luciferase activity (Luc) was then normalized to that of Renilla luciferase (RI) and the uninhibited activity of cells transfected with an unrelated siRNA (nc) was set to 1. Data are the mean \pm s.d. from at least three experiments.

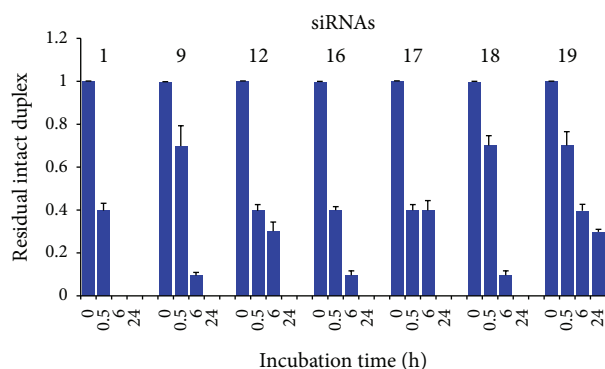


FIGURE 7: Stability of natural and modified siRNAs in 100% fetal bovine serum at 37°C. After incubation, siRNAs were analyzed by PAGE and ethidium bromide staining. Gel images were captured by ChemiDoc XRS (Bio-Rad) and RNA bands were quantified by Image Lab software (Bio-Rad). Signal intensity values at t_0 were set at 1.

and/or 5' ends do not interfere with the typical A conformation of dsRNA. Thermal stability of the siRNAs 2–19 was also considered by thermal denaturation CD experiments highlighting a general thermodynamic destabilization for all modified duplexes. In fact, melting temperatures lower than that of siRNA 1 (76°C) were recorded in all cases suggesting that the presence of the terminal amide linkages caused a limited destabilization of the secondary structure, as inferred from CD-melting values (Table 1).

3.3. Compatibility of Modified siRNAs with the RNAi Machinery. To verify the compatibility of modified siRNAs containing amide linkages with the cellular RNAi machinery, siRNAs 2–19 were evaluated for their ability to specifically inhibit firefly luciferase gene expression in cultured HeLa cells.

siRNA duplexes were cotransfected with the reporter plasmid combination pGL2/phRL-TK using cationic liposomes. pGL2 is transcribed into the *Photinus pyralis* luciferase mRNA, targeted by the siRNA, whereas phRL-TK encodes the *Renilla reniformis* luciferase, used as control to normalize the data with the efficiency of transfection. As shown in Figure 6, the native siRNA 1 effectively and selectively reduced firefly luciferase activity by more than 80% compared to an unrelated siRNA (nc).

We then confirmed that the introduction of PNA modification at the 3' end in either or both strands does not show any loss of interfering effect, because all the modified duplexes (siRNAs 17–19) were as efficient as the siRNA 1. On the other hand, the presence of the amide linkage dramatically decreased the interference activity when it was located at 5' and at both 3', 5' regions of siRNAs, demonstrating that the modification at 5' end mostly controls the silencing activity. Interestingly, "5'-capped" siRNAs partially restored the interfering effect. Therefore, the siRNA 16 appeared to be more effective than all the other 5'-modified duplexes, while the siRNA 18 appeared to be more effective than all the other modified duplexes.

3.4. Serum Stability of Modified siRNAs. Improving the biostability is also crucial for therapeutic purposes of synthetic siRNAs. Experiments were planned to test whether the introduction of the amide linkages at 5' and/or at 3' ends leads to siRNAs more stable than unmodified ones in the extracellular environment. Therefore, the nuclease resistance of 2–19 was investigated through incubation in 100% fetal bovine serum (FBS) at 37°C using unmodified siRNA 1 as control (Figure 7). At various incubation times, aliquots of each siRNA were analyzed by electrophoresis on 15% polyacrylamide gels to detect any degradation products. The unmodified siRNA 1 was greatly degraded within 30 min (Figure 7) as well as almost all siRNAs featuring only one modified strand (data not shown), except for 9 and 12 that exhibited significant amounts of intact duplex at 6 h of incubation. Similar results were obtained with siRNAs 16–18. Finally, the introduction of PNA on both strands markedly increased the resistance to serum-derived nucleases as demonstrated by 19 that showed still evident intact duplex even after 24 h of incubation.

3.5. Molecular Docking Simulations. Molecular docking simulations were attained in order to provide a putative model of the interaction of the newly identified siRNAs with the human Argonaute 2 (hAgo 2) protein at atomistic level. In particular, the software AutoDock4.2 (AD4) [37, 38] was employed to dock the ASs of the siRNAs bearing the most performing modifications at the 3' and 5' ends. In particular, the chimeric 3'-OH-PNA AS of siRNA 17 (oligomer O) and the AS of "5'-capped" siRNA 16 (oligomer M) were docked in the recently published structure of hAgo 2 in complex with miR-20a (PDB code 4F3T) [9]. The modified siRNA ASs were constructed starting from the RNA cocrystal conformation where each nucleotide was mutated to obtain the target sequence, while at the 3' and 5' terminals the proper

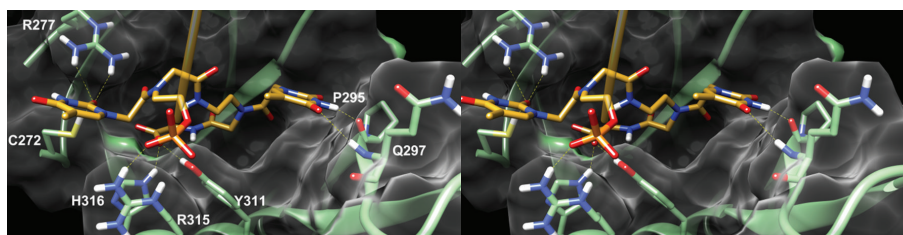


FIGURE 8: Stereoview of the predicted binding mode of the 3'-OH-PNA AS of siRNA 17 in the hAgo 2 X-ray structure. For clarity reasons, the PNA structure is depicted (yellow sticks) while the RNA backbone is shown as an orange transparent ribbon. The protein is depicted as green sticks (interacting residues) and ribbons and white transparent surface. H-bonds are indicated as yellow dashed lined.

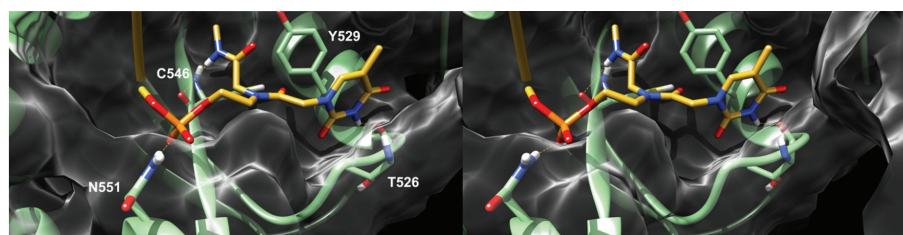


FIGURE 9: Stereoview of the predicted binding mode of the 5'-capped AS of siRNA 16 in the hAgo 2 X-ray structure. For clarity reasons, only the PNA structure is depicted (yellow sticks) while the RNA backbone is shown as an orange transparent ribbon. The protein is depicted as green sticks (interacting residues) and ribbons and white transparent surface. H-bonds are indicated as yellow dashed lined.

modifications were attained. These latter groups were free to move during the docking simulations. For both docking calculations only the lowest energy conformations (ΔG_{AD4}) were considered and analyzed.

In the theoretical complex between the AS of siRNA 17 and hAgo 2 the modified RNA adopted a conformation similar to that of the cocrystal RNA with the 3' end contacting the protein PAZ domain. In this position, the terminal PNA residues are embedded in a wide gorge of the aforementioned protein region establishing several favorable interactions (Figure 8). In particular the phosphate group linking the PNA structure to the RNA one is forming an ionic interaction with R315 while the *heg* residue is able to project the attached thymine base to form two H-bonds with R277 and C272. On the other hand, the second thymine base is pointing towards the opposite site of the gorge H-bonding with P295 and Q297 backbone CO and NH, respectively. Finally, the terminal carboxylate group is able to H-bond H316 and Y311 side-chains.

A well-defined binding pose was also found for the "5'-capped" AS of siRNA 16 where the terminal 5' is pointing towards the hAgo 2 middomain (Figure 9). In this position the phosphate group is H-bonding N551 with the thymine moiety being optimally oriented to establish a π - π interaction with Y529 and an H-bond with T526 backbone CO. Moreover, the terminal methylamide cap can form an additional H-bond interaction with C546 backbone CO.

4. Discussion

A rational design of effective chemically modified siRNAs must consider the 3' and 5' termini of siRNAs as critical

determinants for the silencing activity because these regions interact with the binding domains of hAgo 2, that is, the signature component of the RNAi machinery. In particular, the selective loading of the guide strand into RISC is essential for avoiding undesirable side effects, while the release of the 3' end from the PAZ domain during the cleavage of the mRNA is crucial to perform RNase activity [40]. In this respect, experiments on cell cultures have demonstrated that chemical modifications of siRNAs at 3' end modulate the silencing activity, increase the nuclease resistance, and influence the affinity of the 3'-overhang portion for PAZ [41–44]. Instead, the phosphorylation of the 5' end of siRNA is one of the first steps required for antisense strand selection and for its function in RISC [45, 46]. The 5' end of siRNA is tethered to hAgo 2 through a multitude of interactions to form a very tight binding pocket composed of residues mostly from the middomain and capped on one side by PIWI domain residues [47–50]. All three nonbridging oxygen atoms of the 5' phosphate interact with several protein side chains and it has been suggested that the proper interactions between the 5'-phosphate and hAgo 2 define the position of the RNA guide with respect to the active site to ensure that cleavage of targets occurs at a well-defined and predictable position. In addition, early work on siRNA chemical modifications suggested the importance of the thermal stability of the siRNA duplex, as measured by the melting temperature, T_m , on the gene silencing activity [51–53]. However, there is no obvious correlation between the overall duplex T_m and the gene silencing activity of the siRNA. Rather, specific regions of the siRNA duplex have distinct tolerances toward stabilization and destabilization, resulting in position-specific changes of activity upon incorporation of chemical

modifications that affect thermal stability [54]. Therefore, the thermodynamic properties of siRNA molecules play a central role in determining the molecule's functionality by facilitating several steps, namely, duplex unwinding, correct strand selection, reduced unspecific recognition of target, and mRNA turnover.

siRNAs 2–7, bearing *heg*PNA at 5' end of sense and antisense strands, did not exhibit any mRNA degradation activity and it might be postulated that in these siRNAs the *heg*PNA inhibits phosphorylation event at the 5' terminus. Thus, the absence of the phosphate at 5' end of guide strand in the siRNAs 2 and 5 could result in a loss of specificity and efficiency of target cleavage because the RNA guide might adopt incorrect positions in the RNA binding groove of hAgo 2. This is similar to previously published results [55] where unlocked nucleic acid (UNA) modification at positions 1 and 2 of 5'-terminus prevented phosphorylation by Clp1 kinase abrogating interaction with hAgo 2. Furthermore, it is also reasonable that in siRNAs 2 and 5, the amide-bond linkage placed in substitution of the phosphodiester bridge between the nucleotides 1 and 2 of the 5' region might derange the required interactions between the AS strand and hAgo 2. Modifying siRNAs by introducing *heg*PNA monomer at the 5'-terminus of the sense strand (siRNAs 3 and 6) resulted in a loss of silencing activity. This unexpected result could be explained by the presence of a thermal destabilization due to the structural complexity induced by the PNA in the siRNAs 3 and 6, as confirmed by thermal denaturation studies (Table 1). In this respect, the thermal destabilization would translate in the SS selection by RISC rather the AS and this is consistent with the asymmetry rule of siRNAs. This hypothesis is also confirmed by the observed behavior of siRNAs 4 and 7 where the introduction of PNA at 5' end of both strands resulted again in a loss of silencing activity. Noteworthy, the presence of PNA also at 3' end (siRNAs 5–7) had no improvement on the silencing activity, although the analysis of data resulting from silencing activity of the siRNAs 17–19 showed that the PNA units into 3'-dangling region were well tolerated by RNAi machinery. In particular, the modification of the sense strand of siRNA 18 resulted in an increased silencing activity probably by inducing the correct loading of antisense strand by RISC. In this respect, the theoretical model of the complex between the AS of 17 and the PAZ domain of hAgo 2 would indicate that, in this siRNA, the 3'-OH-PNA is able to establish several and tight interactions with the protein counterpart and thus positively modulating the rates of dislodging and lodging of the AS in and from the PAZ domain and providing, in turn, a further determining factor for its efficiency and potency.

In order to assess the impact of the chemical phosphorylation of *heg*PNA at 5' end on the interfering activity, siRNAs 8–13 were synthesized. As shown in Figure 5, siRNAs 8 and 11 containing a PNA-phosphate at the 5' end of antisense strand were less potent than unmodified siRNA, reproducing the same results obtained for siRNAs 2 and 5. In addition to the lack of the proper AS/hAgo 2 interactions ascribable to the presence of the internucleotidic amide-bond linkage, the low silencing potential may be also caused by the 5'-terminal

phosphate instability. In principle, the 5'-phosphate could be removed in the cellular environment and the 5' terminal *heg* PNA could not be rephosphorylated by cellular kinase Clp1 as already suggested from the behavior of the siRNAs 2–7. Furthermore, siRNAs 9 and 12 resulted in being significantly more active than siRNAs 8 and 11. The only partial restoring of the silencing activity of 9 and 12 may be rationalized considering that both the modified SS (no silencing) and the unmodified AS (silencing) occur.

Finally, we synthesized novel modified siRNAs bearing an *heg*PNA monomer inserted at 5' end of RNA domain by phosphodiester linkage and having at the C-terminus a methylamide function (siRNA 14–16, Table 1). Interestingly, improved silencing performances were observed for siRNAs 14 and 16 in which we suppose that the modified AS is selectively loaded on RISC due to the thermal asymmetry conferred by methylamide PNA at 5' end. In fact, siRNA 15 was not effective, probably, since the modified sense strand is preferentially selected. The “5'-capped” siRNAs 14 and 16 partially restored an interfering effect besides methylamide cap blocks the siRNA versus phosphorylation [56–61]. Also, the specific interaction detected between the methylamide and the hAgo 2 middomain would further substantiate a role of the chemical modification in the selective loading of the AS by the protein. Furthermore, it is worth mentioning that the presence of phosphodiester linkage between residues 1 and 2 in the 5' region of the siRNAs 14 and 16 seems to have an additional role in maintaining the correct binding to direct mRNA degradation.

5. Conclusions

In summary, we reported the synthesis of modified siRNAs containing terminal amide linkages by introducing *heg*PNA moieties at 5', 3', and at both termini. It was revealed that modified siRNAs are only compatible with the RNAi machinery when amide bonds are introduced at 3' end of the siRNAs. In particular, poor efficacy was observed when *heg*PNA or *heg*PNA phosphate moieties are placed at 5' ends because this region plays a crucial role in maintaining the correct binding to address the mRNA-target degradation. Further, “5'-capped” siRNAs partially restored the interfering activity maybe favoring the AS selective loading as well as the correct binding of the AS by the protein. Besides, we examined the biostability of the modified siRNAs and showed the introduction of amide linkages on both strands of siRNAs markedly increased the resistance to serum-derived nucleases. Molecular docking simulations were attained to give at atomistic level a clearer picture of the effect of the most interesting modifications on the interactions with the human Argonaute 2 PAZ, MID, and PIWI domains. In conclusion, this report appends further on the understanding of the effects of chemical modifications and of their location in siRNA structure on the silencing properties and sensitivity to the degradation by ribonucleases and thus opens to the future possibility to exploit these chemical modifications in studying new structure-function relationships.

The following abbreviations are used throughout the test.

Abbreviations

BTT:	5-Benzylthio-1H-tetrazole
CD:	Circular dichroism
CPG:	Controlled pore glass
CPR:	Chemical phosphorylation reagent
DCM:	Dichloromethane
DCA:	dichloroacetic acid
DEPC:	Diethylpirocarbonate
DMF:	N,N-Dimethylformamide
DMT:	Dimethoxytrityl [bis(4-methoxyphenyl) (phenyl)methyl]
ESI:	Electrospray ionization
FBS:	Fetal bovine serum
Fmoc:	9-Fluorenylmethoxycarbonyl
HOBT:	N-Hydroxybenzotriazole
HPLC:	High performance liquid chromatography
MALDI-TOF:	Matrix assisted laser desorption ionization-time of flight
PyBOP:	(Benzotriazol-1-yloxy) tripyrrolidinophosphonium hexafluorophosphate
RNAi:	RNA interference
RISC:	RNA-induced silencing complex
RNase:	Ribonuclease
RP-HPLC:	Reverse phase HPLC
siRNA:	Small interfering RNA
TBDMS:	t-Butyldimethylsilyl
Tm:	Melting temperature.

Conflict of Interests

The authors declare that there is no conflict of interests regarding the publication of this paper.

Acknowledgments

This work was supported by grants from MIUR (PRIN 2009).

References

- [1] A. Fire, S. Xu, M. K. Montgomery, S. A. Kostas, S. E. Driver, and C. C. Mello, "Potent and specific genetic interference by double-stranded RNA in *Caenorhabditis elegans*," *Nature*, vol. 391, no. 6669, pp. 806–811, 1998.
- [2] S. M. Elbashir, J. Harborth, W. Lendeckel, A. Yalcin, K. Weber, and T. Tuschl, "Duplexes of 21-nucleotide RNAs mediate RNA interference in cultured mammalian cells," *Nature*, vol. 411, no. 6836, pp. 494–498, 2001.
- [3] N. J. Caplen, S. Parrish, F. Imani, A. Fire, and R. A. Morgan, "Specific inhibition of gene expression by small double-stranded RNAs in invertebrate and vertebrate systems," *Proceedings of the National Academy of Sciences of the United States of America*, vol. 98, no. 17, pp. 9742–9747, 2001.
- [4] N. C. Lau, L. P. Lim, E. G. Weinstein, and D. P. Bartel, "An abundant class of tiny RNAs with probable regulatory roles in *Caenorhabditis elegans*," *Science*, vol. 294, no. 5543, pp. 858–862, 2001.
- [5] S. Weitzer and J. Martinez, "The human RNA kinase hC1p1 is active on 3' transfer RNA exons and short interfering RNAs," *Nature*, vol. 447, no. 7141, pp. 222–226, 2007.
- [6] D. S. Schwarz, G. Hutvagner, T. Du, Z. Xu, N. Aronin, and P. D. Zamore, "Asymmetry in the assembly of the RNAi enzyme complex," *Cell*, vol. 115, no. 2, pp. 199–208, 2003.
- [7] P. J. F. Leuschner, S. L. Ameres, S. Kueng, and J. Martinez, "Cleavage of the siRNA passenger strand during RISC assembly in human cells," *EMBO Reports*, vol. 7, no. 3, pp. 314–320, 2006.
- [8] J.-B. Ma, K. Ye, and D. J. Patel, "Structural basis for overhang-specific small interfering RNA recognition by the PAZ domain," *Nature*, vol. 429, no. 6989, pp. 318–322, 2004.
- [9] E. Elkayam, C. D. Kuhn, A. Tocilj et al., "The structure of human argonaute-2 in complex with miR-20a," *Cell*, vol. 150, no. 1, pp. 100–110, 2012.
- [10] V. Ambros, "The functions of animal microRNAs," *Nature*, vol. 431, no. 7006, pp. 350–355, 2004.
- [11] B. Berkhout and K.-T. Jeang, "MicroRNAs in viral gene regulation," *Biochimica et Biophysica Acta. Gene Regulatory Mechanisms*, vol. 1809, no. 11-12, p. 587, 2011.
- [12] A. Russo and N. Potenza, "Antiviral effects of human microRNAs and conservation of their target sites," *FEBS Letters*, vol. 585, no. 16, pp. 2551–2555, 2011.
- [13] D. R. Corey, "Chemical modification: the key to clinical application of RNA interference?" *Journal of Clinical Investigation*, vol. 117, no. 12, pp. 3615–3622, 2007.
- [14] S. T. Crooke, "Progress in antisense technology," *Annual Review of Medicine*, vol. 55, pp. 61–95, 2004.
- [15] M. Gaglione and A. Messere, "Recent progress in chemically modified siRNAs," *Mini Reviews in Medicinal Chemistry*, vol. 10, no. 7, pp. 578–595, 2010.
- [16] A. Lingel, B. Simon, E. Izaurralde, and M. Sattler, "Nucleic acid 3'-end recognition by the Argonaute2 PAZ domain," *Nature Structural and Molecular Biology*, vol. 11, no. 6, pp. 576–577, 2004.
- [17] S. Shah and S. H. Friedman, "Tolerance of RNA interference toward modifications of the 5' antisense phosphate of small interfering RNA," *Oligonucleotides*, vol. 17, no. 1, pp. 35–43, 2007.
- [18] J.-B. Ma, Y.-R. Yuan, G. Meister, Y. Pei, T. Tuschl, and D. J. Patel, "Structural basis for 5'-end-specific recognition of guide RNA by the A. *fulgidus* Piwi protein," *Nature*, vol. 434, no. 7033, pp. 666–670, 2005.
- [19] M. Egholm, P. E. Nielsen, O. Buchardt, and R. H. Berg, "Recognition of guanine and adenine in DNA by cytosine and thymine containing peptide nucleic acids (PNA)," *Journal of the American Chemical Society*, vol. 114, no. 24, pp. 9677–9678, 1992.
- [20] B. Hyrup and P. E. Nielsen, "Peptide nucleic acids (PNA): synthesis, properties and potential applications," *Bioorganic and Medicinal Chemistry*, vol. 4, no. 1, pp. 5–23, 1996.
- [21] M. Komiyama, S. Ye, X. Liang et al., "PNA for one-base differentiating protection of DNA from nuclease and its use for SNPs detection," *Journal of the American Chemical Society*, vol. 125, no. 13, pp. 3758–3762, 2003.
- [22] E. Uhlmann, A. Peyman, G. Breipohl, and D. W. Will, "PNA: Synthetic polyamide nucleic acids with unusual binding properties," *Angewandte Chemie. International Edition*, vol. 37, no. 20, pp. 2797–2823, 1998.
- [23] E. Uhlmann, "Peptide nucleic acids (PNA) and PNA-DNA chimeras: from high binding affinity towards biological function," *Biological Chemistry*, vol. 379, no. 8-9, pp. 1045–1052, 1998.

- [24] D. Capasso, L. de Napoli, G. di Fabio et al., "Solid phase synthesis of DNA-3'-PNA chimeras by using Bhoc/Fmoc PNA monomers," *Tetrahedron*, vol. 57, no. 46, pp. 9481-9486, 2001.
- [25] V. Esposito, A. Randazzo, A. Messere et al., "Synthesis and structural characterization of PNA-DNA quadruplex-forming chimeras," *European Journal of Organic Chemistry*, no. 17, pp. 3364-3371, 2003.
- [26] L. Petraccone, E. Erra, A. Messere et al., "Targeting duplex DNA with DNA-PNA chimeras? Physico-chemical characterisation of a triplex DNA-PNA/DNA/DNA," *Biopolymers*, vol. 73, no. 4, pp. 434-442, 2004.
- [27] N. Potenza, L. Moggio, G. Milano et al., "RNA interference in mammalia cells by RNA-3'-PNA chimeras," *International Journal of Molecular Sciences*, vol. 9, no. 3, pp. 299-315, 2008.
- [28] A. Finotti, M. Borgatti, V. Bezzetti et al., "Effects of decoy molecules targeting NF κ B transcription factors in cystic fibrosis IB3-1 cells: recruitment of NF κ B to the IL-8 gene promoter and transcription of the IL-8 gene," *Artificial DNA: PNA & XNA*, vol. 2, no. 3, pp. 97-104, 2012.
- [29] A. Zannetti, S. del Vecchio, A. Romanelli et al., "Inhibition of Sp1 activity by a decoy PNA-DNA chimera prevents urokinase receptor expression and migration of breast cancer cells," *Biochemical Pharmacology*, vol. 70, no. 9, pp. 1277-1287, 2005.
- [30] M. Borgatti, A. Romanelli, M. Saviano et al., "Resistance of decoy PNA-DNA chimeras to enzymatic degradation in cellular extracts and serum," *Oncology Research*, vol. 13, no. 5, pp. 279-287, 2002.
- [31] A. Romanelli, C. Pedone, M. Saviano et al., "Molecular interactions between nuclear factor κ B (NF- κ B) transcription factors and a PNA-DNA chimera mimicking NF- κ B binding sites," *European Journal of Biochemistry*, vol. 268, no. 23, pp. 6066-6075, 2001.
- [32] Y.-L. Chiu, A. Ali, C.-Y. Chu, H. Cao, and T. M. Rana, "Visualizing a correlation between siRNA localization, cellular uptake, and RNAi in living cells," *Chemistry and Biology*, vol. 11, no. 8, pp. 1165-1175, 2004.
- [33] W. Gong and J. P. Desaulniers, "Gene-silencing properties of siRNAs that contain internal amide-bond linkages," *Bioorganic & Medicinal Chemistry Letters*, vol. 22, no. 22, pp. 6934-6937, 2012.
- [34] J. J. Turner, S. Jones, M. M. Fabani, G. Ivanova, A. A. Arzumanov, and M. J. Gait, "RNA targeting with peptide conjugates of oligonucleotides, siRNA and PNA," *Blood Cells, Molecules, and Diseases*, vol. 38, no. 1, pp. 1-7, 2007.
- [35] G. Breipohl, D. W. Will, A. Peyman, and E. Uhlmann, "Novel synthetic routes to PNA monomers and PNA-DNA linker molecules," *Tetrahedron*, vol. 53, no. 43, pp. 14671-14686, 1997.
- [36] A. Guzaev, H. Salo, A. Azhayev, and H. Lonnberg, "A new approach for chemical phosphorylation of oligonucleotides at the 5'-terminus," *Tetrahedron*, vol. 51, no. 34, pp. 9375-9384, 1995.
- [37] R. Huey, G. M. Morris, A. J. Olson, and D. S. Goodsell, "A semiempirical free energy force field with charge-based desolvation," *Journal of Computational Chemistry*, vol. 28, no. 6, pp. 1145-1152, 2007.
- [38] S. Cosconati, S. Forli, A. L. Perryman, R. Harris, D. S. Goodsell, and A. J. Olson, "Virtual screening with AutoDock: theory and practice," *Expert Opinion on Drug Discovery*, vol. 5, no. 6, pp. 597-607, 2010.
- [39] E. F. Pettersen, T. D. Goddard, C. C. Huang et al., "UCSF Chimera—a visualization system for exploratory research and analysis," *Journal of Computational Chemistry*, vol. 25, no. 13, pp. 1605-1612, 2004.
- [40] M. Sano, M. Sierant, M. Miyagishi, M. Nakanishi, Y. Takagi, and S. Sutou, "Effect of asymmetric terminal structures of short RNA duplexes on the RNA interference activity and strand selection," *Nucleic Acids Research*, vol. 36, no. 18, pp. 5812-5821, 2008.
- [41] Y. Ueno, Y. Watanabe, A. Shibata et al., "Synthesis of nuclease-resistant siRNAs possessing universal overhangs," *Bioorganic and Medicinal Chemistry*, vol. 17, no. 5, pp. 1974-1981, 2009.
- [42] Á. Somoza, M. Terrazas, and R. Eritja, "Modified siRNAs for the study of the PAZ domain," *Chemical Communications*, vol. 46, no. 24, pp. 4270-4272, 2010.
- [43] K. Yoshikawa, A. Ogata, C. Matsuda et al., "Incorporation of biaryl units into the 5' and 3' ends of sense and antisense strands of siRNA duplexes improves strand selectivity and nuclease resistance," *Bioconjugate Chemistry*, vol. 22, no. 1, pp. 42-49, 2011.
- [44] M. Gaglione, N. Potenza, G. di Fabio et al., "Tuning RNA interference by enhancing siRNA/PAZ recognition," *ACS Medicinal Chemistry Letters*, vol. 4, pp. 75-78, 2013.
- [45] A. Boutla, C. Delidakis, I. Livadaras, M. Tsagris, and M. Tabler, "Short 5'-phosphorylated double-stranded RNAs induce RNA interference in *Drosophila*," *Current Biology*, vol. 11, no. 22, pp. 1776-1780, 2001.
- [46] D. S. Schwarz, G. Hutvagner, B. Haley, and P. D. Zamore, "Evidence that siRNAs function as guides, not primers, in the *Drosophila* and human RNAi pathways," *Molecular Cell*, vol. 10, no. 3, pp. 537-548, 2002.
- [47] A. Boland, F. Tritschler, S. Heimstädt, E. Izaurralde, and O. Weichenrieder, "Crystal structure and ligand binding of the MID domain of a eukaryotic Argonaute protein," *EMBO Reports*, vol. 11, no. 7, pp. 522-527, 2010.
- [48] A. Boland, E. Huntzinger, S. Schmidt, E. Izaurralde, and O. Weichenrieder, "Crystal structure of the MID-PIWI lobe of a eukaryotic argonaute protein," *Proceedings of the National Academy of Sciences of the United States of America*, vol. 108, no. 26, pp. 10466-10471, 2011.
- [49] F. Frank, N. Sonenberg, and B. Nagar, "Structural basis for 5'-nucleotide base-specific recognition of guide RNA by human AGO2," *Nature*, vol. 465, no. 7299, pp. 818-822, 2010.
- [50] J. S. Parker, S. M. Roe, and D. Barford, "Structural insights into mRNA recognition from a PIWI domain-siRNA guide complex," *Nature*, vol. 434, no. 7033, pp. 663-666, 2005.
- [51] Y.-L. Chiu and T. M. Rana, "siRNA function in RNAi: a chemical modification analysis," *RNA*, vol. 9, no. 9, pp. 1034-1048, 2003.
- [52] T. P. Prakash, C. R. Allerson, P. Dande et al., "Positional effect of chemical modifications on short interference RNA activity in mammalian cells," *Journal of Medicinal Chemistry*, vol. 48, no. 13, pp. 4247-4253, 2005.
- [53] J. K. Watts, N. Choubdar, K. Sadalapure et al., "2'-Fluoro-4'-thioarabino-modified oligonucleotides: conformational switches linked to siRNA activity," *Nucleic Acids Research*, vol. 35, no. 5, pp. 1441-1451, 2007.
- [54] H. Peacock, A. Kannan, P. A. Beal, and C. J. Burrows, "Chemical modification of siRNA bases to probe and enhance RNA interference," *Journal of Organic Chemistry*, vol. 76, no. 18, pp. 7295-7300, 2011.
- [55] D. M. Kenski, A. J. Cooper, J. J. Li et al., "Analysis of acyclic nucleoside modifications in siRNAs finds sensitivity at position 1 that is restored by 5'-terminal phosphorylation both in vitro

- and in vivo," *Nucleic Acids Research*, vol. 38, no. 2, pp. 660–671, 2009.
- [56] Q. Xu, D. Katkevica, and E. Rozners, "Toward amide-modified RNA: synthesis of 3'-aminomethyl-5'-carboxy-3',5'-dideoxy nucleosides," *Journal of Organic Chemistry*, vol. 71, no. 16, pp. 5906–5913, 2006.
- [57] D. R. Corey, "RNA learns from antisense," *Nature Chemical Biology*, vol. 3, no. 1, pp. 8–11, 2007.
- [58] W. Gong and J.-P. Desaulniers, "Synthesis and properties of RNAs that contain a PNA-RNA dimer," *Nucleosides, Nucleotides and Nucleic Acids*, vol. 31, no. 5, pp. 389–400, 2012.
- [59] C. Selvam, S. Thomas, J. Abbott, S. D. Kennedy, and E. Rozners, "Amides as excellent mimics of phosphate linkages in RNA," *Angewandte Chemie. International Edition*, vol. 50, no. 9, pp. 2068–2070, 2011.
- [60] P. S. Pallan, P. von Matt, C. J. Wilds, K.-H. Altmann, and M. Egli, "RNA-binding affinities and crystal structure of oligonucleotides containing five-atom amide-based backbone structures," *Biochemistry*, vol. 45, no. 26, pp. 8048–8057, 2006.
- [61] T. K. Chakraborty, P. K. Gajula, and D. Koley, "Studies directed toward the development of amide-linked RNA mimics: synthesis of the monomeric building blocks," *Journal of Organic Chemistry*, vol. 73, no. 17, pp. 6916–6919, 2008.

Research Article

Transferrin-Conjugated SNALPs Encapsulating 2'-O-Methylated miR-34a for the Treatment of Multiple Myeloma

Immacolata Scognamiglio,¹ Maria Teresa Di Martino,² Virginia Campani,¹ Antonella Virgilio,¹ Aldo Galeone,¹ Annamaria Gullà,² Maria Eugenia Gallo Cantafio,² Gabriella Misso,³ Pierosandro Tagliaferri,² Pierfrancesco Tassone,² Michele Caraglia,³ and Giuseppe De Rosa¹

¹ Department of Pharmacy, Federico II University of Naples, Via Domenico Montesano 49, 80131 Naples, Italy

² Department of Medical Oncology, Department of Experimental and Clinical Medicine, Magna Graecia University and T. Campanella Cancer Center, Salvatore Venuta Campus, 88100 Catanzaro, Italy

³ Department of Biochemistry, Biophysics and General Pathology, Second University of Naples, 80138 Naples, Italy

Correspondence should be addressed to Giuseppe De Rosa; gderosa@unina.it

Received 29 October 2013; Accepted 26 December 2013; Published 13 February 2014

Academic Editor: Maria Chiara Maiuri

Copyright © 2014 Immacolata Scognamiglio et al. This is an open access article distributed under the Creative Commons Attribution License, which permits unrestricted use, distribution, and reproduction in any medium, provided the original work is properly cited.

Stable nucleic acid lipid vesicles (SNALPs) encapsulating miR-34a to treat multiple myeloma (MM) were developed. Wild type or completely 2'-O-methylated (OMet) MiR-34a was used in this study. Moreover, SNALPs were conjugated with transferrin (Tf) in order to target MM cells overexpressing transferrin receptors (TfRs). The type of miR-34a chemical backbone did not significantly affect the characteristics of SNALPs in terms of mean size, polydispersity index, and zeta potential, while the encapsulation of an OMet miR-34a resulted in a significant increase of miRNA encapsulation into the SNALPs. On the other hand, the chemical conjugation of SNALPs with Tf resulted in a significant decrease of the zeta potential, while size characteristics and miR-34a encapsulation into SNALPs were not significantly affected. In an experimental model of MM, all the animals treated with SNALPs encapsulating miR-34a showed a significant inhibition of the tumor growth. However, the use of SNALPs conjugated with Tf and encapsulating OMet miR-34a resulted in the highest increase of mice survival. These results may represent the proof of concept for the use of SNALPs encapsulating miR-34a for the treatment of MM.

1. Introduction

MicroRNAs (miRNAs) are noncoding nucleic acids able to regulate basic biological functions and pathways essential to tumor development and progression [1]. In the last years, the development of miRNA-based anticancer therapies received growing attention. Some miRNAs, such as miR-34a, have a tumor suppressor activity and their reintroduction into diseased tissues can drive a therapeutic response [2]. The development of therapies based on miRNAs, as well as in general on nucleic acids, is hampered by several drawbacks, including cost and production of clinical grade material [3], degradation and inactivation by nucleases in plasma and cells [4], poor intracellular delivery [5, 6], rapid plasma elimination

[7–9], and renal and dose-limiting hemodynamic toxicities [10]. For antisense oligonucleotides (ONs), which are furthest along the clinical development, nuclease sensitivity has been minimized through chemical modifications to the nucleic acid backbones and/or sugars [11], while hemodynamic toxicities have been reduced through the use of repeated, slow infusions (2 h) or continual infusion protocols up to 21 days [12]. The use of nanovectors for the delivery of nucleic acids represents a valid and widely investigated approach to overcome the previously described biopharmaceutical issues [11, 13]. This will be particularly critical for RNA agents on which modifications would be increasingly more complicated and costly. Conventional and cationic liposomes have been used extensively to increase the therapeutic index of a variety

of ONs by changing their pharmacokinetic and pharmacodynamic characteristics [14–16]. However, the low ONs encapsulation efficiency (especially for neutral liposomes), the instability in serum, and the toxicity issues associated with the use of cationic lipid [13] limited the *in vivo* use of cationic liposomes. The use of an ionizable aminolipid into the lipid vesicles allowed facilitating the encapsulation of nucleic acids into the vesicle that can subsequently be brought at physiological pH with consequent increased stability in serum [17]. These nanocarriers, the so-called stable nucleic acid lipid vesicles (SNALPs), have shown promising results to deliver plasmids, antisense oligonucleotides, and small interfering RNAs (siRNA) *in vivo* [18–20].

Previously, our group developed SNALPs encapsulating miR-34a for the treatment of medulloblastoma cells [21]. The miR-34 is a family of noncoding RNAs directly regulated by the transcription factor p53 [22–24]. miR-34a activates the p53 oncosuppressor activity, by inhibiting cell growth, inducing apoptosis, and causing a senescence-like phenotype [25]. Several studies have confirmed that the miR-34 family is required for normal cell responses to DNA damage following irradiation *in vivo*.

Multiple myeloma is a hematologic malignancy, incurable in most cases, which needs development of novel therapeutic strategies [26]. Deregulated expression of miR-34a in MM patients had been evidenced [27], thus suggesting an interest for these molecules as antitumor therapeutic agents. In this light, a recent report by our group has demonstrated that miR-34a replacement strategies are active in controlling the proliferation of several MM cell lines in different animal models [28]. However, the optimization of the delivery of miR-34a is required in order to translate these models in the clinical setting.

The aim of this study was to develop SNALPs encapsulating miR-34a with enhanced delivery properties for MM. In particular, we investigated the possibility to encapsulate synthetic miRNAs, namely, wild type miR-34a and a completely 2'-O-methylated (OMet) miR-34a, into the SNALPs. Moreover, SNALPs encapsulating miR-34a were conjugated with transferrin (Tf), in order to achieve improved transfection efficiency and targeting types of tumor cells. Antitumor properties of the different miR-34a, encapsulated in SNALPs or Tf-conjugated SNALPs (Tf-SNALPs), were investigated in preclinical experimental model of MM.

2. Materials and Methods

1,2-Dioleoyl-3-dimethylammonium propane (DODAP) and N-palmitoyl-sphingosine-1-{succinyl[methoxy(polyethylene glycol)2000]} (PEG₂₀₀₀-Cer₁₆) were purchased from Avanti Polar Lipids. Distearoylphosphatidylcholine (DSPC) was kindly offered from Lipoid GmbH (Cam, Switzerland). Cholesterol (CHOL), human transferrin (Tf), sodium chloride, sodium phosphate, HEPES, citric acid, and sodium citrate were purchased from Sigma Aldrich (USA). Ethanol and other solvents were obtained from Carlo Erba Reagenti (Italy). MiR-34a wild type sequence obtained by miR.org database (5'-UGG CAG UGU CUU AGC UGG UUG U-3')

was directly synthesized by MWG (Germany). As control an oligonucleotide with scrambled sequence (miR-NC) was used (Life Technologies).

2.1. 2'-OMet Oligonucleotide Synthesis and Purification. The 2'-OMet Oligonucleotide were synthesized on a Millipore Cyclone Plus DNA synthesizer at 1 μ mol scale, using commercially available 5'-O-(4,4'-dimethoxytrityl)-2'-O-methyl-3'-O-(2-cyanoethyl-N,N-diisopropyl) RNA phosphoramidite monomers and 2'-OMet RNA SynBase CPG 1000/110 as solid phase support (Link technologies). The oligomers were detached from the support and deprotected by treatment with concentrated aqueous ammonia at 55°C for 12 h. The combined filtrates and washings were concentrated under reduced pressure, redissolved in H₂O, analysed, and purified by anion-exchange high-performance liquid chromatography (HPLC) on a Nucleogel SAX column (Macherey-Nagel, 1000-8/46), using buffer A: 20 mM KH₂PO₄/K₂HPO₄ aqueous solution (pH 7.0), containing 20% (v/v) CH₃CN, and buffer B: 1 M KCl, 20 mM KH₂PO₄/K₂HPO₄ aqueous solution (pH 7.0), containing 20% (v/v) CH₃CN; a linear gradient from 0 to 100% B for 45 min and flow rate 1 mL/min were used. The purified oligomers were successively desalted by Sep-Pak C-18 cartridges (Waters) and characterized by ESI mass spectrometry.

2.2. Preparation of miR-34a Encapsulating SNALPs Conjugated or Not with Tf. SNALPs formulations were prepared by modified ethanol injection method. Briefly, lipid stock solutions were prepared in ethanol. Aliquots (0.4 mL total volume) of stock lipids (CHOL/DSPC/DODAP/PEG₂₀₀₀-Cer₁₆ or CHOL/DSPC/DODAP/DSPE-PEG₂₀₀₀-Mal/PEG₂₀₀₀-Cer₁₆) were added to a glass tube. In a separated tube, 0.2 mg of miRNA was dissolved in 0.6 mL of 20 mM citric acid at pH 4.0. The two solutions were warmed for 2–3 min to 65°C and the lipid solution was quickly added to the miRNA solution under stirring. The mixture was passed 5 times through 200 nm and 20 times through 100 nm polycarbonate filters using a thermobarrel extruder (Northern Lipids Inc., Vancouver, BC, Canada) maintained at approximately 65°C. Therefore, the preparation was dialyzed (3.5 kDa cutoff) against 20 mM citrate buffer at pH 4.0 for approximately 1 h to remove excess of ethanol, followed by further dialysis against HBS (20 mM HEPES, 145 mM NaCl, and pH 7.4) for 12–18 h to remove the citrate buffer and to neutralize the DODAP. Unencapsulated miRNA was removed by DEAE-Sepharose CL-6B column chromatography. A typical 1 mL formulation consisted of DSPC/CHOL/DODAP/PEG₂₀₀₀-Cer₁₆ or DSPC/CHOL/DODAP/DSPE-PEG₂₀₀₀-Mal/PEG₂₀₀₀-Cer₁₆ (25/45/20/10 or 25/45/20/5/5 mol/mol/mol/mol, resp.) and 0.2 mg of miR in a final solution. Tf was coupled on the preformed SNALPs vesicles containing DSPE-PEG-Mal in the lipid mix (SNALPs-Mal). Briefly, Tf was thiolated using 2-iminothiolane (Traut's reagent). Tf was dissolved in 0.1 M Na-borate buffer/0.1 mM EDTA, pH 8, followed by the addition of Traut's reagent (1:40 mol/mol). After incubation for 60 min at room temperature, thiolated Tf was immediately

used for conjugation with SNALPs-Mal overnight at room temperature. The excess of Tf was removed by molecular exclusion chromatography, Sepharose CL-B4 column.

2.3. SNALPs Characterization: Mean Diameter, Polydispersity Index, and Zeta Potential. The mean diameter and size distribution of SNALPs were determined at 20°C by photon correlation spectroscopy (PCS) (N5, Beckman Coulter, Miami, USA). Each sample was diluted in deionized/filtered (0.22 µm pore size, polycarbonate filters, MF-Millipore, Microglass Heim, Italy) water and analysed with detector at 90° angle. As measure of the particle size distribution, polydispersity index (PI) was used. For each batch, mean diameter and size distribution were the mean of three measures. For each formulation, the mean diameter and PI were calculated as the mean of three different batches. The zeta potential (ZP) of the SNALPs was determined in distilled water at 20°C by Zetasizer Nano Z (Malvern, UK). For each batch, mean diameter, size distribution, and ZP were the mean of three measures.

2.4. miR-34a Encapsulation into SNALPs Formulations. The amount of miRNA encapsulated into the SNALPs was measured spectrophotometrically. Briefly, 10 µL of SNALPs suspension was dissolved in 990 µL of methanol and analysed at 260 nm. Actual loading was calculated as amount (mg) of miRNA/mg of mg total lipids. The amount of miRNA loaded into the nanocarriers was expressed as miRNA actual loading and encapsulation efficiency, calculated as mg of miRNA/mg of total lipids and percent ratio between miR actually loaded into SNALPs and miR theoretical loading, respectively. For each batch, the results were the mean of three measures. For each formulation, the results were calculated as the mean of the measures obtained in three different batches ($n = 3$). The phospholipid content of the carrier suspension was determined by the Stewart assay [29]. Briefly, an aliquot of the SNALPs suspension was added to a two-phase system, consisting of an aqueous ammonium ferrothiocyanate solution (0.1 N) and chloroform. The concentration of DSPC was obtained by measuring the absorbance at 485 nm into the organic layer. The concentration of the total lipid content was calculated considering a constant ratio between the lipids.

2.5. Animals and In Vivo Models of Human MM. Male CB-17 severe combined immunodeficient (SCID) mice (6- to 8-week old; Harlan Laboratories, Inc., Indianapolis) were housed and monitored in our Animal Research Facility. All experimental procedures and protocols had been approved by the Institutional Ethical Committee (Magna Graecia University) and conducted according to protocols approved by the National Directorate of Veterinary Services (Italy). In accordance with institutional guidelines, mice were sacrificed when their tumors reached 2 cm in diameter or in the event of paralysis or major compromise in their quality of life, to prevent unnecessary suffering. For our study 25 SCID mice were inoculated in the interscapular area (sc) with 5×10^6 MM cells in 100 µL RPMI-1640 medium. After detection of palpable tumors, approximately 3 weeks following injection of

MM cells, animals were randomized into 5 groups including 5 mice per group, and treatments were initiated. Each animal received a dose of 20 µg of miR-34a SNALPs formulation. The treatment schedule included 5 treatments, three days apart, via tail vein. The tumor sizes were measured every two days until the day of first mouse sacrifice, using a caliper, and volume was calculated using the formula $V = 0.5 \times a \times b^2$, where a and b are the long and short diameters of the tumor, respectively.

2.6. Survival Analysis and Kaplan-Meier Plot. Survival was evaluated from the first day of treatment until death or sacrifice of animals. The observations were followed until last animal death or the tumors reached 2 cm in diameter according to our institutional guidelines. Percent of mice that survive with respect to the totality of animals included in each group is calculated and used to plot the survival curves (Kaplan-Meier curve).

2.7. FACS Analysis of TfR Expression in SKMM-1 Multiple Myeloma Cells. For determination of cell surface expression of TfR, fluorescence-activated cell sorting (FACS) analysis was performed using indirect staining of TfR (CD71). Briefly, we have seeded 50,000 SKMM-1 cells/well in 6 multiwell plates and incubated at 37°C for 24, 48, and 72 h. At the established times, the cells were collected, counted in a Burkert chamber, and centrifuged at 1,300 rpm for 5 min at 4°C in order to remove the medium. The cells were suspended in PBS in order to obtain 500,000 cells for each time point. After another centrifugation at 2,000 rpm at 4°C for 5 min, the cells were suspended in 4% paraformaldehyde and incubated for 15 min at 4°C in the dark. Thereafter, after another centrifugation the cells were suspended in PBS/BSA (1% w/v) and incubated for 10 min at 4°C. Thereafter, the cells were incubated with a primary mouse monoclonal antibody raised against human TfR (CD71, H68.4, dilution: 1:100; Santa Cruz Biotechnology, Santa Cruz, CA, USA) or with an irrelevant immunoglobulin (IgG1) or in PBS overnight at 4°C. After incubation with primary antibody, the cells were again centrifuged and incubated with the secondary antibody (anti-mouse-FITC), in the dark for 1 h at 4°C. After washing, FACS sorting was performed using a FACScan (Becton Dickinson, Mountain View, CA, USA), and analysis was performed using CellQuest 2.0 (Becton Dickinson).

2.8. Statistical Analysis. Student's t -test, two-tailed test, and Log rank test were used to calculate all reported P values using GraphPad software (<http://www.graphpad.com/>). Graphs were obtained using SigmaPlot version 11.0.

3. Results and Discussion

In this study, we investigated the possible use of miR-34a in the treatment of MM. We have previously investigated the activity of miR-34a in different preclinical models using a commercial available lipidic emulsion [28]. Moreover, we previously developed SNALPs encapsulating miR-34a to treat medulloblastoma cells *in vitro* [21]. Here we proposed the use

TABLE 1: Mean diameter, polydispersity index, and zeta potential of the different SNALPs-based formulations.

Formulations	miRNA chemistry	Targeting ligand	Mean diameter (nm) \pm SD	PI \pm SD	ZP (mV) \pm SD
SNALP1	Wild type	—	157.18 \pm 17.18	0.16 \pm 0.03	-13.52 \pm 2.28
SNALP2	OMet	—	127.75 \pm 10.68	0.25 \pm 0.03	-5.19 \pm 5.38
Tf-SNALP1	Wild type	Tf	158.32 \pm 10.25	0.14 \pm 0.05	-23.62 \pm 1.54
Tf-SNALP2	OMet	Tf	130.84 \pm 8.41	0.21 \pm 0.02	-18.13 \pm 4.39

TABLE 2: miRNA encapsulation into the SNALPs.

Formulations	Actual loading (μ g miRNA/mg lipids)	Encapsulation efficiency (%)
SNALP1	160.0 \pm 4.8	80 \pm 3
SNALP2	196.5 \pm 10.6	98 \pm 5

Theoretical loading: 200 μ g miRNA/mg lipids.

of SNALPs encapsulating miR-34a to treat MM *in vivo*. We also investigated the possibility to modify the previously developed SNALPs in order to obtain enhanced antitumor activity. To do this, as first strategy, we encapsulated a chemically modified miRNA into the SNALPs. In particular, OMet miR-34a was selected due to substantial degree of nuclease resistance and high binding affinity with the target [30]. A second strategy consisted of Tf conjugation with SNALPs in order to enhance targeting and delivery to cancer cells *in vivo*. In fact, SKMM-1 MM cells (used in our study) expressed on their surface significantly high levels of the TfR as demonstrated by the analysis of TfR expression performed during FACS analysis (Figure 1). Interestingly, the expression of the receptor increased in a time-dependent manner during the culture of SKMM-1 cells suggesting its role in the survival of these cells. Moreover, MM cells are characterized by an over-expression of the Tf receptor [33, 34]. On the basis of these data and on the known high rate of internalization of the TfR, we were prompted to develop SNALPs armed with Tf for the treatment of MM.

In Table 1, the developed formulations, as well as their characteristics in terms of mean diameter, PI, and ZP, are reported. SNALPs have a mean diameter ranging between about 128 and 158 nm; the use of an OMet miRNA slightly decreased mean diameter. All the formulations have a narrow size distribution, although a slight increase from 0.16 to 0.25 was observed when encapsulating an OMet miR-34a.

In Table 2, the amount of miR-34a encapsulated into the SNALPs is reported. All the formulations displayed a high amount of miR-34a encapsulated into the SNALPs. In particular, wild type miR-34a was encapsulated with an efficiency of about 80%. This result was not surprising and in agreement with other previously developed SNALPs formulations [17, 21]. Interestingly, the use of an OMet miRNA led to a significant increase of the encapsulation efficiency (about 98% of the miRNA initially used in the formulation). The interaction between the negative charge of nucleic acid and the positive one of cationic lipid is the driving force for the encapsulation of nucleic acids into the SNALPs [17]. However, an OMet miR-34a, if compared to a wild type miR-34a, is more lipophilic, due to the presence of the methyl residue

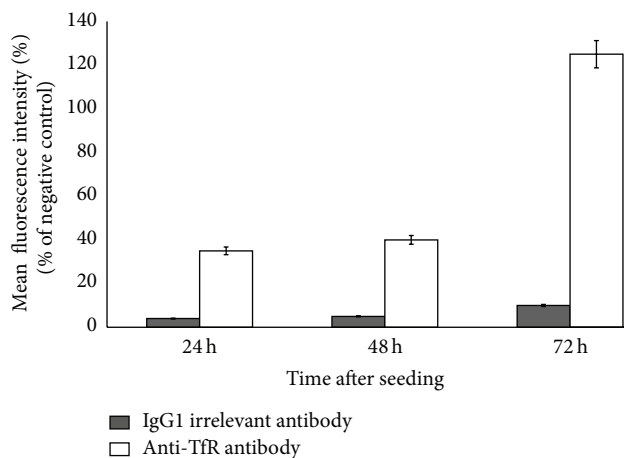


FIGURE 1: FACS analysis of the surface expression of TfR in SKMM-1 cells. SKMM-1 cells were cultured for 24, 48, and 72 h and the expression of CD71 (TfR) was evaluated at FACS as reported in Section 2. The intensity of TfR expression was represented as % of mean fluorescence intensity (MFI) calculated by comparing the MFI of cells incubated with antibodies with that of cells incubated in PBS. A significant increase of MFI was observed in cells labelled with anti-TfR (empty squares) if compared with that of cells labelled with irrelevant IgG1 (full squares) suggesting a significant expression of TfR on the surface of SKMM-1 cells. Each value was the mean of at least three different determinations performed in three different experiments. Bars, SEs.

bound to 2'-position of the sugar moiety of each nucleotide. Therefore, in our study, an additive hydrophobic interaction between the miRNA and the lipid bilayer can represent an additional contribution to high miRNA loading into the SNALPs, when encapsulating a completely 2'-O methylated miRNA.

Thereafter, we modified the surface of SNALPs with Tf in order to achieve an additional improvement of the delivery in MM cells. SNALPs modified with targeting ligands have previously been reported for glioblastoma cells [31]. In the study from Costa et al., SNALPs were modified by postinsertion method. In the present work, we preferred to use a different approach and Tf was coupled to preformed SNALPs. Tf binding to the nanoparticle surface did not significantly affect the size characteristics of the vesicles. On the contrary, a slight decrease of the PI, from 0.16 to 0.14 and from 0.25 to 0.21, was observed for both SNALP1 and SNALP2, respectively. This slight increase of PI can be explained with the further purification step after the conjugation with Tf. Tf-SNALPs also showed a significant decrease of the zeta

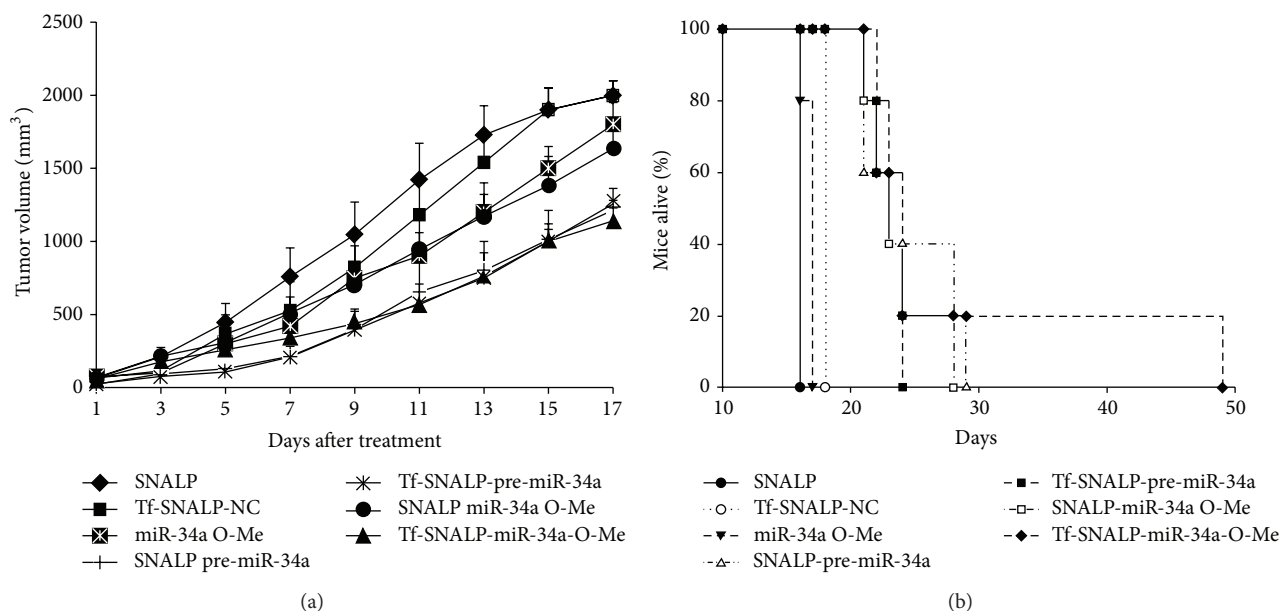


FIGURE 2: Systemic delivery of miR-34a SNALPs formulations inhibits growth of human MM tumors in mice. (a) Mice carrying palpable subcutaneous SKMM-1 tumor xenografts were treated with 20 μ g of pre-miR-34a or miR-34a OMe SNALPs or Tf-SNALPs formulations by intravenous tail vein injections. Caliper measurement of tumors was taken every 2 days from the day of first treatment. Averaged tumor volumes of 5 mice per group are reported \pm SD. (b) Survival curves (Kaplan-Meier) of treated mice show prolongation of survival after formulated miR-34a treatment compared to controls (log-rank test, $P < 0.005$). Survival was evaluated from the first day of treatment until death or sacrifice.

potential (Table 1), as expected by the presence of the protein on the vesicle surface. The Tf conjugation on the preformed SNALPs did not affect miRNA encapsulation into the vesicles (data not shown).

We next explored the effects of the systemic delivery of miR-34a SNALPs formulations in controlling the growth of SKMM-1 xenografts. When subcutaneous MM tumors became palpable, mice were randomized and systemically treated, via tail vein, with different miR-34a or miR-NC SNALPs formulations at a concentration of 1 mg miR-34a/kg per mouse. Following 5 injections (3 days apart), a significant antitumor effect of miR-34a SNALPs formulation (SNALP 1) versus the control was detected (Figure 2(a)). The treatment with plain SNALPs did not elicit any effect on the tumor growth (Figure 2(a)). The use of SNALPs encapsulating OMe miR-34a resulted in a lower inhibition of tumor growth, compared to SNALPs encapsulating wild type miR-34a. If we consider that the ONs modification with a 2'-O-methyl group maintains a strong base-pairing with target [32], a different delivery mechanism of the miRNA from the vesicle could be responsible for the lower antitumor activity when using SNALPs encapsulating OMe miR-34a. The modification of Tf conjugation with SNALPs affected miRNA antitumor activity, depending on the RNA chemistry. In particular, the SNALPs conjugation with Tf significantly increased the effect of OMe miR-34a on tumor growth (Figure 2(a)). In particular, after 9 days from the beginning of the treatment, the effect of Tf-SNALPs encapsulating OMe miR-34 was comparable to that obtained in animal treated with SNALPs encapsulating wild type miR-34a. Surprisingly, conjugation

with Tf had no effect on SNALPs encapsulating wild type miR-34a. The increased efficacy of the treatment, observed in the case of Tf-SNALP2, can be explained with a higher interaction and uptake of SNALPs in MM cells, characterized by an overexpression of TfR (see also Figure 1) [33, 34]. The importance of the TfR for the development of malignant human hematopoietic has been well established [35]. Moreover, in the case of metastasis originated by the MM cells, an increased growth of vessel characterizes the tumor mass. It has been demonstrated that SNALPs predominantly deliver siRNA to areas adjacent to functional tumor blood vessels [36]. Therefore, in our study, a targeting of tumor vessel, characterized by an enhanced expression of the TfR, can also be hypothesized. It is worthy of note that the use of Tf was beneficial only in the case of SNALPs encapsulating wild type miR-34a. To justify these findings, we hypothesize that the animal treatment with SNALP1 led to the highest miRNA delivery, in these experimental conditions. For this reason, animal treatment with Tf-SNALP1 did not result in an increased inhibition of the tumor growth; in line with this hypothesis, the use of Tf-SNALP2 led to an increased inhibition of the tumor growth, which was similar to that obtained in animals treated with SNALP1 and Tf-SNALP1.

In Figure 2(b), the mice survival following treatment with the different SNALP-based formulations is reported. All the animals treated with plain SNALPs died after 17 days of treatment. Mice survival was prolonged with all the SNALP-based formulations encapsulating miR-34a. In particular, mice treatment with SNALPs containing wild type miR-34a or OMe miR-34a resulted in mice survival until 28-29 days

from the beginning of the treatment. The conjugation of Tf with SNALPs containing wild type miR-34a did not prolong mice survival. Surprisingly, the use of Tf-conjugated SNALPs encapsulating OMet miR-34a resulted in a significant prolongation of the mice survival until 49 days. This could be explained with the higher biological stability of OMet miR-34a that can result in the highest persistence of the miR-34a into the cells. Of course, the superiority of the formulation Tf-SNALP2 was not observed in the experiments of tumor growth, where the animals were sacrificed, according with the institutional guidelines, following 17 days from the beginning of the treatment.

4. Conclusions

In this work, we developed SNALPs to deliver miR-34a. SNALPs were also modified to enhance miR-34a delivery in cancer. The two strategies used, the encapsulation of a chemically modified OMet miR-34a and the binding Tf on the nanoparticle surface, did not affect the technological properties of the nanocarriers. The antitumor effect of miR-34a was demonstrated in an experimental animal model of MM. A significant inhibition of the tumor growth was observed in animals treated with all the formulations. However, only the combination of OMet miR-34a and Tf-conjugation with SNALPs resulted in a significant prolongation of the mice survival.

This study demonstrated that miR-34a represents a powerful tool to treat tumors as MM, for which present treatment can only prolong the survival. However, this kind of therapy will need to develop *ad hoc* delivery systems in order to optimize the anticancer activity of miRNAs. As shown in this work, chemical modifications aimed to improve the biological stability of the miRNA that could be successfully combined with targeting approaches based upon the active delivery of the nanotechnological devices. This approach can be reasonably extended to deliver miRNA and other nucleic acids in other tumors characterized by over-expression of TfR. Additional studies are required to investigate if the developed treatment can be associated to toxicity in healthy tissue.

Authors' Contribution

Immacolata Scognamiglio and Maria Teresa Di Martino contributed equally to this work.

Conflict of Interests

The authors declare that there is no conflict of interests regarding the publication of this paper.

Acknowledgments

This work has been supported by the Italian Association for Cancer Research (AIRC), PI: PT, "Special Program Molecular Clinical Oncology-5 per mille" no. 9980, 2010/15. Giuseppe De Rosa and Michele Caraglia received partial support from

the Italian Ministry of Education, University and Research (MIUR) with a project (FIRB-ACCORDI DI PROGRAMMA 2011) entitled Application of High-Throughput Technology Platforms for the Characterization of New Biomarkers and Molecular Targets in Nanovectors for the Diagnosis and Treatment of Human Cancer and from Regione Campania with a project entitled Laboratori Pubblici Progetto Hauteville.

References

- [1] S. P. Nana-Sinkam and C. M. Croce, "Clinical applications for microRNAs in cancer," *Clinical Pharmacology & Therapeutics*, vol. 93, pp. 98–104, 2013.
- [2] A. G. Bader, "miR-34—a microRNA replacement therapy is headed to the clinic," *Frontiers in Genetics*, vol. 3, article 120, 2012.
- [3] D. M. Prazeres, G. N. Ferreira, G. A. Monteiro, C. L. Cooney, and J. M. Cabral, "Large-scale production of pharmaceutical-grade plasmid DNA for gene therapy: problems and bottlenecks," *Trends in Biotechnology*, vol. 17, no. 4, pp. 169–174, 1999.
- [4] S. Akhtar, R. Kole, and R. L. Juliano, "Stability of antisense DNA oligodeoxynucleotide analogs in cellular extracts and sera," *Life Sciences*, vol. 49, no. 24, pp. 1793–1801, 1991.
- [5] V. G. Budker, D. G. Knorre, and V. V. Vlassov, "Cell membranes as barriers for antisense constructions," *Antisense Research and Development*, vol. 2, no. 2, pp. 177–184, 1992.
- [6] R. M. Crooke, "In vitro toxicology and pharmacokinetics of antisense oligonucleotides," *Anti-Cancer Drug Design*, vol. 6, no. 6, pp. 609–646, 1991.
- [7] S. Agrawal and R. Zhang, "Pharmacokinetics of oligonucleotides," *Ciba Foundation Symposium*, vol. 209, pp. 60–78, 1997.
- [8] S. Akhtar and S. Agrawal, "In vivo studies with antisense oligonucleotides," *Trends in Pharmacological Sciences*, vol. 18, no. 1, pp. 12–18, 1997.
- [9] S. T. Crooke and C. F. Bennett, "Progress in antisense oligonucleotide therapeutics," *Annual Review of Pharmacology and Toxicology*, vol. 36, pp. 107–129, 1996.
- [10] S. P. Henry, P. C. Giclas, J. Leeds et al., "Activation of the alternative pathway of complement by a phosphorothioate oligonucleotide: potential mechanism of action," *Journal of Pharmacology and Experimental Therapeutics*, vol. 281, no. 2, pp. 810–816, 1997.
- [11] G. De Rosa, D. De Stefano, and A. Galeone, "Oligonucleotide delivery in cancer therapy," *Expert Opinion on Drug Delivery*, vol. 7, no. 11, pp. 1263–1278, 2010.
- [12] J. T. Holmlund, B. P. Monia, T. J. Kwok, and F. A. Dorr, "Toward antisense oligonucleotide therapy for cancer: ISIS compounds in clinical development," *Current Opinion in Molecular Therapeutics*, vol. 1, no. 3, pp. 372–385, 1999.
- [13] G. De Rosa and M. I. La Rotonda, "Nano and microtechnologies for the delivery of oligonucleotides with gene silencing properties," *Molecules*, vol. 14, no. 8, pp. 2801–2823, 2009.
- [14] M. J. Hope, B. Mui, S. Ansell, and Q. F. Ahkong, "Cationic lipids, phosphatidylethanolamine and the intracellular delivery of polymeric, nucleic acid-based drugs," *Molecular Membrane Biology*, vol. 15, no. 1, pp. 1–14, 1998.
- [15] O. Zelphati and F. C. Szoka Jr., "Cationic liposomes as an oligonucleotide carrier: mechanism of action," *Journal of Liposome Research*, vol. 7, no. 1, pp. 31–49, 1997.

- [16] N. Smyth-Templeton, D. D. Lasic, P. M. Frederik, H. H. Strey, D. D. Roberts, and G. N. Pavlakis, "Improved DNA: liposome complexes for increased systemic delivery and gene expression," *Nature Biotechnology*, vol. 15, no. 7, pp. 647–652, 1997.
- [17] S. C. Semple, S. K. Klimuk, T. O. Harasym et al., "Efficient encapsulation of antisense oligonucleotides in lipid vesicles using ionizable aminolipids: formation of novel small multilamellar vesicle structures," *Biochimica et Biophysica Acta*, vol. 1510, no. 1-2, pp. 152–166, 2001.
- [18] D. V. Morrissey, J. A. Lockridge, L. Shaw et al., "Potent and persistent *in vivo* anti-HBV activity of chemically modified siRNAs," *Nature Biotechnology*, vol. 23, no. 8, pp. 1002–1007, 2005.
- [19] T. S. Zimmermann, A. C. Lee, A. Akinc et al., "RNAi-mediated gene silencing in non-human primates," *Nature*, vol. 441, pp. 111–114, 2006.
- [20] T. W. Geisbert, A. C. Lee, M. Robbins et al., "Postexposure protection of non-human primates against a lethal Ebola virus challenge with RNA interference: a proof-of-concept study," *The Lancet*, vol. 375, no. 9729, pp. 1896–1905, 2010.
- [21] P. de Antonellis, C. Medaglia, E. Cusanelli et al., "MiR-34a targeting of notch ligand delta-like 1 impairs CD15⁺/CD133⁺ tumor-propagating cells and supports neural differentiation in medulloblastoma," *PLoS ONE*, vol. 6, no. 9, Article ID e24584, 2011.
- [22] H. Hermeking, "The miR-34 family in cancer and apoptosis," *Cell Death and Differentiation*, vol. 17, no. 2, pp. 193–199, 2010.
- [23] T.-C. Chang, E. A. Wentzel, O. A. Kent et al., "Transactivation of miR-34a by p53 broadly influences gene expression and promotes apoptosis," *Molecular Cell*, vol. 26, no. 5, pp. 745–752, 2007.
- [24] V. Tarasov, P. Jung, B. Verdoodt et al., "Differential regulation of microRNAs by p53 revealed by massively parallel sequencing: miR-34a is a p53 target that induces apoptosis and G1-arrest," *Cell Cycle*, vol. 6, no. 13, pp. 1586–1593, 2007.
- [25] N. Raver-Shapira, E. Marciano, E. Meiri et al., "Transcriptional activation of miR-34a contributes to p53-mediated apoptosis," *Molecular Cell*, vol. 26, no. 5, pp. 731–743, 2007.
- [26] C. Welch, Y. Chen, and R. L. Stallings, "MicroRNA-34a functions as a potential tumor suppressor by inducing apoptosis in neuroblastoma cells," *Oncogene*, vol. 26, no. 34, pp. 5017–5022, 2007.
- [27] L. He, X. He, L. P. Lim et al., "A microRNA component of the p53 tumour suppressor network," *Nature*, vol. 447, no. 7148, pp. 1130–1134, 2007.
- [28] M. T. Di Martino, E. Leone, N. Amodio et al., "Synthetic miR-34a mimics as a novel therapeutic agent for multiple myeloma: *in vitro* and *in vivo* evidence," *Clinical Cancer Research*, vol. 18, pp. 6260–6270, 2012.
- [29] J. C. Stewart, "Colorimetric determination of phospholipids with ammonium ferrothiocyanate," *Analytical Biochemistry*, vol. 104, no. 1, pp. 10–14, 1980.
- [30] M. Cotten, B. Oberhauser, H. Brunar et al., "2'-O-methyl, 2'-O-ethyl oligoribonucleotides and phosphorothioate oligodeoxyribonucleotides as inhibitors of the *in vitro* U7 snRNP-dependent mRNA processing event," *Nucleic Acids Research*, vol. 19, no. 10, pp. 2629–2635, 1991.
- [31] P. M. Costa, A. L. Cardoso, L. S. Mendonça et al., "Tumor-targeted chlorotoxin-coupled nanoparticles for nucleic acid delivery to glioblastoma cells: a promising system for glioblastoma treatment," *Molecular Therapy—Nucleic Acids*, vol. 2, article e100, 2013.
- [32] C. Wilson and A. D. Keefe, "Building oligonucleotide therapeutics using non-natural chemistries," *Current Opinion in Chemical Biology*, vol. 10, no. 6, pp. 607–614, 2006.
- [33] C. J. Yeh, C. G. Taylor, and W. P. Faulk, "Transferrin binding by peripheral blood mononuclear cells in human lymphomas, myelomas and leukemias," *Vox Sanguinis*, vol. 46, no. 4, pp. 217–223, 1984.
- [34] Y. Kohgo, T. Nishisato, H. Kondo, N. Tsushima, Y. Niitsu, and I. Urushizaki, "Circulating transferrin receptor in human serum," *British Journal of Haematology*, vol. 64, no. 2, pp. 277–281, 1986.
- [35] P. P. Ng, G. Helguera, T. R. Daniels et al., "Molecular events contributing to cell death in malignant human hematopoietic cells elicited by an IgG3-avidin fusion protein targeting the transferrin receptor," *Blood*, vol. 108, no. 8, pp. 2745–2754, 2006.
- [36] L. Li, R. Wang, D. Wilcox et al., "Tumor vasculature is a key determinant for the efficiency of nanoparticle-mediated siRNA delivery," *Gene Therapy*, vol. 19, pp. 775–780, 2011.